TÉCNICO LISBOA

# Interaction of silver nanoparticles with aerobic granular sludge in textile wastewater treatment bioreactors

**João André Tomás Borges Bento**

Thesis to obtain the Master of Science Degree in

**Biotechnology**

Supervisors: Profª. Nídia Dana Mariano Lourenço de Almeida

Profª. Maria Teresa Ferreira Marques Pinheiro

## Examination Committee

Chairperson: Profª. Leonilde de Fátima Morais Moreira

Supervisor: Profª. Nídia Dana Mariano Lourenço de Almeida

Member of the Committee: Profª. Helena Maria Rodrigues Vasconcelos Pinheiro

**November 2016**

# Acknowledgments

Um agradecimento muito especial às professoras, Nídia Lourenço e Teresa Pinheiro, pelos conhecimentos transmitidos, pelo constante apoio, motivação, paciência e carinho.

Quero agradecer também à Rita Franca pela paciência e disponibilidade para ensinar-me todas as técnicas e protocolos necessários para a monitorização dos reatores. Muitos dos resultados desta tese devem-se à tua ajuda e colaboração. A tua dedicação e capacidade de trabalho foram, sem dúvida, uma influência muito positiva.

À professora Helena Pinheiro, pela sabedoria, simpatia e disponibilidade para ajudar sempre que necessário.

Ao professor Manuel Francisco pela sua colaboração com as análises de microtomografia de raio-X.

À "coronela" Renata, pelos conhecimentos transmitidos, por toda a ajuda no laboratório, pela paciência, motivação e boa disposição.

À Lília e à Laura a "minha família do laboratório" e aos restantes colegas do laboratório pela contagiante alegria que em muito contribuiu para ótimo ambiente de trabalho existente. Obrigado também pela amizade e pela ajuda que me ofereceram sempre que necessitei.

À Ana Rosa do 7º piso pelos conhecimentos transmitidos e pela preciosa ajuda com na análise da distribuição de tamanhos das partículas através de *Dynamic light scattering* (DLS).

À Dª Rosa pela sua simpatia, disponibilidade e ajuda.

Aos meus pais pela educação, confiança e ânimo que me foram transmitidos desde sempre.

À minha irmã, familiares e amigos pela amizade, força e companheirismo.

Este trabalho foi financiado pela Fundação para a Ciência e a Tecnologia (FCT, Portugal) através do projecto "Impact of engineered nanoparticle and microplastics on textile wastewater treatment with aerobic granular technology – NanoMicroImpact", PTDC/AAG-TEC/4501/2014

# Abstract

The use of silver nanoparticles (Ag NPs) in textile industry has been increasing and their occurrence in wastewater is expected to rise accordingly. The antimicrobial properties of Ag NPs suggest a potential negative impact on biological wastewater treatment systems. This study assessed the impacts of 5mg $L^{-1}$ Ag NPs on aerobic granular sludge (AGS) in sequencing batch reactors treating textile wastewater. Nuclear microscopy (NM) was applied for imaging and quantitative elemental analysis. Successful granulation was achieved after 35 days, irrespective of Ag NP presence. Although Ag NPs had induced an early AGS deterioration, in the long term they seemed to enhance AGS settling properties. Furthermore, AGS treatment performance and cell integrity were not affected by Ag NPs. A quantitative analysis of the major fractions of the extracellular polymeric substances (EPS) suggested that Ag NPs interacted with the protein fraction, which was further confirmed by NM. The Ag NPs-containing sample examination through NM also showed that < 10μm Ag NPs agglomerates were presumably distributed uniformly in the surface of both granular and floc-like structures, although in AGS it was preferentially associated with an external EPS layer. The Ag distribution in AGS demonstrated that the granule outer layers hindered the dispersion of Ag NPs into the central part. Overall, AGS showed the ability to withstand Ag NPs toxicity, but granule structural stability was negatively influenced by Ag NPs. Furthermore, the detailed NM compartmentalization of Ag NPs in sludge components provided new and relevant information concerning the pattern of Ag NPs retention.



**Keywords:** silver nanoparticles; aerobic granular sludge; extracellular polymeric substances; textile wastewater; sequencing batch reactor; nuclear microscopy.

# Resumo

O uso de nanopartículas de prata (Ag NPs) na indústria têxtil tem vindo a aumentar e a sua ocorrência em águas residuais deverá aumentar em conformidade. As propriedades antimicrobianas das Ag NPs sugerem um potencial impacto negativo nos sistemas biológicos de tratamento de águas residuais. Este estudo avaliou os impactos de 5mg $L^{-1}$ Ag NPs em grânulos aeróbios (GA) em reatores descontínuos sequenciais tratando efluentes têxteis. A microscopia nuclear (MN) foi aplicada para análise quantitativa e mapeamento de elementos. A granulação foi conseguida após 35 dias, independentemente da presença das Ag NPs. Embora as Ag NPs tivessem induzido uma deterioração precoce dos GA, a longo prazo pareceram melhorar as suas propriedades de sedimentação. Além disso, as Ag NPs não afetaram o desempenho do tratamento, nem a integridade das membranas celulares. A análise quantitativa das substâncias poliméricas extracelulares (SPE) sugeriu que as Ag NPs interagiam com a fração protéica, como confirmado por MN. MN também mostrou que aglomerados de Ag <10 μm estavam presumivelmente distribuídos uniformemente na superfície de estruturas granulares e floculares, embora nos grânulos estivessem preferencialmente associados a uma camada de SPE. A distribuição de Ag em GA revelou que as camadas externas impediam a dispersão de Ag NPs para as camadas interiores dos grânulos. Em geral, os GA mostraram resistência à toxicidade das Ag NPs, mas a sua estabilidade estrutural foi negativamente influenciada. A compartimentação de Ag NPs nos componentes das lamas obtida com MN forneceu informações novas e relevantes sobre o padrão de retenção das Ag NPs.

**Palavras-chave:** Nanopartículas de prata; Grânulos aeróbios; Substâncias poliméricas extracelulares; Águas residuais têxteis; Reatores descontínuos sequenciais; Microscopia nuclear.

# Table of Contents

# Figure Index

# Table Index

# Abbreviations

| | |
|---|---|
| Ag NPs | Silver Nanoparticles |
| AGS | Aerobic granular sludge |
| AMO | Ammonia monooxygenase |
| AOPs | Advanced oxidation processes |
| AQDS | Anthraquinone-2,6-disulfonate |
| AQS | Anthraquinone-2-sulfonate |
| AR14 | Acid Red 14 |
| AS | Activated sludge |
| BCA | Bicinchoninic acid |
| BOD | Biochemical Oxygen Demand |
| CER | Cation exchange resins |
| CM | Cytoplasmic membrane |
| CMC | Carboxymethyl Cellulose |
| COD | Chemical Oxygen Demand |
| CotA-Lac | Bacterial laccase |
| CymA | Tetraheme quinol dehydrogenase |
| DyPs | Dye decolorizing peroxidases |
| EDS | Energy-dispersive spectrometry |
| EDTA | Ethylenediamine tetraacetic acid |
| ELVs | Emission limit values |
| EM | Electron microscopy |
| EPS | Extracellular polymeric substances |
| EVSS | Volatile suspended solids in the discharged effluent |
| FAD | Flavin adenine dinucleotide |
| Feed - C | Carbon feed solution |
| Feed - N | Nitrogen dye-containing feed solution |
| FMN | Flavin mononucleotide |
| GAOs | Glycogen accumulating organisms |
| HO• | Hydroxyl radical |
| HRT | Hydraulic retention time |
| HRTEM | High-resolution transmission electron microscopy |
| IC | Integrity Coefficient |
| ICP-AES | Inductively-coupled plasma atomic emission spectroscopy |
| ICP-MS | Inductively-coupled plasma mass spectrometry |
| IQ | Interquartile |
| Lac | Laccase |
| LB-EPS | Loosely bound – extracellular polymeric substances |
| LDH | Lactate dehydrogenase |

| | |
|---|---|
| LiP | Lignin peroxidase |
| MF | Microfiltration |
| MLVSS | Volatile suspended solids in the mixed liquor |
| MnP | Manganese peroxidase |
| MQ | Menaquinone |
| MtrA | Periplasmic protein c-type cytochrome |
| MWCO | Molecular weight cut-off |
| NADPH | Reduced nicotinamide adenine dinucleotide phosphate |
| NAR | Nitrate reductase |
| NM | Nuclear microscopy |
| OLR | Organic loading rate |
| OM | Outer membrane |
| OmcB | Decaheme c-type cytochrome |
| PAOs | Phosphate accumulating organisms |
| PI | Propidium iodide |
| PIXE | Particle induced X-ray emission |
| PN | Proteins |
| PS | Polysaccharides |
| PVA | Polyvinyl Alcohol |
| RBS | Rutherford backscattering |
| RO | Reverse Osmosis |
| ROS | Reactive oxygen species |
| SBR | Sequencing batch reactor |
| SEM | Scanning electron microscopy |
| STIM | Scanning transmission ion microscopy |
| SVI | Sludge Volume Index |
| $SVI_{30}$ | SVI after 30 min of settling |
| $SVI_5$ | SVI after 5 min of settling |
| TB-EPS | Tightly bound – extracellular polymeric substances |
| TEM | Transmission electron microscopy |
| TOC | Total organic carbon |
| TSS | Total Suspended Solids |
| Tyr | Tyrosinase |
| UASB | Upflow anaerobic sludge blanket |
| UF | Ultrafiltration |
| VSS | Volatile Suspended Solids |
| WWTP | Wastewater treatment plant |
| XPS | X-ray photoelectron spectroscopy |
| µCT | Microcomputerized tomography |

# 1. Introduction

## 1.1 Textile industry

Textile processing involves many different steps and in almost all of them, wastewater is generated. The amount and composition of the generated wastewaters depend on different factors, including the processed fabric and the type of process. The textile industry not only applies a large quantity of different dyes and chemicals, but also consumes large quantities of water. (Ghaly et al., 2013). In Europe, a consumption of water between 50 - 240 $m^3$/ton of textile product (Mattioli et al., 2005) has been estimated. The data from a study involving 34 Portuguese companies points to similar values, 35 - 325 $m^3$/ton (Citeve, 2012). As a consequence, the textile industry generates large amounts of wastewater with complex and extremely variable characteristics, which makes it one of the most polluting of all industrial sectors (Vandevivere et al. 1998; Vajnhandl & Valh 2014; Lourenço et al. 2015).

### 1.1.1 Textile processing operations

Textile industries receive and prepare the fibers, which can be natural (e.g. cotton, wool, silk and linen) or synthetic (e.g. polyester, nylon and polypropylen) (Ghaly et al., 2013); transform these fibers into yarns; alter the yarns into fabrics and then these fabrics go through several stages of wet processing (Babu et al., 2007). The volume and composition of the wastewater generated by the textile industry arises mainly from the wet processing stages. The operations involved in the wet processing of textiles and the corresponding wastewater generated are discussed in the subsequent sections.

**Desizing**

In the upstream stages of wet fabric processing, sizing agents such as starch, polyvinyl alcohol (PVA) and carboxymethyl cellulose (CMC) are added to provide strength to the fibers and minimize breakage due to friction in the weaving process. Nonetheless, textile wet processes like dyeing and printing are affected by the presence of sizing agents in the fabric, since they cover the yarn and act as a barrier to dyes and other chemicals. Consequently, these size agents must be removed from the fabric by the process of desizing (dos Santos et al. 2007; Sarayu & Sandhya 2012; Holkar et al. 2016). Depending on the size agent used, alkalis, acids, enzymes or surfactants are applied in the desizing process. As result, the wastewater characteristic of this stage contains the sizes and the agents used for desizing. The contribution of this stage to the overall Biochemical Oxygen Demand (BOD) and Total Solids load of a textile wastewater can be very high. Up to 50% of the total BOD in fabric processing can be originated from the desizing step when starch is applied as size (Bisschops and Spanjers, 2003).

**Scouring**

In the scouring step an alkali solution (commonly NaOH) is used to breakdown natural oils, fats, waxes and surfactants, as well as to emulsify and suspend impurities in the scouring bath (dos Santos et al., 2007; Sarayu and Sandhya, 2012). Due to the chemicals used for scouring and to the compounds released from the fabric, the generated wastewater is chemically aggressive and may be toxic. This

wastewater is characterized by high Chemical Oxygen Demand (COD), BOD and solids content and its pH is highly alkaline (Bisschops & Spanjers 2003; Sarayu & Sandhya 2012).

**Bleaching**

To get a white fabric it is essential to remove its natural color by the process of bleaching. Mostly sodium hypochlorite, hydrogen peroxide, and peracetic acid are used as bleaching agents, but some auxiliary compounds can also be added and are released in the wastewater. BOD levels are low, but the solids content of the wastewater from bleaching can be high (Bisschops and Spanjers, 2003; Holkar et al., 2016).

**Mercerization**

Mercerization of fabrics is carried out after bleaching to confer shine and advance dye uptake. It is done by treating the fabric with a high concentration of NaOH (Holkar et al., 2016). Sometimes wax is also applied to improve the luster. As a consequence, the wastewater from this step is highly alkaline and in spite of its low BOD, it contains natural oils and waxes (Sarayu and Sandhya, 2012).

**Dyeing**

Different dyestuffs are used to confer color to the final textile product. The chromophore group, i.e., a delocalized electron system with conjugated double or simple bonds, is the major structure element responsible for light absorption in dye molecules. Common chromophores include azo (–N=N–), carbonyl (–C=O), methine (=CH–), nitro ($–NO_2$), and quinoid groups (Gürses et al., 2016; Sarayu and Sandhya, 2012). Electron withdrawing or donating substituents, denominated as auxochromes, are also used to generate or intensify the color of the chromophores. The most important auxochromes are amine ($–NH_3$), carboxyl (–COOH), sulfonate ($–SO_3H$), and hydroxyl (–OH) (Chequer et al., 2013). These groups also have the property of conferring a higher affinity to the fiber (Pereira and Alves, 2012). It is estimated that over 10,000 different dyes and pigments are used industrially and over $7 \times 10^5$ tons of synthetic dyes are annually produced worldwide. The textile industry consumes about two-thirds of all the world production (Chequer et al., 2013; Ventura and Marin, 2013).

Dyes are commonly classified through the Color Index. It lists dyes using two systems: one corresponds to the assignment of a generic name based on its mode of application, color and an identification number (e.g. Acid Red 14); another is numeric with 5-digit color index number based on its chemical structure (e.g. 14720, corresponding to the previous example). According to the type of chromophore group present in their chemical structures, dyes are classified as azo, anthraquinone, indigoid, xanthene, arylmethane and phthalocyanine. On the basis of the technique employed for their application, dyes are classified as acid, basic, direct, disperse, metallic, mordant, pigment, reactive, solvent, sulphur and vat dyes (Pereira and Alves, 2012).

The textile dyeing process normally requires large volumes of water, not only in the dye bath, but also during the rinsing step. Depending on the class of the dye, there is always a portion of unfixed dye which gets washed away along with water (Ghaly et al., 2013). The losses in wastewaters can vary from 2% for basic dyes to as high as 50% for reactive dyes. It is estimated that globally 280 000 tons of textile dyes are discharged in textile industrial wastewater every year (Pereira and Alves, 2012). Apart

from dyes, different auxiliary chemicals such as metals, salts, surfactants, organic processing assistants, sulfide, and formaldehyde are also used and end up in the wastewater. Dyeing contributes to most of the metals and almost all the salts in the overall textile wastewater. In fact, for some dyeing processes, about 75% of the salts end up in the wastewater (Bisschops and Spanjers, 2003).

**Printing**

The important reactions involved in the printing process are similar to those in the dyeing process, with the difference that color is only applied to specific parts of the fabric. Furthermore, while in the dyeing process the dye is applied in a solution form, in printing it is applied in a thick paste form (Babu et al., 2007; Holkar et al., 2016). The print pastes consist of water, thickeners, dyes, urea and various other chemicals like surfactants and solvents. A common disposal method is dilution of the residual pastes and disposal with the other wastewater streams, where they considerably increase COD, nitrogen and dye loads. Printing wastewaters are small in volume, but difficult to treat. (Bisschops and Spanjers, 2003).

**Finishing**

Finishing processes impart certain properties to the fabrics, including softening, waterproofing, antimicrobial and UV protective (Holkar et al., 2016). Specially, due to the rapid global production growth of textile materials for medical, healthcare, hygiene, and sports applications, the interest for antimicrobial finishing has been renewed in the last decade. The microbial growth on textile materials can lead to unpleasant odors, staining, fabric deterioration, and even physical irritation, such as skin allergies and skin infections. Various antimicrobial agents like metal salts, quaternary ammonium compounds, polyhexamethylene biguanides, triclosan, biopolymer chitosan, N-halamine, and peroxyacid, etc., have been used in the antimicrobial finishing of textile materials. Although many of them met the desired antimicrobial demands, they were not acceptable from economic, environmental, or long-term efficiency standpoint. As a consequece, the textile industry has been recognizing the promising potentials of silver. Silver possesses bactericidal activity against more than 650 pathogens (bacteria, fungi, and viruses). However, ionic silver stains textile materials when exposed to light and the color of the material turns from white to black–brown. This disadvantage can be avoided by the application of silver nanoparticles (Ag NPs). Unlike the conventional finishing methods, which often do not provide the desired long-term efficiency, the functionalization of textiles with Ag NPs not only improves antimicrobial durability, but also does not alter the fabric breathability and handle. Due to the high surface to volume ratio of Ag NPs, a considerable amount of silver atoms is exposed toward the surrounding medium, providing an extraordinary bactericidal efficiency (Radetić, 2013). Nonetheless, these processes also contribute to water pollution and very few data have been reported concerning the wastewater generated in the actual finishing steps (Bisschops and Spanjers, 2003).

### 1.1.2 Textile wastewater characteristics

Despite its extremely variable characteristics, untreated wastewater is usually high in color, chemical oxygen demand (COD), biochemical oxygen demand (BOD), total organic carbon (TOC), suspended solids (SS), pH, temperature, turbidity, and toxicity. Most of the BOD:COD ratios are found

to be around 1:4, indicating the presence of non-biodegradable substances (Ghaly et al., 2013; Pang and Abdullah, 2013).

Regarding color, it is difficult to find typical values reported for their content in textile wastewater due to their extreme variability. The quantity of a dye in textile wastewater depends on the type of dye and on the process carried out. Literature cites a dye concentration range from 0.01 to 0.25 g $dm^{-3}$ as being typically present in textile wastewater (O'Neill et al. 1999; Ghaly et al. 2013). Different methods with different units are used to describe the color content of a textile effluent (Bisschops and Spanjers, 2003). Some legal limits of color discharge are expressed in terms of the requirement of its absence after a certain degree of dilution (Citeve, 2012).

The wastewaters of the textile industry can be discharged in the water environment or into a collector (municipal or inter-municipal). In the case of discharge in the water environment, the wastewater must undergo a prior treatment due to its characteristics, so companies must have a wastewater treatment plant (WWTP). In Portugal, the emission limit values (ELVs) for discharge into the water environment normally follow the values defined by the Annex XVIII of Decree-Law 236/98 or the ordinance 423/97. In the case of discharge into a collector, the ELVs can vary, since each collector has its defined emission limits. However, as the wastewater discharged into the collector is further subject to treatment, most of the parameters exceed the limits defined in Decree-Law 236/98. Table 1 presents ranges of values for some representative physicochemical characteristics of untreated wastewater based on a study (Citeve, 2012) involving 34 Portuguese textile companies and the respective ELVs for discharge into the collector (e.g. Águas do Nordeste collector) and in the water environment.

Table 1. Typical ranges of values for pH, Temperature, COD, $BOD_5$ and Total suspended soldis (TSS) of untreated wastewater from 34 Portuguese textile companies and the respective ELVs for discharge into the collector (e.g. Águas do Nordeste collector) and in the water environment (Citeve, 2012).

| **Physicochemical Parameters** | **Range of values** | **ELVs - Discharge into collector (Águas do Noroeste)** | **ELVs - Discharge in water environment (Ordinance 423/97)** | **ELVs - Discharge in water environment (Decree-Law 236/98)** |
|---|---|---|---|---|
| pH | 4.7 - 11.8 | 5.5 - 9.5 | 5.5 - 9 | 6 – 9 |
| Temperature (ºC) | 16 - 41 | 30 | - | - |
| COD (mg/L $O_2$) | 102 - 11000 | 1 000 | 250 | 150 |
| $BOD_5$ (mg/L $O_2$) | 9 - 2580 | 500 | 100 | 40 |
| TSS (mg/L) | <3 - 2500 | 1 000 | - | 60 |
| Color | - | - | Not visible in the dilution 1:40 | Not visible in the dilution 1:20 |

### 1.1.3 Environmental impact

Color is usually the first contaminant to be recognized in textile wastewater. Even a very small amount of a synthetic dye in water (< 1 ppm) is highly visible and affects its aesthetic quality and transparency (Carmen and Daniela, 2010). The accumulation of color in aqueous ecosystems leads to

a reduction in sunlight penetration, which in turn decreases photosynthetic activity, dissolved oxygen concentration and water quality, disturbing biological activity in aquatic life (Saratale et al. 2011; Malik et al. 2014).

The organic components present in textile wastewater are found to undergo chemical and biological changes that result in the removal of oxygen from water (Masupha, 2007). Some of the inorganic chemicals, like hydrochloric acid, sodium hypochlorite, sodium hydroxide are poisonous to marine life (Blomqvist, 1996; Masupha, 2007). The suspended solids concentration in the effluents play an important role in affecting the environment as they combine with oily layers and interfere with the oxygen transfer mechanism in the air-water interface. Heavy metals, such as Cr, As, Cu and Zn, can also be toxic to aquatic life (Ghaly et al., 2013).

The overwhelming majority of synthetic dyes currently used are azo derivatives, due to their ease of synthesis, stability and variety of colors (Lourenço et al., 2015). Azo dyes account for 60-70% of all dyes produced annually in the world (dos Santos et al., 2007). These dyes are characterized by the presence of one or more azo groups (–N=N–), linked to phenyl and naphthyl radicals, which are usually substituted with some combinations of functional groups including amino ($–NH_2$), chlorine (–Cl), hydroxyl (–OH), methyl ($–CH_3$), nitro ($–NO_2$), sulphonic acid and sodium salts ($–SO_3Na$) (Ventura and Marin, 2013). Due to their xenobiotic and recalcitrant nature, they represent a long-term challenge for the different ecosystems if discharged without proper treatment. The ecosystems have natural remediation potential to modify the dyes, but not always produce non-toxic or less toxic metabolites. In fact, in certain conditions, the degradation of these compounds lead to conversion of non-toxic dyes into toxic metabolites. The ecological fate and consequences of azo dyes is a result of interactions of microbes and dyes in the background of various environmental processes (Rawat et al., 2016). These interactions are summarized in Figure 1.

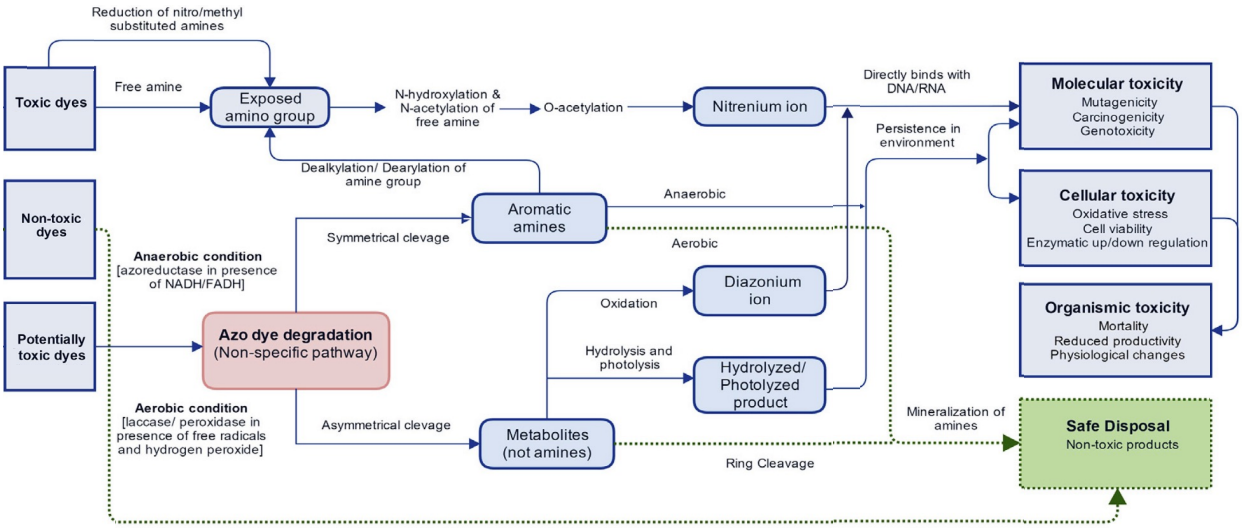


Figure 1. Schematic diagram showing complex interactions between azo dyes and environmental factors (extrinsic: oxygen, light, moisture, etc.; and intrinsic: microbial enzymes, etc.), which determine the ecological fate and consequences of these dyes. The solid lines represent pathways leading to toxic metabolites, whereas dotted lines represent pathways leading to non-toxic environmentally safe metabolites (adapted from Rawat et al. 2016).

Toxic azo dyes can directly impact the living organisms without the reduction of azo bond to yield hazardous products. In this case, the toxicity is a direct function of the low molecular weight and lipophilicity of the parent dye, which facilitate diffusion of the dye through cell membranes. Toxic dyes develop genotoxicity (mutagenicity) and carcinogenicity when free amines and N-acetylated amines undergo biochemical activation, forming nitrenium ion ($–NH^+$). This ion is able to interact with electron-rich sites in DNA molecules, causing DNA adducts, mutations and subsequent adverse effects on the cells (Pinheiro et al. 2004; Maria et al. 2011; Rawat et al. 2016).

Potentially toxic azo dyes cause toxicity after degradation in the environment. Most of these dyes do not show immediate toxicity due to the bulkiness of their structure and to the high polarity imparted by substitution with multiple sulfonic acid ($SO_3H$) groups. These properties restrict their entry through cell membranes, reducing their bioavailability. However, after degradation these dyes generate small hydrophobic metabolites, which can easily pass through cell membranes and have drastic cellular and ecological implications. These metabolites can promote oxidative genotoxicity inside mammalian bodies, cause cyto/organismic toxicity, hinder the growth of microbial communities, and trigger unscheduled DNA synthesis in organisms. The microbial actions play a key role in altering the behavior of these azo dyes. Daily and seasonal fluctuations in oxygen availability, light, moisture, and temperature determine the activity and distribution of microbes that directly affect the azo dye degradation. These factors not only differ between ecosystems, but also within ecosystems (both aquatic and terrestrial) creating microheterogeneity in the habitat, which might lead to uneven distribution of diverse toxic metabolites (Majcen et al., 2012; Rawat et al., 2016).

Therefore, treatment of textile wastewater containing azo dyes and their metabolites is necessary prior to their final discharge to the environment.

## 1.2 Conventional wastewater treatments

Various treatment techniques are in use to mitigate the contaminant levels of textile wastewaters and reduce their environmental impact. These include physicochemical and biological methods.

### 1.2.1 Physicochemical methods

**Coagulation-flocculation**

The coagulation-flocculation method has been employed for the removal of colloidal and small suspended particles (e.g. dyes, heavy metals, organic solids, oil) from textile wastewaters. Coagulation involves the addition of coagulants to destabilize particles and causing them to clump together ( Eyvaz et al. 2016). Ferrous sulfate, lime, alum, ferric sulfate and ferric chloride are some of the most commonly used coagulants (Ghaly et al., 2013). This step also comprises a rapid mixing to promote collision between the particles. Coagulation is usually followed by flocculation to increase the particle size. In the flocculation step, the particles formed at the step of coagulation are induce to form bulky floccules through the binding action of flocculants aids, such as long chain polymers and polyelectrolytes (Verma et al., 2012). This step also involves a mechanical mixing, but at a slower speed to allow maximum interaction between the particles and flocs, without destruction of those already formed (Ebeling et al., 2003). The resulting flocs can settle more easily and be removed from the effluent as sludge (Ghaly et

al., 2013). This method is successfully applied for color removal of sulfur and disperse dyes. However, acid, direct, reactive and vat dyes present very low coagulation–flocculation capacity (dos Santos et al., 2007; Saratale et al., 2011). In addition to the ineffective decolorization of some soluble dyes, these techniques demand large chemical inputs leading to the production of high volumes of polluted sludge (dos Santos et al., 2007). The cost of treating the sludge and the increasing restrictions concerning their disposal, limits the application of this method to textile wastewater treatment (Babu et al. 2007; Pereira & Alves 2012).

**Adsorption**

The adsorption process is usually applied to remove residual dissolved organic and inorganic pollutants from textile wastewaters (Eyvaz et al., 2016). In this process, when a solution containing absorbable solute comes into contact with a solid with a highly porous surface structure, liquid–solid intermolecular forces of attraction cause some of the solute molecules from the solution to be concentrated or deposited at the solid surface (Rashed, 2013). The color removal from wastewater is influenced by many physicochemical factors, such as dye/sorbent interaction, sorbent surface area, particle size, temperature, pH, and contact time. Adsorption is also related to the molecular size of the dye and to the number of sulfonic groups present in its structure. Smaller dyes have higher adsorption, whereas bigger molecules are more difficult to adsorb due to diffusion limitations (Pereira and Alves, 2012). The selection of an adsorbent is based on characteristics such as high affinity, capacity for target compounds and the possibility of adsorbent regeneration (Verma et al. 2012; Holkar et al. 2016). Activated carbon is the most commonly used adsorbent and can be very effective for many dyes. However, its high price and the difficulty in its regeneration, limits its application (Grassi et al., 2012). Furthermore, this procedure is only feasible in combination with a pre-treatment process, due to the rapid clogging of flow channels of the carbon bed caused by residual suspended solids (Babu et al., 2007). In recent years, the search for low-cost adsorbents with high pollutant-binding capacities has intensified. Materials locally available such as natural materials, agricultural and industrial wastes can be utilized as low-cost adsorbents (Rashed, 2013). However, the practical application of these adsorbents has been restricted by problems associated toh their regeneration or disposal, high sludge production and low effectiveness regarding a wide range of dyes (Saratale et al., 2011).

**Membrane Filtration**

Wastewater treatment based on membrane filtration processes, which include Microfiltration (MF), Ultrafiltration (UF), Nanofiltration (NF), Reverse Osmosis (RO) or hybridization of two or more of these membranes are normally addressed as clean and environmentally benign technologies (Dasgupta et al., 2015). NF and RO are the main processes used for the treatment of colored textile effluents. The rejection of species by NF membranes is governed mostly by steric and charge repulsion. It allows the separation of low-molecular weight organic compounds, divalent ions, large monovalent ions, hydrolyzed reactive dyes, and dyeing auxiliaries (Babu et al., 2007). Additionally, the production of a quality permeate allows the reuse of treated wastewaters in primary processes of the textile industry, such as dyeing and finishing (Dasgupta et al., 2015). NF is often used in combination with an upstream adsorption process since NF modules are extremely sensitive to fouling by colloidal material and

macromolecules (Wang et al., 2011). In turn, RO membranes have a retention rate of 90% or more for most types of ionic compounds and produce a high quality permeate. However, the use of dense polymeric membranes and the high osmotic pressure build up due to presence of high salt concentrations considerably limit the permeate flux. In order to maintain a reasonable permeate flux, higher transmembrane pressures are necessary, which increases the energy required for the separation process (Babu et al., 2007; Dasgupta et al., 2015). UF and MF have limited application in colored textile wastewater treatment, mainly because the molecular weights of most dyes present in the textile effluents are much lower than the molecular weight cut-off (MWCO) of these membranes. Nonetheless, UF membrane enables the separation of macromolecules and colloids, but the elimination of dyes is never complete (Babu et al., 2007). The water recovered through UF can be reused, but only in subsidiary processes of the textile industry. MF membranes can be used for removal of particles and colloidal dyes from exhausted dye bath and discarded rinsing bath (Wang et al., 2011). However, it permits the unconsumed auxiliary chemicals, dissolved organic pollutants and other soluble contaminants to escape with the permeate. As such, UF and MF are mostly employed as a pre-treatment step in hybrid systems so as to complement other concomitant processes, which target dyes and other soluble pollutants (Babu et al. 2007). The main drawbacks of membrane technology are the initial investment cost, potential membrane fouling, requirement of different pre-treatments depending upon the type of effluent wastewaters and production of concentrated dyebath, which further needs proper treatment before its safe disposal to the environment (Holkar et al., 2016; Verma et al., 2012).

**Advanced Oxidation processes**

Advanced oxidation processes (AOPs) are based on the generation of highly reactive species, such as the hydroxyl radical ($HO^{\bullet}$), which has a high oxidation potential and can promote the quick and non-selective degradation of a broad range of dye pollutants. Generally, $HO^{\bullet}$ radicals are generated by reactions involving oxidizing agents such as $O_3$ and $H_2O_2$ or heterogeneous catalysis, with catalysts such as $TiO_2$, $ZnO_2$, Mn and Fe in the presence (photocatalysis) or absence of an irradiation (UV) source. (dos Santos et al. 2007; Saratale et al. 2011).

Ozonation is an effective method for textile wastewater treatment due to high reactivity of $O_3$ with some azo dyes and consequent good color removal efficiencies. However, the major advantage of ozonation is that $O_3$ is used in its gaseous state and, therefore, it does not increase the volume of wastewater and residual sludge (Pereira and Alves, 2012). $O_3$ can also react directly with the dye molecules in addition to their action via $OH^{\bullet}$. In the presence of other oxidants or irradiation, the $OH^{\bullet}$ yield can be significantly improved. For example, in the so-called peroxone ($O_3/H_2O_2$) and $O_3$/ultraviolet (UV) irradiation systems (Yang and Zhao, 2015). The disadvantages of ozonation are the short half-life of $O_3$, demanding its continuous application and thereby making it a costly process; its ineffectiveness towards dispersed dyes and those insoluble in water; as well as low COD removal capacity (dos Santos et al., 2007). However, ozonation has been successfully used in combination with biological treatments, either as pre- or as a post-treatment (Solís et al., 2012).

The Fenton reaction method is relatively cheap comparing to ozonation and has high COD removal and decolorization efficiencies for both soluble and insoluble dyes. The classic Fenton reaction uses $H_2O_2$ to react with $Fe^{2+}$ at acidic pH conditions, producing $Fe^{3+}$ and $OH^{\bullet}$ according to reaction (1).

$$H_2O_2 + Fe^{2+} \rightarrow Fe^{3+} + OH^{\bullet} + OH^{-} \quad (1)$$

$$Fe^{3+} + H_2O_2 \rightarrow Fe^{2+} + HO_2^{\bullet} + H^{+} \quad (2)$$

$Fe^{2+}$can be regenerated from $Fe^{3+}$ through reaction (2), to further catalyze Fenton reaction. However, reaction (2) is much slower than reaction (1). As consequence, $Fe^{3+}$ accumulates in the solution, which precipitates as $Fe(OH)_3$ sludge flocs at typical wastewater conditions (Yang and Zhao, 2015). Consequently, the sludge flocs should be separately disposed, increasing the treatment complexity and operational costs. Furthermore, this reaction is most effective only at an acidic pH condition. As the wastewater pH in many cases is neutral or alkaline, the necessity to acidify the reaction medium limits the applicability of the process. Based on the classical Fenton treatment ($Fe^{2+}/H_2O_2$), modified process have been proposed, including the Fenton-like system ($Fe^{3+}/H_2O_2$), photo-Fenton system ($Fe_{2+}/H_2O_2$/UV) and electro-Fenton system. In the Fenton-like reaction, $Fe^{2+}$ is replaced by the lower cost $Fe^{3+}$ salts. The series of reactions in the Fenton-like system are initiated from equation (2) rather than from equation (1) in the traditional Fenton treatment. However, several studies have shown that the rate of decomposition of $H_2O_2$ and the rate of oxidation of organic solutes are much slower and more sensitive to pH using $Fe^{3+}/H_2O_2$ than $Fe^{2+}/H_2O_2$ (Jiang et al., 2010; Yang and Zhao, 2015). In the photo-Fenton reaction, UV irradiation is applied with the traditional Fenton system with the major purpose of enhancing the reduction of dissolved $Fe^{3+}$ to $Fe^{2+}$, decreasing the consumption of Fenton's reagent in the process (Goi and Trapido, 2002). Furthermore, this method can significantly enhance the decomposition of many refractory organic compounds. In the electro-Fenton reaction, either or both Fenton reagents may be generated through electrochemical methods.

Ultraviolet (UV) light has been tested in combination with $H_2O_2$ and catalysts, such as $TiO_2$, for the decoloration of azo dyes (Solís et al., 2012). In $H_2O_2$ /UV process, $OH^{\bullet}$ are yielded when water-containing $H_2O_2$ is exposed to UV light, normally in the range of 200–280 nm (dos Santos et al., 2007). The photolysis of $H_2O_2$ follows reaction (3).

$$H_2O_2 + h\upsilon \rightarrow 2HO^{\bullet} \quad (3)$$

The major advantages of the $H_2O_2$ /UV process are the low initial capital cost and the lack of undesirable residual sludge formation during or after the oxidation. More than 95% decolorization was achieved in treating reactive, basic, acid and direct dyes at pH 5, although disperse and vat dyes were only partially decolorized (dos Santos et al., 2007). Furthermore, the decomposition rate of dyes is dependent of UV light intensity, which is a disadvantage since the $H_2O_2$ /UV process requires extensive electricity consumption (Solís et al., 2012). The $TiO_2$/UV process has also shown to be effective for color removal. When UV light with appropriate energy irradiates $TiO_2$ particles, an electron from the valence band is promoted to the conduction band, leaving an electron deficiency or hole, $h\upsilon^{+}_{vb}$, in the valence band with oxidative capacity and an excess of negative charge in the conduction band, $e^{-}_{cb}$, with reductive capacity. These $h\upsilon^{+}_{vb}$ and $e^{-}_{cb}$ can further form $HO^{\bullet}$ by reacting with $OH^{-}$, $H_2O$, and $O_2$ at the surface of $TiO_2$, as represented by equations (4)-(6):

$$h\upsilon^{+}_{vb} + OH^{-} \rightarrow HO^{\bullet} \quad (4)$$

$$h\upsilon^{+}_{vb} + H_2O \rightarrow HO^{\bullet} + H^{+} \quad (5)$$

$$e^{-}_{cb} + O_2 \rightarrow O_2^{\bullet -} \quad (6)$$

In the presence of oxidants, such as $H_2O_2$ or $O_3$, additional $HO^{\bullet}$ may be yielded under the UV irradiation (Yang and Zhao, 2015). However, these methods are enormously influenced by the type of dye, dye concentration and pH (dos Santos et al., 2007).

### 1.2.2 Biological methods

The application of microorganisms for the biodegradation of azo dyes is an attractive alternative to the development of bioremediation processes for the treatment of textile wastewater. Biological methods are a cost-competitive and environmentally friendly solution; potentially yield end products that are non-toxic or have complete mineralization; produce less sludge and require less water consumption compared to physicochemical systems. Microbial decolorization can occur via biosorption on growing/living and dead microbial cells, enzymatic degradation or a combination of both (Pereira and Alves, 2012; Solís et al., 2012). The effectiveness of the decolorization techniques depends on dye class, its substituent groups and physicochemical characteristics of the effluent, such as pH, temperature, salt content and the presence of organic pollutants (Solís et al., 2012).

Several organisms can decolorize a wide range of dyes, including bacteria, filamentous fungi, yeasts, algae and plants (phytoremediation) and some of these organisms can also mineralize many azo dyes under certain environmental conditions (Saratale et al., 2011).

Filamentous fungi can degrade various complex organic pollutants, including dyes. The ability of fungi to oxidize such a range of organic compounds results from the non-specific nature of their ligninolytic enzymes, such as lignin peroxidase (LiP), manganese peroxidase (MnP) and laccase (Lac) (Saratale et al., 2011). The application of filamentous fungi in the decolorization process is an attractive alternative due to its low cost and to the possibility of total dye mineralization. Decolorization can be accomplished not only by enzymatic degradation, but also by adsorption (Solís et al., 2012). However, the application of fungi for the removal of dyes from textile wastewater has some inherent drawbacks, such as a long growth cycle and the need for nitrogen limiting conditions (Saratale et al., 2011).

Only a few studies have been done to explore the decolorization ability of yeasts and most of them are related to their biosorption capacity (Saratale et al., 2011). Yeast strains have some advantages, such as high capacity to accumulate dyes and heavy metals, fast growth, faster color removal than filamentous fungi and the ability to survive unfavorable environments. Dye biodegradation is associated to the yeast growth process and its primary metabolism and requires a carbon source. The presence of azo dyes induces the production of oxidases and reductases, such as MnP, Tyr and NADH-DCIP reductase by yeasts (Solís et al., 2012).

Algae are receiving increasing attention in the field of wastewater decolorization due to its capacity to survive in unfavorable environments. Some azo dyes exhibit high toxicity to aquatic life but do not significantly reduce algae growth (Solís et al., 2012). Furthermore, algae do not require the addition of a carbon source, making its mass cultivation less expensive. Algae obtain their energy from

sunlight and use inorganic carbon for growth. The mechanisms of algae decolorization can involve enzymatic degradation, adsorption, or both. A survey of the literature suggests that algae can degrade azo dyes through an induced form of an azoreductase, resulting in the production of aromatic amines, which can be further metabolized to simpler organic compounds or $CO_2$ (Saratale et al. 2011).

Phytoremediation is an emerging technology for the remediation of soils and groundwater contaminated with heavy metals and organic pollutants. This autotrophic system requires little nutrient input, is easy to manage and is generally approved by the public due to both its aesthetic appeal and environmental sustainability. However, large scale application of phytoremediation presently faces a few obstacles, including the level of pollutants tolerated by the plant, the bioavailable fraction of the contaminants and evapotranspiration of volatile organic pollutants, as well as the large areas required to implant the treatment (Saratale et al., 2011).

Bacteria are the most frequently applied microorganisms for the bioremediation of textile effluents. These microorganisms are generally easy to cultivate, grow rapidly under aerobic or anaerobic conditions and can be facultative (Solís et al., 2012). Furthermore, bacteria can be adapted to survive in extreme conditions of salinity and temperature and express different types of oxidoreductases. Under anaerobic conditions, bacteria reduce azo dyes to give colorless aromatic amines. The bacterial enzymes involved in this process are usually non-specific azoreductases. Azo dyes are generally recalcitrant under aerobic conditions because the presence of oxygen usually inhibits azo bond reduction activity. Some selected aerobic bacterial strains possess the ability to reduce the azo linkage by oxygen-insensitive or aerobic azoreductases. However, contrary to the unspecific mechanism of azo dye bacterial reduction under anaerobic conditions, aerobic bacteria usually need to be specifically adapted to achieve a significant reductive process. Bacteria also possess oxidative enzymes including laccases, tyrosinases and dye decolorizing peroxidases (DyPs). Bacterial laccases are the most common oxidases involved in the degradation and mineralization of azo dyes (Solís et al., 2012). Laccases have been largely isolated and characterized from fungi (Pereira et al., 2009; Saratale et al., 2011) However, fungal laccases are sensitive to high pH and chloride. These disadvantages make bacterial laccases better alternatives because they are highly active and much more stable at high temperatures, pH and salt concentrations.

Treatment systems composed of mixed microbial populations achieve a high degree of dye biodegradation and mineralization due to the synergistic metabolic activities of the microbial community. In a microbial consortium, the individual strains can attack the dye molecule at different positions or utilize metabolites produced by the co-existing strains for further decomposition (Saratale et al., 2011). Microbial consortia can be constructed with bacteria, fungi, or a mixture of both (Solís et al., 2012). However, mixed cultures only provide an average macroscopic view of what is happening in the system and the results are not easily reproduced. For these reasons, a substantial amount of research about color removal has been carried out using single bacterial cultures. The use of a pure culture system ensures that data are reproducible and that the interpretation of experimental observations is easier (Pearce et al., 2003).

**Anaerobic mechanisms of microbial color removal**

The azo bond (–N=N–) reduction is regarded as the rate-limiting step in the overall dye degradation process and is most common achieved under anaerobic conditions (Brigé et al., 2008). The anaerobic azo bond cleavage involves a transfer of four electrons (reducing equivalents), which proceeds through two stages at the azo linkage, as described by equations (7) and (8).

$$R_1–N=N–R_2 + 2e^- + 2H^+ \rightarrow R_1–HN–NH–R_2 \text{ (Hydroazo intermediate)} \quad (7)$$

$$R_1–HN–NH–R_2 + + 2e^- + 2H^+ \rightarrow R_1–NH_2 + R_2–NH_2 \text{ (Colorless aromatic amines)} \quad (8)$$

In each stage, two electrons are transferred to the azo dye ($R_1$–N=N–$R_2$), which acts as a final electron acceptor, resulting in color removal with formation of aromatic amines.

The exact mechanism of anaerobic azo dye reduction is still a subject of investigation. In earlier studies with anaerobic bacteria, it was repeatedly suggested that reduced flavins generated by cytosolic flavin-dependent reductases were responsible for the unspecific reduction of azo dyes. Reduced flavins act as an electron shuttle from nicotinamide adenine dinucleotide phosphate (NADPH)-dependent flavoproteins to azo dye as electron acceptor (dos Santos et al., 2007). However, studies with cell extracts showed much higher rates for the anaerobic reduction of azo dyes than the preparations of resting cells. This was explained by the low permeability of the cell membranes for the highly polar sulfonated azo compounds. In addition, Russ et al. (2000) also suggest that bacterial membranes are almost impermeable to flavin-containing cofactors and, therefore, restrict the transfer of reduction equivalents by flavins from the cytoplasm to the sulfonated azo dyes. Therefore, it appears reasonable that, in vivo, intracellular enzymes like flavin reductases are of little importance for the reduction of sulfonated azo compounds (Pandey et al., 2007; Stolz, 2001).

A different mechanism for the reduction of azo dyes that does not require transport of the azo dyes or reduced flavins through the cell membranes has been suggested. This mechanism involves the electron transport-linked reduction of azo dyes in the extracellular environment. To achieve this, the bacteria must establish a link between their intracellular electron transport systems and the sulfonated azo dye molecules. For such a link to be established, the electron transport components must be localized in the outer membrane (OM) of the bacterial cells. Thus, they can make direct contact with either the azo dye substrate or a redox mediator at the cell surface. Redox mediators can act as electron shuttles between the azo dye and an NADH-dependent azo reductase that is in the OM. Such mediators are either formed during the aerobic metabolism of certain substrates by the bacteria or be added externally (Pearce et al., 2003). Flavin-based compounds like FAD, FMN and riboflavin, as well as quinone-based compounds like anthraquinone-2-sulfonate (AQS), anthraquinone-2,6-disulfonate (AQDS) and lawsone, have been extensively reported as redox mediators during azo dye reduction (dos Santos et al., 2007). Reductive decolorization of azo dyes in the presence of redox mediators occurs in two distinct steps, the first step being a non-specific enzymatic mediator reduction, and the second step being a chemical re-oxidation of the mediator by the azo dyes (Figure 2). It is also possible that this non-enzymatic reaction works in conjunction with a direct enzymatic reaction involving an azoreductase that is synthesized throughout the cytoplasm and secreted without accumulation inside the cell (Pearce et al., 2003).

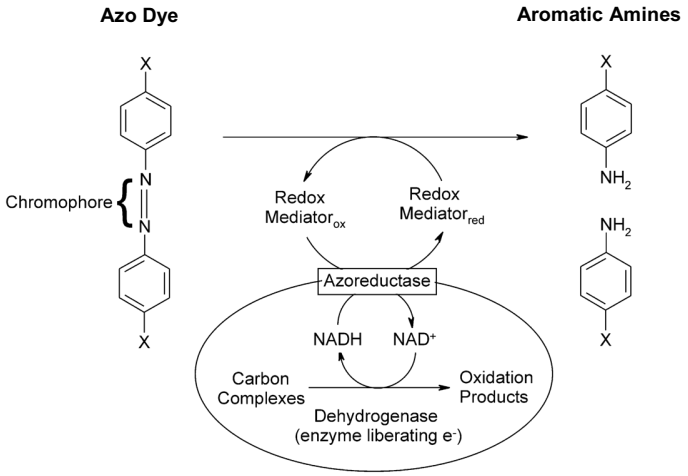


Figure 2. Proposed mechanism for reduction of azo dyes by bacterial cells. (Adapted from Keck et al. (1997)). Redox mediators are reduced intracellularly. Then, these reduced mediator compounds reduce the extracellular azo group in a purely chemical reaction.

Recent investigations on bacterial azo reduction have led to a new recognition that azo reduction by certain bacteria is related to the electron transport chain on the cellular membrane. Brigé et al. (2008) demonstrated that decolorization is an extracellular reduction process requiring a multicomponent electron transfer pathway, which comprises cytoplasmic membrane (CM), periplasmic and outer membrane (OM) components. A model of the multicomponent pathway is given in Figure 3.

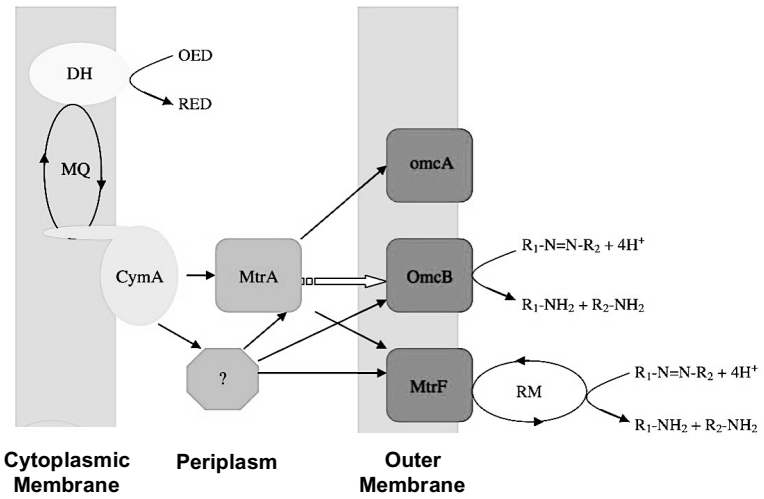


Figure 3. Model of the decolorization mechanism *S. oneidensis*. The arrows indicate the possible routes of electron transfer to the extracellular dye resulting in colorless reduction products. The pathway starts when the electron donor is oxidized from the reduced type (RED) into oxidized one (OED) in the cytoplasmic membrane, electrons enter the menaquinone (MQ) pool via membrane-bound dehydrogenase (DH) from which they are transferred to CymA. The white arrow represents the principal pathway for the downstream electron transport of CymA, where MtrA and OmcB proteins play the key roles. The alternative routes of electron flow are represented by (?). The MtrF, OmcA, and OmcB proteins work as terminal azoreductases, which can interact with azo dyes directly or indirectly through the redox mediators (RM). (Adapted from Brigé et al. (2008)).

When the electron donor is oxidized in the CM, electrons enter the menaquinones (MQ)/quinol pool via membrane-bound dehydrogenase from which they are transferred to CymA (tetraheme quinol dehydrogenase). The MtrA (periplasmic protein c-type cytochrome) and OmcB (decaheme c-type cytochrome in the OM) proteins are the main constituents of the pathway downstream of CymA. However, alternative routes of electron flow to the dyes via a network of cytochromes *c* appear to be present. Given their location in the OM, the multiheme cytochromes MtrF, OmcA and OmcB fulfil a function as terminal dye reductase, which can interact with azo dyes directly or through the redox mediators leading to the reduction (Brigé et al., 2008; Hong and Gu, 2010).

In addition, azo dye decolorization can further occur from purely chemical reactions with inorganic compounds such as sulfide and ferrous ion that are formed as end products of metabolic reactions, under anaerobic conditions. $H_2S$ generation by sulfate reduction has been proven to reduce azo dyes extracellularly (Hong and Gu, 2010; Pandey et al., 2007). However, according to some authors the contribution of this reaction to the anaerobic decolorization *in vivo* appears to be inconsistent (dos Santos et al., 2007).

**Aerobic mechanisms of microbial color removal**

Azo dyes are generally resistant to aerobic degradation (dos Santos et al., 2007; Pearce et al., 2003; Solís et al., 2012). The presence of oxygen usually inhibits the reduction of azo bond probably because oxygen is a more effective electron acceptor and, therefore, having more preference for reducing equivalents than the azo dye (dos Santos et al 2007; Solis et al 2012). Furthermore, azo dyes are electron-deficient xenobiotic components because of their azo linkage and, in many cases, sulfonic or other electron-withdrawing groups, which generate an electron deficiency and make the dye quite recalcitrant to degradation by microorganisms (dos Santos et al., 2007; Solís et al., 2012).

However, azo dye reduction processes have been described for some aerobic bacteria, which can grow with (rather simple) azo compounds (Stolz, 2001). These microorganisms synthesize specific azoreductases, which reductively cleave the azo group in the presence of molecular oxygen. However, aerobic bacteria must be specifically adapted to be significant in the reductive process. Nonetheless, this adaptation involves long-term aerobic growth in continuous pure culture in the presence of very simple azo compounds (Pearce et al., 2003).

Azo dyes can also be oxidized under aerobic conditions without the cleavage of the azo bond through a highly non-specific free radical mechanism, forming phenolic type compounds. This mechanism avoids the formation of the toxic aromatic amines arising under reductive conditions (Pearce et al., 2003; Pereira and Alves, 2012). The aerobic oxidation of azo dyes and/or metabolites from reductive metabolism (e.g aromatic amines) can be catalyzed by peroxidases and phenoloxidases, such as manganese peroxidase (MnP), lignin peroxidase (LiP), laccase (Lac), tyrosinase (Tyr) and dye-decolorizing peroxidases. These oxidases have been found in filamentous fungi, bacteria and yeast.

Peroxidases, including LiP and MnP, are hemoproteins that catalyze the oxidation of phenols, biphenols, anilines, benzidines and related hetereoaromatic compounds, for which $H_2O_2$ is the final electron acceptor. The mechanism of azo dye degradation by LiP involves two successive one-electron oxidations in the phenolic ring by the $H_2O_2$-oxidized forms of LiP. The resulting carbonium undergoes nucleophilic attack by water, leading to the formation of a phenyldiazene and the corresponding quinone.

The phenyldiazine is oxidized by $O_2$ to a phenyl radical and the azo linkage is eliminated as $N_2$. The phenyl radical abstracts an hydrogen radical from its surroundings to yield stable aromatic compounds. (dos Santos et al., 2007; Solís et al., 2012) LiP has been used to mineralize a variety of recalcitrant aromatic compounds, including synthetic dyes (Saratale et al., 2011). Although LiP is able to oxidize both phenolic and non-phenolic aromatic compounds, MnP only oxidizes phenolic compounds (dos Santos et al., 2007). MnP mechanism differs from that of LiP in using $Mn^{2+}$ as a mediator. The catalytic cycle of MnP proceeds through an initial oxidation by $H_2O_2$ to an intermediary that promotes the oxidation of $Mn^{2+}$ to $Mn^{3+}$, which is chelated by organic acids. The $Mn^{3+}$- organic acid complex formed can then acts as an active oxidant of azo dyes (Solís et al., 2012). Recently, a new family of microbial peroxidases, known as dye decolorizing peroxidases (DyPs), have demonstrated successful degradation of synthetic dyes, including azo dyes. The physiological function of these enzymes is at present unclear, but there are increasing evidences of their involvement in the degradation of lignin. (Singh, 2014)

Phenoloxidases, including Lac and Tyr, are copper containing enzymes that catalyze the oxidation of several aromatic and inorganic substances with the concomitant reduction of oxygen to water. According to the mechanism proposed by Pereira et al. 2009, CotA-Lac (bacterial Lac) oxidizes, in a single electron transfer reaction, a hydroxyl group of the azo dye, generating the phenoxyl radical, that will be sequentially oxidized to carbonium ion. The water nucleophilic attack on the phenolic carbonium, bearing the azo linkage, followed by N–C bond cleavage, produces phenyldiazene and the corresponding quinone. The phenyldiazene can form a radical and then, a benzene radical, upon loss of a nitrogen molecule. This benzene radical can undergo hydrogen radical addition or get involved in further coupling reactions. The free radicals resulting from the biotransformation process have a high reactivity and all species can participate in coupling reactions with intact dye and/or intermediate product molecules (Pereira et al., 2009). These enzymes have potential to be used in bioremediation due lack of requirement for cofactors and to the use of readily available $O_2$ as an electron acceptor, while peroxidases require the addition of $H_2O_2$ to the reaction medium (Solís et al., 2012).

**Aromatic amine mineralization**

The decolorization of azo dyes can be accomplished through anaerobic azo bond cleavage, whereas partial or complete mineralization of the corresponding aromatic amines is an almost exclusively aerobic process (Lourenço et al., 2003). Despite the notable success in the anaerobic decolorization of azo dyes, studies regarding the fate of the breakdown aromatic amines under aerobic conditions are scarce and do not reveal the underlying mechanism. However, the involvement of specific aerobic microbial populations capable of metabolizing such compounds has been suggested (Franca et al., 2015; Van Der Zee and Villaverde, 2005).

**Combination of Anaerobic-Aerobic Processes**

A wastewater treatment system in which anaerobic and aerobic conditions are combined is the most logical strategy for effective decolorization and mineralization of azo dyes (Lourenço et al., 2003; Van Der Zee and Villaverde, 2005)

The simplest approach for the anaerobic–aerobic treatment is the use of aerated stabilization

ponds, aerated and non-aerated lagoons, as well as natural and artificial wetland systems. Aerobic treatment occurs in the upper part of these systems, while anaerobic treatment occurs at the bottom end. However, these systems usually comprise large ponds connected in series and are frequently characterized by long hydraulic retention time (HRT), low organic loading rate (OLR), as well as vast area of land. These disadvantages can be overcome using high rate bioreactors.

In recent years, substantial attention has been paid towards the more compact high-rate bioreactors with integrated anaerobic–aerobic systems for wastewater treatment to meet the strict constraints with respect to space, odor, view, and biosolids production. The combination of aerobic and anaerobic degradation pathways in a single reactor can enhance the overall degradation efficiency, are cost effective, efficient and have smaller footprints as compared to the aforementioned anaerobic–aerobic systems. Essentially, there are three types of integrated anaerobic–aerobic bioreactors. These are integrated bioreactors with physical separation of the anaerobic and aerobic zones; Sequencing Batch Reactors (SBR) based on temporal separation of the anaerobic and the aerobic phases; and combined anaerobic–aerobic culture systems based on the principle of limited oxygen diffusion in microbial biofilms.

**SBR systems using the conventional flocculent activated sludge (AS)**

The activated sludge (AS) process is commonly used in aerobic wastewater treatment. The conventional AS system consists of two basic units: a bioreactor, in which a flocculent suspension of a mixed microbial population responsible for treatment is aerated and a secondary settling tank for solid-liquid separation. An essential feature of the process is recirculation of part of the solids removed from the solid-liquid separation unit back to the aeration unit to maintain a high concentration of microorganisms in the aeration tank (Chan et al., 2009a).

The SBR is an improved version of the conventional fill and draw AS system that does not require the secondary settling tank and the recirculation of sludge, i.e. the different treatment stages take place in the same tank. These systems consist of five discrete sequential phases, namely fill, reaction, settle, discharge and idle in a cyclic operation with aeration during the reaction period to oxidize the organic matter and nitrify the ammonium–nitrogen of wastewater. Recently, SBR systems have been modified by adjusting the steps in the reaction period to provide anaerobic and aerobic phases in certain number and sequence for biological nutrient (N and P) removal. The staged anaerobic–aerobic SBR systems with flocculent activated sludge have been largely tested for textile wastewater treatment with efficient color and COD removal. However, intrinsic operational features of this technology, such as poor settling properties of the flocculent sludge, compromise the treatment efficiency and lead to large footprint requirements (Giesen et al., 2013; Kreuk and van Loosdrecht, 2004; Lourenço et al., 2015).

## 1.3 Aerobic granular sludge (AGS) technology

### 1.3.1 Definition

Considering the environmental problems raised by textile industry wastewater and the limitations of the treatment processes currently used, SBR systems using the novel aerobic granular sludge (AGS) technology have been proposed as an effective alternative to the conventional flocculent AS (Lourenço et al., 2015). The formation and use of AGS in SBR began to be reported in the end of the 1990s (Beun et al., 1999) and has recently been scale-up and implemented with success in industrial and municipal WWTPs with low investment costs and significant reductions in footprint and energy (Giesen et al. 2013; Pronk, de Kreuk, et al. 2015).

Aerobic granules are compact and dense self-aggregated microorganism clusters embedded in extracellular polymeric substances (EPS) formed under specific SBR operation conditions (Quan et al., 2015). They have a well-defined appearance and are visible as separate entities (Liu and Tay, 2004). The definition of AGS was only made during the first AGS workshop, in 2004:

*"Granules making up aerobic granular activated sludge are to be understood as aggregates of microbial origin, which do not coagulate under reduced hydrodynamic shear, and which settle significantly faster than activated sludge flocs."*

In the second AGS workshop in 2006, a further extension of the definition was discussed (Kreuk et al., 2007):

- Speaking of aerobic granular activated sludge implies that aerobic granules need to contain active microorganisms. The microbial population in AGS is expected to be similar to that of activated sludge, thus there is no need to describe specific groups of microorganisms in the definition. Furthermore, this part implies that no carrier material is involved or added;
- Flocculent activated sludge tends to coagulate when it settles, while AGS does not coagulate, each granule settling as a separate unit. AGS settles significantly faster than activated sludge flocs. This means that $SVI_5$ (SVI after 5 min of settling) in combination with $SVI_{30}$ should be used for characterizing the settleability of AGS. The difference between the $SVI_5$ and $SVI_{30}$ values gives an excellent indication about granule formation and the extent of thickening after settling;
- The minimum granule size was set to 0.2mm. This limit could be adjusted per case/granule type, as long as the other demands of the definition hold;
- Sieving is considered a proper method to harvest granules from activated sludge tanks or from aerobic granule reactors.

When an aggregate fulfils all characteristics described above, it can be called an aerobic granule.

In addition to the general advantages of the staged SBR technology, AGS systems present several unique attributes: excellent settling properties, allowing shorter settling times for good solid–liquid separation and requiring lower construction area; good biomass retention, allowing higher concentration

in the SBR and consequently lower reaction time and/or reactor volume; ability to withstand toxicity and high organic loading rates (Adav et al., 2008); aerobic and anoxic/anaerobic zones within the granules, allowing organic matter, nitrogen and phosphorus removal in the same system (Pronk et al., 2015b); maintenance of stability during a storage or starvation period of weeks or months (Gao et al., 2011). These particular characteristics make this compact technology suitable for the treatment of the highly variable textile wastewaters (Lourenço et al., 2015).

### 1.3.2 Aerobic granulation

The formation of AGS is a gradual process involving the progression from seed flocculent sludge to compact aggregates, further to granular sludge and finally to mature granules (J. Tay et al., 2001). Aerobic granulation occurs mostly in SBR systems applying short settling times, sufficiently high shear stress and a feast–famine regime (de Kreuk and van Loosdrecht, 2004).

#### Settling time

The sludge settling time acts as a major hydraulic selection pressure on the microbial community. A short settling time promotes the growth of fast-settling microorganisms and the washout of flocculent sludge with poor settling properties (Adav et al., 2008; Gao et al., 2011; Qin et al., 2004). It has been reported that AGS is successfully cultivated and becomes dominant in SBR operated at a sludge settling time of 5 min (Qin et al., 2004). In addition, short settling times select the cells with a higher surface hydrophobicity and stimulate the production of EPS in the sludge (Gao et al., 2011; Liu and Tay, 2004; Qin et al., 2004).

#### Hydrodynamic shear force

The hydrodynamic shear force exerted on AGS is an important factor in the formation and structure of the granules. The shear force is mainly generated by aeration that can be described by the upflow air velocity in SBR (Liu et al., 2005). Previous research showed that aerobic granules can be formed only above a threshold value of superficial upflow air velocity (1.2 cm $s^{-1}$) in SBR. Under low superficial air velocity (0.6-1.2 cm $s^{-1}$), small granules are formed with massive growth of filamentous bacteria (J. H. Tay et al., 2001; Zhu et al., 2013). A higher hydrodynamic shear force causes the detachment of filamentous outgrowth from the surface of the granules and promotes the formation of smooth and compact granular structures (Adav et al., 2008; Beun et al., 1999). In addition, the high shear force also stimulates the production of EPS and improves the hydrophobicity of cells, which can contribute to the compact and strong structure of aerobic granules (Gao et al., 2011; Liu and Tay, 2004; Zhu et al., 2013). However, when the superficial air velocity is too high, the granules are subjected to disintegration. (J. H. Tay et al., 2001; Zhu et al., 2013).

#### Feast – famine regime and feeding strategies

The formation of stable and compact AGS through the selection of slow growing bacteria is achieved by applying a feast - famine regime (de Kreuk and van Loosdrecht, 2004; Pronk et al., 2015a). The feast phase corresponds to the period in which abundant external substrates are available for growth and storage, while the famine phase is the period in which the organisms use their internally

stored substrates. Thus, short feeding periods must be selected to create feast and famine phases (Beun et al., 2002; de Kreuk and van Loosdrecht, 2004).

In an anaerobic feeding strategy (Figure 4), all easily biodegradable substrates are taken up by phosphate accumulating organisms (PAO) or glycogen accumulating organisms (GAO) and are converted into storage polymers during the feast phase. The substrates are in this way stored in a larger fraction of the granule volume. In a subsequent aerobic period, these storage polymers are used for growth throughout the granule at a relatively slow rate (de Kreuk and van Loosdrecht, 2004). While no oxygen is present in the deeper regions of the granules, the stored polymers can be oxidized by other electron acceptors such as nitrite and nitrate. These are produced by nitrification on the aerobic outer layer of the granules. Therefore, an anaerobic feeding strategy not only selects for stable granules, but also ensures optimal phosphate and nitrogen removal (Pronk et al., 2015a; Winkler et al., 2013; Xavier et al., 2007).

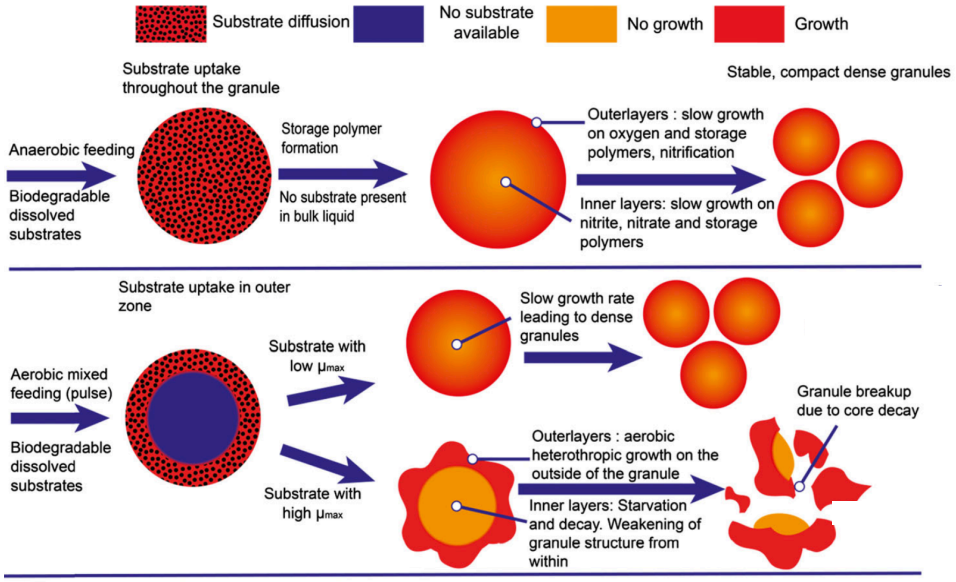


Figure 4. Effect of different SBR feeding regimes on AGS formation. On top is represented the anaerobic feeding strategy with biodegradable dissolved substrates and their impact on AGS morphology; at the bottom is represented the aerobic feeding strategy with biodegradable dissolved substrates and their impact on AGS morphology. (Adapted from Pronk et al. (2015)).

In an aerobic feeding strategy (Figure 4), the substrates are used for simultaneous growth and formation of storage polymers, mainly limited to the outer layers of the granules, while the inner regions are deprived of oxygen. The fast consumption of easily biodegradable substrates in the presence of oxygen on the outside fraction of the granules leads to filamentous outgrowth. Consequently, an increased hydrodynamic shear force is needed to ensure smooth and stable granulation (Beun et al., 1999).

Granules formed under this strategy are more prone to breaking under shear stress since the inner regions are inactive and will eventually decay and weaken the granule. This will result in unstable granulation and poor settling characteristics combined with higher suspended solids (flocs and loose cells) in the liquid after fast settling. Also, the nitrification and phosphorus removal potential is decreased. Nonetheless, some substrates lead to good granulation even if they are converted aerobically. They are converted with oxygen by relatively slow growing bacteria, which leads to a denser AGS formation

(Figure 4). In AGS systems, substrates that induce slow growth aerobically are therefore generally expected to lead to stable granulation.

### 1.3.3 Morphology and size

The morphology of AGS is completely different from that of flocculent activated sludge. Compared to the loose, fluffy, and irregular conventional activated sludge, AGS is known to have a dense and compact structure with a regular, smooth and normally spherical shape and a well-defined outer surface (Liu and Tay, 2004).

The granule size is an important parameter that may influence the biological composition of the granule as well as its physical characteristics, such as SVI, settling velocity and granule strength (Muda et al., 2013; Toh et al., 2003). The size of the granule is a net result of the balance between growth and abrasive detachment due to the shear force in SBR (Liu and Tay, 2004; Verawaty et al., 2013). Verawaty et al. (2013) demonstrated that a certain critical granule size exists for particular process operating conditions, including reactor geometry, wastewater characteristics, settling speed, shear forces, feed mode, mixing and aeration. Theses authors suggested that granules larger than the critical size would be more prone to undergo breakage or attrition, such that size reduction outweighs growth, and these granules decrease down to the critical size. Conversely, for granules smaller than the critical size, growth outweighs size reduction and the net result is an increase in granule size up to the critical size. The overall effect is a steady-state granule size distribution around the critical size. In the study of Toh et al. (2003) granules with smaller size, i.e. below 2–3 mm in diameter, appeared to be more compact, whereas granules of larger size ranges presented a loose architectural assembly. Beyond the size of 4 mm in diameter, certain detrimental effects were inflicted on granules, causing severe problems in the operation of the AGS SBR system. In view of the biological viability, the maximal size range would be less than 1 mm in diameter. These authors observed that for granules in the 1–4 mm diameter range, the nutrient availability in their inner region was limited as consequence of limitations in diffusion and mass transport, whereby certain starved bacterial cells started to consume EPS to sustain their growth. Additionally, their metabolic products, such as inhibitors, hydrolytic exoenzymes and toxic substances, also accumulated in the inner region, affecting the EPS matrix and biomass growth. This phenomenon was responsible for the increasing number of cavities spotted in the core region of the aerobic granules. It also accounted for the fact that granule biomass density was more susceptible to size increment rather than total density. Nonetheless, beyond the 4 mm in diameter, the granules presented peculiar high values of biomass and total density. The increment in diameter and the deterioration of the EPS matrix caused the fragmentation of the outer layer of the granules, forming new “micro passages” that penetrated into the inner regions. These new passages allowed the diffusion and mass transport of both substrates and products, re-establishing the growth of certain microflora. Nonetheless, the increase of solids content and density had a positive influence on the settling velocity, while the deterioration of the inner and outer structure had negative effects on this property. Toh et al. (2003) also reported that granules with smaller size-ranges presented lower SVI values. Smaller granules were more irregular in shape and could pack more effectively in the reactor, leaving no gaps. Granules with a bigger size were more spherical in shape and exhibited voluminous packing (Toh et al., 2003). However, for a large-scale

reactor operating under high organic loadings, in order to maintain this small size range (<1mm), a very high shear force would be necessary, which is unpractical and costly. Consequently, Toh et al. 2003 suggested that the optimal granule size-range for large-scale SBR operation is 1–3 mm in diameter.

### 1.3.4 Granule strength

Aerobic granules have enough physical strength to maintain the stability of their granular form and structure during bioreactor operation (Gao et al., 2011). The granule strength is defined as the resistance to attrition and/or breaking by a mechanical force or the hydrodynamic shear stress (Nor-Anuar et al., 2012).The physical strength of aerobic granules has been examined indirectly by measuring the integrity coefficient (IC) as proposed by Tay et al. (2002). This parameter is determined by measuring the weight ratio of the residual granules after 5min of shaking at 200 rpm on a platform shaker versus the total weight of the granular sludge. The higher the IC value, the higher the strength and ability of the granules to remain as high structurally intact granules during the aeration phase that caused the shear force (Muda et al., 2010). Although the IC is an indirect measurement, it provides an overall and practical indication of the shear resistance of the sludge particles in a dynamic fluid condition (Tay et al., 2002).

### 1.3.5 Granule porosity

Liu and Tay (2004) reported that channels and pores of aerobic granules penetrated to a depth of 900 μm below their surface. The porosity peaked at depths of 300 to 500 μm from the granule surface (Liu and Tay, 2004). The pore size distribution is closely related to the substrate and metabolite transport throughout the granules. Consequently, their pore size distribution and porosity will have a significant influence on the fraction of active bacteria and bioactivity of the granules (Zheng and Yu, 2007).

Confocal laser scanning microscopy together with specific flourochromes has been used to evaluate the porosity profiles in granules (Tay et al., 2003). However, such analysis only provides qualitative information (Zheng and Yu, 2007). Zheng and Yu (2007) showed that size-exclusion chromatography can be adequately and effectively applied for determining the porosities and internal pore size distribution of aerobic granules. Based on this analysis, it has been found that the porosity of aerobic granules decreased with the increasing granule diameter. For the small-size granules with a diameter of 0.2–0.6 mm, molecules greater than 137,000 Da could not penetrate the pores, while the exclusion limits of the middle-size granules with a diameter of 0.6–0.9 mm and of large-size ones with a diameter of 0.9–1.5 mm was 76,000 and 29,000 Da, respectively. The EPS of the granules might clog the pores and could be responsible for the reduced porosity (Gao et al., 2011; Zheng and Yu, 2007).

### 1.3.6 Cell surface hydrophobicity

Cell surface hydrophobicity is an important affinity force in cell self-immobilization processes (Liu et al., 2003b). According to the thermodynamic theory, the increase in the cell hydrophobicity can cause a corresponding decrease of the excess Gibbs energy in the cell, and thereby promote cell-to-cell interaction, leading to self-aggregation of bacteria out of the suspending liquid. Thus, high cell hydrophobicity facilitates and strengthens cell-to-cell interaction to form a more compact microbial

structure (Qin et al., 2004).

Several analytical methods have been used to characterize the cell hydrophobicity of AGS, including contact angle measurements and bacterial adherence to hydrocarbons (Gao et al., 2011; Zhang et al., 2007; Zheng et al., 2005). The cell surface hydrophobicity of AGS is much higher than that of flocculent sludge. Mean contact angle values of 35° and 46.3° have been reported for flocculent sludge and AGS, respectively (Zheng et al., 2005). The cell surface hydrophobicity, in terms of adherence to hydrocarbons, was reported to increase from 43.2% to about 78.2% as the sludge changed from flocculent to granular form in a SBR (Zhang et al., 2007). Qin et al. (2004) also found that the cell surface hydrophobicity of granules was increased by 2.5 to 3.5 times as compared to that of flocculent sludge.

Cell surface hydrophobicity is influenced by the structure of the granules and the bioreactor operating conditions (Gao et al., 2011). High shear force resulted in a significant increase in the cell surface hydrophobicity (Adav et al., 2008; Liu and Tay, 2004; Qin et al., 2004). The cell hydrophobicity was also increased as the settling time and the cycle time were shortened (Qin et al., 2004). In addition, Toh et al. (2003) observed that the specific surface hydrophobicity increased with the increase of granule diameter.

### 1.3.7 Settling and biomass retention capacity

The settling ability of AGS is an important characteristic which directly relates to the biomass retention capacity and to the efficiency of solid–liquid separation in the reactor. The SVI is a parameter of sludge settling ability. The SVI of AGS can be lower than 50 mL/g, which is much lower than that of conventional activated sludge (above 150 mL/g) (Qin et al., 2004; J. Tay et al., 2001). High settling velocities allow shorter settling times and the use of relatively high hydraulic loads to the reactor without concerns about biomass washout. Consequently, AGS promotes a high biomass retention in the reactors, which can improve their performance (Liu and Tay, 2004). Additionally, AGS can be settled in a more compact construction and dispensing with the traditional settlers, necessary in the activated sludge process (Chan et al., 2009b; Liu and Tay, 2004; Xavier et al., 2007).

### 1.3.8 Microbial structure and diversity

AGS structure can provide different ecological niches due to substrate gradients, shear stress phenomena, as well as protozoa grazing on the outer layers of the granules (Winkler et al., 2012). Granules can harbor slow-growing organisms due to higher retention time for the biomass located in the deeper parts of the granule (Winkler et al., 2013). In addition, there is also segregation of biomass over the sludge bed column in SBR. Granules with larger radius or higher specific density will develop more rapidly settling characteristics, are therefore often at the bottom of the sludge bed. Consequently, the microbial population at the bottom of the reactor will be different from that present at the top (Winkler et al., 2011).

The aerobic granule structure is characterized by the presence of an aerobic outer layer and an anaerobic/anoxic core. This structure enables the co-existence of aerobic nitrifying organisms in the outer layers and of phosphate accumulating organisms (PAO), glycogen accumulating organisms

(GAO), denitrifying bacteria, as well as (facultative) anaerobic organisms towards the center (Figure 5) (Winkler et al., 2012; Xavier et al., 2007). It has been reported that aerobic nitrifying organisms are mainly at a depth of 70 to 100 µm from the granule surface, while anaerobic organisms are at a depth of 800 to 900 µm from the granule surface. Toh et al. (2003) noted a layer of dead microbial cells at a depth of 800 to 1000 µm (Adav et al., 2008; Liu and Tay, 2004; Toh et al., 2003) Due to this microbial structure, AGS allows the simultaneous removal of phosphorus, nitrogen and organic matter in the same system .

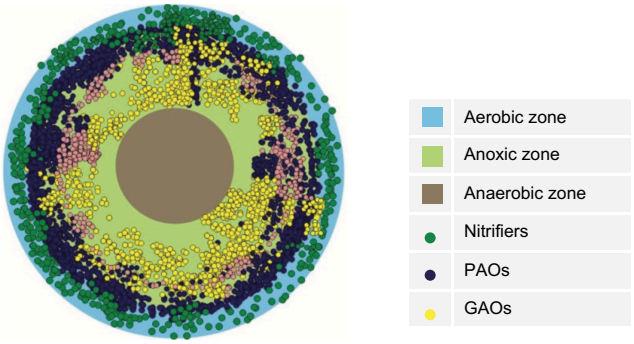


Figure 5. Typical structure of aerobic granules with nitrifiers in the aerobic zone followed by phosphate accumulating organisms (PAOs) and glycogen accumulating organisms (GAOs) and denitrifies in the up following anoxic zone (adapted from Windler et al. (2013)).

### 1.3.9 Extracellular polymeric substances (EPS)

Extracellular polymeric substances (EPS) are metabolic products accumulating on the surface of bacterial cells (Adav et al., 2008). The major components of EPS are polysaccharides (PS) and proteins (PN). Humic substances, lipids, nucleic acids, uronic acids and some inorganic components have also been found in EPS matrices (Gao et al., 2011; Sheng et al., 2010). In AGS systems, polymer synthesis is influenced by the type of reactors used, wastewater composition and its loading rate, hydraulic retention time, hydrodynamic shear force, settling time and periodical feast-famine regime in SBR, culture temperature, among other variables (Chen et al., 2010). EPS can be subdivided into bound EPS and soluble EPS (Jang et al., 2007). Bound EPS are closely bound to cells, while soluble EPS are weakly bound or dissolved into the solution. Generally, these two types of EPS can be separated by centrifugation, with those remaining in the supernatant being soluble EPS and those forming microbial pellets being bound EPS (Sheng et al., 2010). The structure of bound EPS is generally depicted by a dynamic two-layer model (Figure 6): 1) tightly bound EPS (TB-EPS) forms the inner layer; 2) loosely bound EPS (LB-EPS) diffuses in outer layer. The LB-EPS have a highly hydrated matrix, which tend to form a dispersible and loose slime layer.

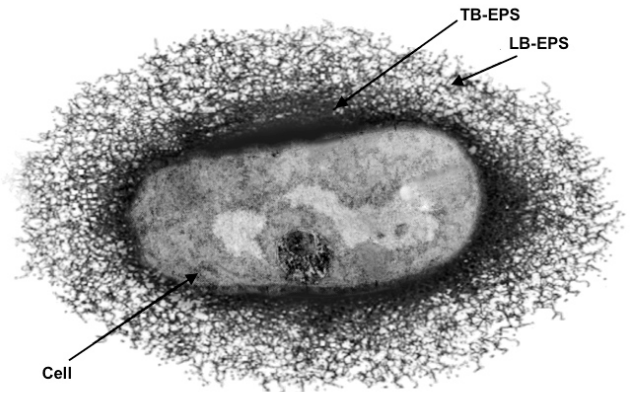


Figure 6. Two-layer model of the EPS structure. EPS surrounding bacteria possess a dynamic double-layered structure where tightly bound EPSs (TB-EPSs) form inner layer and loosely bound EPSs (LB-EPSs) diffuse in outer layer (adapted from Lin et al. (2014)).

The spatial distribution of the major components of EPS, i.e. PN and PS, is reported to be heterogeneous in aerobic granules (Sheng et al., 2010). Wang et al. (2005) observed that aerobic granules had an outer layer composed of β-D-glucopyranose polysaccharides (non-biodegradable) with high cell density, whereas its core part was filled with readily soluble and biodegradable EPS and presented a relatively low cell density. Mcswain et al. (2005) also observed that cells and α-D-glucopyranose polysaccharides were present in the outer layer of AGS, whereas most of the proteins were found in the core. Adav & Lee (2008) also observed substantial proteins and β-polysaccharides in the interior of the granules, with cells, lipids and α-polysaccharides accumulating at the outer layer. Comparable results were obtained in a study carried out by Lee et al., (2010). These authors reported that the aerobic granules had an outer surface composed mostly of lipids and α-polysaccharides and a core composed of proteins and β-polysaccharides, which provide mechanical strength for the granule to resist shear stress.

EPS matrix plays an important role in the formation of AGS and in the maintenance of granule structure and mechanical stability (Quan et al., 2015; Sheng et al., 2010). Part of the EPS can also serve as carbon or energy sources in conditions of nutrient limitation (Geyik and Çeçen, 2015; Wang et al., 2006). Furthermore, EPS can play a significant protective role to the inner microorganisms against harsh external environmental conditions, such as exposure to heavy metals. EPS constituents are amphiphilic in nature and contain multiple active functional groups and/or charged moieties (e.g., carboxyl, phosphoric, sulfhydryl, phenolic and hydroxyl groups), as well as hydrophobic moieties that can complex with heavy metals and act as a permeability barrier to hinder their intracellular penetration, thus attenuating toxicity (Kang et al., 2014; Sheng et al., 2010; Wang et al., 2016). Geyik & Çeçen (2016) demonstrated that EPS can biosorb both $Ag^+$ and Ag NPs. Furthermore, Kang et al. (2014) concluded that EPS constitute a permeability barrier with reducing constituents that mitigate the antibacterial activity of $Ag^+$. These authors, through high-resolution transmission electron microscopy (HRTEM) combined with X-ray photoelectron spectroscopy (XPS) and energy-dispersive spectrometry (EDS) analyses, showed that Ag+ was reduced to Ag NPs, which were entrapped within the EPS matrix. Other researchers have suggested that these extracellular biomolecules can effectively adsorb on NPs forming a protein corona which impart them with biological identity, thereby altering the cell membrane

affinity, uptake, and retention of NPs and reducing their bactericidal activity (Albanese et al., 2014; Fleischer and Payne, 2015; Miclăuş et al., 2016; Wei et al., 2016).

**EPS extraction methods**

An ideal EPS extraction method should be effective, cause minimal cell lysis and not disrupt or modify the EPS structure. The extraction efficiency can be defined as the total quantity of EPS extracted from the total organic matter, or the total quantity of EPS extracted from the total EPS pool, for a given cell sample. A typical EPS extraction procedure is as follows: (1) *pre-treatment*, including sampling, washing, and physical disruption. This step allows the microbial cells to be dispersed. For EPS extraction from microbial granules, physical disruption is needed; (2) *EPS extraction*; (3) *Purification*; (4) *Analysis*. The EPS are usually analyzed for macromolecular composition (e. g. polysaccharides and proteins) and, in some cases, a more detailed investigation of the chemical composition or other characteristics is performed (Sheng et al., 2010).

The EPS extraction step is carried out through physical or chemical methods or combinations of both. Physical extraction methods usually involve low- and high-speed centrifugation, sonication or heat treatment, whereas common chemically extractions include the addition of ethylenediamine tetraacetic acid (EDTA), alkaline reagents and the use of cation exchange resins (CER). The extraction efficiencies of chemical methods are generally higher than that of physical methods, but the application of chemicals can cause significant interferences, either in the extraction process or in the subsequent EPS analysis (Bourven et al., 2013; Caudan et al., 2012).

The physical EPS extraction methods apply a shear force to promote the detachment of EPS from the cells and its dissolution (Sheng et al., 2010). Centrifugation is often used to separate the soluble EPS fraction from cells and other particles. However, it does not provide a significant extraction of the bound EPS from microbial aggregates (Antonelli et al., 2011). EPS extraction with low energy sonication does not cause significant cellular disruption, but it simultaneously appears to be ineffective (Antonelli et al., 2011). However, Adav & Lee 2008 noted that the use of pre- or post-sonication improved the EPS extraction efficiency from compact microbial aggregates. Heat treatment enhances the kinetic energy of the molecules, accelerating the EPS dissolution (Sheng et al., 2010) and leading to higher EPS extraction levels when compared to other physical extraction techniques. In addition, it is easy and inexpensive to perform, it does not require sophisticated equipment and, therefore, it is sometimes the preferred EPS extraction technique (Antonelli et al., 2011). Nonetheless, the extracts were reported to contain DNA, suggesting the occurrence of cell lysis and the release of intracellular components during the extraction procedure (Sheng et al., 2010).

Chemical treatments include addition of various reagents to the sludge sample to break different linkages in the EPS matrix, facilitating the release of EPS to the aqueous medium. Alkaline treatment (NaOH addition) causes ionization of charged groups, such as carboxylic groups in proteins and polysaccharides, because their isoelectric points are generally below pH 4-6. It induces a strong repulsion between EPS components, increasing their water solubility (Nielsen and Jahn, 1999). Nonetheless, this method can cause severe cell lysis and hydrolysis of macromolecules. Some studies used fixative reagents, such as formaldehyde (Liu and Fang, 2002) or glutaraldehyde (Azeredo et al., 1998), to protect the cells and prevent cell lysis during alkaline EPS extraction. Furthermore, the addition

of these reagents seems also to increase the EPS extraction yield from aerobic granules (Adav and Lee, 2008). For instance, formaldehyde can react with amino groups of proteins or amino-polysaccharides to alkylate cell wall molecules or EPS, destabilizing the structure of granules and, consequently, increasing the release of EPS. But residual formaldehyde can remain in the EPS solution, or the molecules present in the EPS solution can be modified by reaction with the formaldehyde on their amino group, which can alter their properties (D'Abzac et al., 2010). Adav & Lee (2008) replaced formaldehyde with formamide and found that its cell shrinkage action can also enhance the efficiency of EPS extraction.

Divalent cations, mainly $Ca^{2+}$ and $Mg^{2+}$, are essential for crosslinking of charged compounds in the EPS matrix and, by removing them, the EPS matrix tends to destabilize and lose its structure. The divalent cations can be removed by a chelating agent such as ethylenediaminetetraacetic acid (EDTA) or by using a cation exchange resin (CER). The EDTA method has a high extraction efficiency and causes a low degree of cell lysis. However, the residual EDTA interfere with protein quantification methods. CER methods are the most widely accepted EPS extraction methods because the resin can be removed readily after extraction, which means that the contamination of the extracts by chemical reagents is avoided and the subsequent analysis is easier (Pal and Paul, 2008a; Sheng et al., 2010). In addition, this method does not affect the cell membrane, despite that long extraction times can cause significant cell lysis. However, the yield of extracted EPS was reported as being dependent on the amount of CER added, stirring intensity and extraction time (Frolund et al., 1996). On the other hand, there have been some divergences regarding CER effectiveness. Frolund et al. (1996) evaluated the CER method as highly efficient, yielding significant concentrations of extracted EPS, contrarily to the results reported by Liu & Fang (2002) and Mcswain et al. (2005). Besides, proteins seem preferentially extracted by CER. In fact, Dignac et al. (1998) demonstrated that proteins have more affinity for multivalent cations than the polysaccharides in the EPS matrix. Consequently, the use of CER to extract EPS facilitates the protein extraction.

The strategies of EPS extraction from aerobic granules are often inspired by protocols applied to activated sludge flocs. However, extracting EPS from aerobic granules is more difficult than from sludge flocs due to the low surface-to-volume ratio of exposure (Adav and Lee, 2008; Liu and Fang, 2002; Mcswain et al., 2005). Mcswain et al. 2005 extracted EPS from aerobic granules by heating the samples at 80ºC in the presence of NaOH or by mixing them with CER and noted that, due to the large size of the granules, effective EPS extraction required the pre-homogenization (980rpm) of the aggregates before chemical extraction. Adav & Lee 2008 also reported that using pre-ultrasound (120W) before chemical treatment largely improved the EPS extraction from compact aerobic granules. In contrast, the use of ultrasounds did not enhance EPS extraction from sludge flocs, probably due to the correspondingly loose attachment between EPS and flocculent cells.

There is not a standard method established for EPS extraction from aerobic granules and the efficiency of the available methods varies significantly. Furthermore, the selected method can influence the qualitative composition of the recovered EPS. It is clear by Table 2 that protein to polysaccharide ratio (PN/PS) is linked to the extraction procedure. Chemical methods are more selective towards proteins than polysaccharides, since the PN/PS values range between 4.4 and 7.6. Physical methods

lead to lower PN/PS values (from 1.4 to 4.9), suggesting better ability of these methods for polysaccharide extraction than the chemical ones. Therefore, an appropriate method should be chosen and adapted to the properties of the sludge under study with the aims of effective EPS recovery with minimal cell lysis, avoiding EPS destruction and incompatibility with EPS analysis methods (Adav and Lee, 2008; Caudan et al., 2012; Mcswain et al., 2005).

Table 2. Comparison of methods for the extraction of proteins (PN) and polysaccharides (PS) from granular sludge.

| Method | Protocol | mg $g^{-1}$ VSS | | | PN/PS | Reference |
|---|---|---|---|---|---|---|
| | | PN | PS | Total | | |
| Physical | Crushing — Heating 80ºC (1h) – Centrifugation 2100*g* (15min) – Centrifugation 12 000*g* (30 min) | 156.7 | 54.5 | 258.3 | 2.9 | Li et al. 2008 |
| | Heating 80ºC (30min) – Centrifugation 10 000*g* (20 min) | 238.2 | 57.2 | - | 3.6 | Adav & Lee 2008 |
| | Heating 80ºC (30min) – Centrifugation 7 000 rpm (10 min) | 22.6 | 15.4 | - | 1.4 | Li et al. 2014 |
| | Heating 80ºC (30min) – Centrifugation 4 000*g* (15min) | 15.05 | 9.94 | - | 1.5 | Lv et al. 2014 |
| Chemical | Cation-Exchange Resin – Centrifugation 10 000 rpm (1min + 10 min) | 23 | 3 | 15 | 7.6 | Mcswain et al. 2005 |
| | Homogenization – Cation-Exchange Resin – Centrifugation 10 000 rpm (1min + 10 min) | 73 | 11 | 69 | 6.7 | Mcswain et al. 2005 |
| | Formaldehyde – NaOH 1M – Centrifugation 10 000g (20 min) | 309.5 | 70 | - | 4.4 | Adav & Lee 2008 |
| | Formamide – NaOH 1M – Centrifugation 10 000g (20 min) | 374.9 | 61 | - | 6.2 | Adav & Lee 2008 |
| Combined | NaOH 1M + Heating 80ºC (30min) – Centrifugation 10 000 rpm (1min + 10 min) | 185 | 18 | 86 | 10.9 | Mcswain et al. 2005 |
| | Homogenization – NaOH 1M + Heating 80ºC (30min) – Centrifugation 10 000 rpm (1min + 10 min) | 210 | 26 | 203 | 7.9 | Mcswain et al. 2005 |
| | Sonication – Formaldehyde – NaOH 1M – Centrifugation 10 000g (20 min) | 455.2 | 85.1 | - | 5.3 | Adav & Lee 2008 |
| | Sonication – Formamide – NaOH 1M – Centrifugation 10 000g (20 min) | 537.2 | 109.3 | - | 4.9 | Adav & Lee 2008 |
| | 3 x (Sonication 37W – 0.25% Tween 20 – EDTA 2%), Centrifugation 10000rpm after each step | 64 | 38 | 102 | 1.7 | Caudan et al. 2012 |
| | 3 x (Sonication 120W – 0.25% Tween 20 – EDTA 2%) Centrifugation 10000rpm (10 min) after each step | 270 | 102 | 270.3 | 3.6 | Caudan et al. 2012 |

## 1.4 Silver nanoparticles as an emerging problem in textile wastewaters

The use of silver nanoparticles (Ag NPs) in the textile industry has been rapidly increasing and their occurrence in wastewater is expected to rise accordingly, constituting an emerging environmental concern (Som et al., 2011; Windler et al., 2013). Worldwide, markets for silver-containing nano-functionalized products have started to grow significantly (Blaser et al., 2008). In 2000, the global production of textiles exhibiting antimicrobial properties was estimated to be around 100,000 tons with a European annual growth of more than 15% (Voelker et al., 2015). Based on the information of the staff working paper of the European Commission, the annual global market for Ag NPs in antimicrobial uses is estimated at 22 tons (European Commission 2012). In turn, Windler et al. (2013), from publications among 2008 to 2011, estimated that up to 36 tons of Ag NPs were applied in textiles globally

(Windler et al., 2013). Ag NPs are used in t-shirts, socks, underwear, sports clothing and many other commercial textile products (Benn and Westerhoff, 2008). Ag NPs may be discharged into the environment during synthesis; manufacturing and incorporation of NPs into textiles; usage and washing of textiles; and recycling or disposal of textiles and Ag NPs. However, only a few studies considered Ag NPs release from textile fibers into wastewater and reported the possibility of their removal from the wastewater (Radetić, 2013).

In the study of Benn & Westerhoff (2008), six types of socks containing up to a maximum of 1360 µg Ag/g sock leached as much as 650 µg of silver in 500 mL of distilled water. Sock material and wash water revealed the presence of silver particles from 10 to 500 nm in diameter. Both particulate and ionic silver were leached from the socks. (Benn and Westerhoff, 2008). In another study concerning the release of silver from textiles, Geranio et al. (2009) revealed that the amount of silver released from nine types of textiles during one washing was up to 45% of total silver mass and that the majority of the silver released was in the size fraction >450 nm (Geranio et al., 2009). Also, Lorenz et al. (2012) investigated the release of silver from eight different commercial silver textiles during a washing and rinsing cycle. The initial silver content of the textiles was up to 2925 mg Ag/kg. The majority of the investigated textiles leached detectable amounts of silver. In fact, these were released up to 38.5 mg $L^{-1}$ into the washing solution (575 mg Ag $kg^{-1}$ textile) and 22.7 mg $L^{-1}$ into the rinsing solution (113 mg Ag $kg^{-1}$textile), of which 34-80% were in the form of particles larger than 450 nm (Lorenz et al., 2012).

Wastewater treatment plants (WWTPs) are important barriers to prevent NPs from directly entering the environment (Quan et al., 2015). Blaser et al. (2008) predicted that the amount of silver released from silver-containing products into water systems would reach a maximum of 410 tons per year in 2010, for European countries alone. Of these, up to 15% accounts for silver incorporated in textiles, of which Ag NPs are a significant fraction. These authors also predicted that silver concentration in sewage treatment plants would be from 2 to 18 mg/L. Nonetheless, some WWTPs have registered a higher concentration (e.g., 105 mg/L of total silver) in the wastewater influent receiving periodic silver discharges from the industry (Shafer et al., 1998).

A considerable amount of Ag NPs could be removed in WWTPs via aggregation, settling, precipitation, biosorption, or other sludge mediated processes (Kiser et al., 2010; Liang et al., 2010). However, little is known about how the discharge of Ag NPs affects bacterial growth and the properties of sludge in WWTPs (Liang et al., 2010).

## 1.5 Interaction of Ag NPs with AGS

Ag NPs can impose toxicity to microorganisms through several mechanisms: Ag NPs can attach to cell membranes and cause changes in their permeability; small Ag NPs (<10 nm) and released $Ag^{+}$ may enter the bacterial cell and cause cellular enzyme deactivation, membrane permeability disruption and accumulation of intracellular radicals, resulting in microbial growth inhibition, cell lysis and death (Gu et al., 2014; Liang et al., 2010). These antimicrobial properties of Ag NPs suggest a potential negative impact on biological sludge in wastewater treatment plants.

Several studies have been reported on the interactions of Ag NPs with flocculent activated sludge (Eduok et al., 2015; Kiser et al., 2010; Liang et al., 2010). Kiser et al. 2010 studied the removal

of eight types of NPs using activated sludge as sorbent and found that 97% of non-functionalized Ag NPs were removed by aggregation and sedimentation. Liang et al. (2010) investigated the bacterial response to a shock load of Ag NPs (1 mg/L, 12 h) in an activated sludge treatment system, and found a significant inhibition of nitrification (46.5%) after more than one-month operation. However, only a few studies have been reported on the interactions of Ag NPs with AGS and their impacts in AGS treatment performance (Gu et al., 2014; Quan et al., 2015).

Gu et al. 2014 investigated the effect of different sludge types on Ag NPs removal from aqueous suspensions at different Ag NP concentrations (1 - 8mg $L^{-1}$) after 3h of contact. AGS contributed only to 2.5 - 9.4% removal of Ag NPs (relatively to the sludge-free control), which was lower than Ag NP removal by flocculent sludge (30-58%). The authors attributed the higher removal of Ag NPs by flocculent sludge than by AGS to the differences in sludge particle shape and structure. Flocculent sludge has large specific surface area with a loose structure and a large number of bacterial cells embedded in the EPS, which favors the adsorption of Ag NPs. In addition, the presence of flocculent sludge may also raise the ionic strength of wastewater, which may make Ag NPs more susceptible to aggregation by increasing electric double layer suppression and destabilization. Sludge granules are much larger and denser than flocs, and have significantly smaller specific surface area and, hence, lower adsorption capacity.

In the study of Quan et al. (2015), an AGS SBR with Ag NPs showed an EPS level similar to that of the Ag NPs-free control SBR after 69 days of operation, but its EPS components significantly changed, with an apparent PN content increase and PS content decrease. One possible explanation for the elevated production of proteins was the induction of heat shock-like proteins as a defense mechanism against high concentrations of heavy metal ions. The EPS secreted from AGS might protect the cells from the toxic effects of Ag NPs.

The level of extracellular lactate dehydrogenase (LDH) released from damaged cells is an indicator of membrane permeability and integrity (Quan et al., 2015). Reactive oxygen species (ROS) are an indicator of oxidative stress (Choi and Hu, 2008). Both Gu et al. (2014) and Quan et al. (2015) measured these two parameters aiming to reveal the toxic mechanisms of Ag NPs in sludge. Both studies reported that exposure of AGS to high Ag NPs dosage (50mg/L) induced the generation of ROS and the release of LDH. These results indicated that the integrity of AGS cells was damaged and that oxidative stress increased in the presence of Ag NPs.

In the study of Quan et al. (2015), the ratio of dead cells to the total cells increased after 69 days of exposure to Ag NPs (5 mg $L^{-1}$ and 50 mg $L^{-1}$) compared to the Ag NPs-free control. The AGS Ag NPs-free control showed a compact structure, while the AGS treated with Ag NPs showed a loose structure with relatively more dead cells on the surface. Gu et al. (2014) also found a higher ratio of dead cells to the total cells after 12-h exposure to 100 mg/L Ag NPs than that in Ag NPs-free control. Nonetheless, these authors observed that in AGS Ag NPs-free control, dead cells were mainly located at the outer layer of the granules and that after exposure to Ag NPs, more dead cells were found in the inner part of the granules. This suggests that Ag NPs or the released $Ag^{+}$ can penetrate into the inner part of sludge granules and cause toxicity to the interior cells. Therefore, both studies confirmed that exposure to Ag NPs induced chronic toxicity on AGS and led to cell death, which corresponded to the result of microbial activity inhibition (Gu et al., 2014; Quan et al., 2015).

According Quan et al. (2015) the special physical structure and microbial distribution in AGS allowed the microbial community of AGS to remain stable after long-term exposure (69 days) to 5 and 50 mg/L of Ag NPs. The AGS served as a good shelter for the vulnerable bacteria, which were protected against toxic environments deep within the specially organized consortium. In addition, the microbial community interactions in AGS may be another important reason for the high resistance to toxicity. Interactions within a symbiotic microbial community such as protocooperation, mutualism and even competition, can increase its tolerance against antimicrobial agents (Gu et al. 2014; Quan et al. 2015).

The ammonia oxidizing rate of AGS in the study of Gu et al. (2014) did not significantly change at both short- (12h) and long-term (22h) exposure to Ag NPs. In turn, Quan et al. (2015) reported that the ammonia oxidizing rate of AGS remained stable during the first 35 days of Ag NPs exposure, but significant inhibition was observed from day 56 on. In this study, the ammonia monooxygenase (AMO) activity of AGS was also measured and it was found that it decreased relatively to the Ag NPs-free control on day 69. AMO is used by autotrophic ammonia oxidizing bacteria to catalyze ammonia oxidation. This finding indicated that the decrease in the ammonia oxidizing rate might be primarily due to the reduction of AMO (Quan et al., 2015).

For the denitrification rate of AGS, Quan et al. (2015) observed inhibition with a 5 mg/L Ag NPs dosage but not with a 50 mg/L Ag NPs dosage on day 35. The authors suggested that this could be possibly due to the sheltered location of denitrifying bacteria. The dissolved silver ($Ag^+$), to cause inhibition to the denitrifying bacterial populations, has to penetrate from the bulk solution into the granule structure. Ag NPs at high concentrations are unstable and easily aggregate in wastewater, leading to reduced adsorption of Ag NPs on the sludge and less $Ag^+$ release (Gu et al., 2014; Quan et al., 2015). Thus, as Ag NPs at 5 mg/L are more stable than those at 50 mg/L, there can be more $Ag^+$ penetrating into the inner parts of the granules and contacting with the denitrifying bacteria. Thereafter, AGS at 5 mg/L Ag NPs dosage reclaimed denitrification activity possibly due to its acclimation to Ag NPs and secretion of more EPS to resist the toxicity. On day 69, Ag NPs at 50 mg/L dosage caused a slight inhibition of the denitrification rate. The authors suggested that it might be due to the reduction of nitrate reductase (NAR) activity. NAR is one of the main enzymes that catalyze the denitrification (Quan et al., 2015). In turn, Gu et al. (2014) observed that 50mg/L Ag NPs did not inhibit the denitrification rate of AGS at short- (12 h) and long-term (22 days) exposure (Gu et al., 2014).

The oxygen uptake rate of the AGS according to Gu et al. (2014) was inhibited at high Ag NPs concentrations (50 and 100 mg/L) in short-term exposure (12h). However, such inhibition disappeared after long-term (22 days) exposure, possibly due to adaptation of the granular sludge (Gu et al., 2014). Quan et al. (2015) reported that the oxygen uptake rate did not significantly change during the first 56 days of Ag NPs exposure, but it declined on day 69 at Ag NPs dosages of 5 and 50 mg/L (Quan et al., 2015).

In the study of Quan et al. (2015) the Ag NP exposed reactors maintained a high removal of COD and ammonia nitrogen, similarly to the Ag NPs-free control reactor, despite that the oxygen respiration rate and ammonia oxidation rate of AGS declined to a certain extent from day 56 on. Ag NPs exposure did not influence COD and ammonia nitrogen removal possibly due to the relatively low COD (1000 mg $O_2$ $L^{-1}$) and ammonia (50 mg/L) loadings applied in this study (Quan et al., 2015). The authors

also showed that long-term exposure of Ag NPs reduced the production of biomass in the AGS reactor.

The AGS maintained its good settling ability, since the SVI values did not significantly change in Ag NPs-dosed reactors compared to the Ag NPs-free control. Regarding its granular size, the long-term exposure of Ag NPs (>40 days) promoted the growth of AGS granules. This phenomenon could be explained by a growing silver accumulation in the AGS along the operation time, leading to chronic toxicity to microbial cells and higher EPS production, which in turn could promote the adsorption and attachment of more cells to the granule surfaces.

These results showed that AGS can contribute to the removal of Ag NPs, although with low efficiency. AGS also showed good tolerance to the presence of Ag NPs and maintained stable microbial activities within the first 35 days of exposure. Toxic effects occurred thereafter and the AGS was significantly inhibited on oxygen respiration rate, ammonia oxidation rate and denitrification rate. However, the long-term Ag NP exposure did not cause significant changes in sludge properties, as the AGS maintained a large granule size (about 900 nm) and good settling ability. The microbial community of AGS also remained stable. Overall, Ag NPs did not cause acute toxicity to the AGS, but their chronic toxic effects are cause for great concern (Gu et al., 2014; Quan et al., 2015).

In order to better understand the causes of Ag NPs chronic toxic effects and further operate AGS systems to overcome these toxic effects it is essential to study the fate, the transformations and the toxicity mechanisms of Ag NPs. However, this information is very limited and the lack of proper techniques to trace Ag NPs in complex matrices hinders the investigation (Liu et al., 2012).

## 1.6 Methods for identification, characterization and quantification of Ag NPs in biological samples

### 1.6.1 Current methods for identification and characterization of Ag NPs

Due to their nanoscale dimensions, Ag NPs are beyond the detection ability of traditional optical microscopy. Electron microscopy (EM) techniques have a much higher resolution, which makes them a current option in visualization and characterization of NPs. In this field, the most applied techniques are transmission electron microscopy (TEM) and scanning electron microscopy (SEM).

In TEM, a high-energy electron beam (80–300 keV) is transmitted through a very thin layer of the sample. A fraction of the beam is scattered from the sample while some electrons can be transmitted. (Dudkiewicz et al., 2011). TEM images provide not only the size and the shape of the particles, but also the morphology and the aggregation state. However, TEM specimens are required to be dry and at most hundreds of nm thick, so the main task is to prepare a proper sample. For biological materials, in order to keep their original state and to enhance contrast, chemical fixation and a straining procedure is often needed. Moreover, the samples also need to be embedded in resin and cut into thin sections to allow the electron beam to pass through (Liu et al., 2012).

SEM creates an image of the sample by scanning the sample surface with a low-energy beam of electrons (1– 30 keV) and detecting the electrons scattered off the sample (Dudkiewicz et al., 2011). Though the SEM samples need not be as thin as TEM, to avoid the accumulation of static electric charge on the specimen during electron irradiation, the specimen, at least the surface, must be conducting, so

sometimes it is necessary to coat the sample with a layer of conductive material. However, there is a risk that some of the surface information could be lost. This problem could be solved by the application of environmental SEM, which allows the samples to be imaged under vacuum. Nonetheless, the resolution of this technique is reduced (Liu et al., 2012).

EM imaging as an analytical technique is not sufficient for comprehensive characterization and detection of Ag NPs in complex matrices, so supporting information is essential for element identification (Dudkiewicz et al., 2011). Energy-dispersive X-ray spectroscopy (EDS) is an analytical method for elemental determination that is usually combined with TEM or SEM to give an element distribution of the Ag NPs (Liu et al., 2012).

### 1.6.2 Current methods for quantification of Ag NPs

Inductively-coupled plasma atomic emission spectroscopy (ICP-AES) and inductively-coupled plasma mass spectrometry (ICP-MS) allow the detection Ag NPs and are the most popular techniques in the quantitative determination of metal ions. Since the existence of particles may block or clog the sample tips within the spray chamber, and the presence of ligands or other organic substances could hinder complete atomization of the sample, a sample-digestion process is always required before the sample is pipetted and analyzed. This destructive procedure leads to some drawbacks (e.g., it cannot distinguish $Ag^{+}$ and Ag NPs, unless a pre-separation performance is carried out before digestion) (Liu et al., 2012).

### 1.6.3 Nuclear microscopy

Nuclear microscopy (NM) employs a variety of high energy (MeV) ion beam techniques at submicron spatial resolutions to provide simultaneously elemental imaging and quantitative elemental analysis of biological material down to the parts per million (ppm) level of analytical sensitivity (Mulware, 2015). This tool is also particularly suited for biological analysis since that only need a simple and non-destructive sample preparation, contrary of TEM and SEM (Gontier et al., 2008; Liu et al., 2012; Pinheiro et al., 2007; Veríssimo et al., 2007).

In NM, the detection of scattered and transmitted protons, induced X-rays, emitted secondary electrons, among others, can be done simultaneously and the images produced display features of the sample that cannot promptly be imaged by other techniques (e.g. TEM and SEM). This capacity derives from the ability of MeV ion beams to penetrate deep beneath the sample surface with low scattering to produce signals from hidden features. On contrary, electrons impinging on the sample are subject to multiple scattering and energy attenuation, producing a significant background of continuous radiation. This means that in elemental analysis for instance, the weak signal of trace elements is hidden in the background what justifies the low sensitivity of EM when compared to the NM (Pinheiro et al., 2007; Watt et al., 2013) .

#### Nuclear Microscopy techniques

Scanning transmission ion microscopy (STIM), particle induced X-ray emission (PIXE), and Rutherford backscattering (RBS) constitutes a group of techniques widely used in nuclear microscopy

to image density variations in relatively thick samples, map trace elements leveling those samples to the microgram per gram (dry weight) level, and extract quantitative information on these elements.

STIM is based on the measurement of the energy loss of the incident particles after passing through the sample. The energy loss is proportional to the stopping power of the sample and describes its atomic density. By measuring density variations, high spatial resolution (<0.5μm) density maps of the sample can be obtained (Carmona et al., 2008; Ortega et al., 2009; Pinheiro et al., 2007). STIM is often used to investigate samples thin enough to transmit a 2 - 3 MeV proton beam. For thin organic samples (30 μm or less), essentially all incident protons which are not backscattered will be transmitted (Mulware, 2015). Therefore, this technique is well suited to the analysis of single cells that are typically of the order of 10 μm thick (Ortega et al., 2009)

PIXE is a well-established technique for minor and trace element analysis. This technique is based on the detection of characteristic X-rays emitted by the sample elements when excited with an MeV ion beam. It is generally performed with protons, better than with heavier particles, because the ionization cross sections follow an $A^{-4}$ law, where A is the atomic weight of the incoming particle (Carmona et al., 2008; Ortega et al., 2009). Thus, when the energy transfer of the incident proton is higher than the electron binding energy from the inner shell, the ejection of this electron occurs creating an inner shell vacancy. This vacancy will be filled by an electron transition from the outer shell with the emission of an X-ray (Mulware, 2015). The energy of the emitted X-rays is characteristic of the excited element. It corresponds to the difference between the two electronic levels' binding energies. The emission energies of all chemical elements are tabulated, thus enabling the identification of the composition of the atoms constituting the sample (Ortega et al., 2009). PIXE is a non-destructive procedure that enables the simultaneous detection of multiple elements (from sodium to uranium) with excellent quantitative precision and analytical sensitivity (1–10 μg/g on a dry weight basis), especially for transition elements (Pinheiro et al., 2007; Watt, 2006).

RBS is based on the energy of elastically backscattered particles after interaction with the nuclei of target atoms in the sample (Mulware, 2015). The energy loss of the backscattered particle depends on the mass of the nucleus involved in the collision (Ortega et al., 2009). During its path in and out of the sample the backscattered proton also lose energy due to electronic interactions. Thus, the incoming particle are 'sorted' according to the atomic nucleus involved in the collision and according to the depth of the interaction, allowing not only an elemental identification, but also determines the thickness of the sample (Carmona et al., 2008; Ortega et al., 2009). The RBS analysis provides valuable information on the matrix composition being complementary to PIXE because information on matrix composition is needed to normalize PIXE data and produce quantitative results (Grime and Dawson, 1995).

**Quantitative elemental concentration**

The energy of the emitted X-ray is characteristic of the sample atom and thus the full collected energy spectrum enables the identification of the elements present in the sample. The measured X-ray yield allows the quantization of trace element concentrations. Assuming that the concentration depth profile $C_{(Z)}$ of the zth element of atomic number Z in the sample is constant, the X-ray intensity I(Z) for the characteristic X-ray of the zth element in the sample is given by (9):

$$I_{(z)} = Q\ C_{(Z)}\ K_{(Z)} \qquad (9)$$

where Q is the total beam charge and K(Z) is a calibration constant independent of the sample, in the case that both experimental geometry and sample matrix composition are constant. However, in microbeam PIXE the composition of the matrix may vary strongly over a scale comparable with the beam diameter. In addition, the precise quantification of beam charge proves to be experimentally difficult, since the beam current is in the order of nA and spatially variable. This problem was addressed by using a simultaneous RBS analysis (Grime and Dawson, 1995). Assuming a precise modeled RBS spectrum, it is possible to obtain information on the local matrix composition by its shape, and on the total beam charge, by its integral. Thus, it is possible to normalize the PIXE data using matrix estimation and by the ratio between the true beam charge and the measured charge, also known as Q-factor (Grime and Dawson, 1995).

**The proton microprobe components**

In nuclear microscopy the ion beams, most frequently protons or $He^{+}$, are produced in an accelerator. The energy range required in most of the applications, 1 to 3 MeV, means that small accelerators, preferably with a bright ion source, are suitable (Pinheiro et al. 2007). The essential components of the nuclear microprobe consist of a focusing system, a scanning system, an irradiation chamber where several detectors and devices can be connected, and adequate data collection modules (Figure 7) (Veríssimo et al., 2007).

The focusing system contains two sets of slits in addition to the lens system. The first set of slits is called the object slits from which the system of lenses produces their demagnified image on the sample at the focal plane. The opening of these slits controls the beam transmission/resolution parameters. The second set of slits, the collimation slits, define the beam divergence into the lens system by limiting lens aberrations, such as the spherical aberration (Veríssimo et al., 2007). A steering magnet located close to the object aperture can be used to optimize the amount of beam that is transmitted through the collimator aperture. The focused beam is raster scanned over the sample surface using scanning coils that are located before the lenses. The typical distances between object slits and collimation slits and between the lens system exit and focus plane are 2-8 m and 8-16 cm, respectively.

The vaccum irradiation chamber can accommodate a Si(Li) detector for X-rays (PIXE), a Si surface barrier detector for backscattered particles (RBS), a collimated windowless photodiode or a Si surface barrier detector for transmitted particles (STIM), and a Faraday-cup for beam charge measurements (Teresa Pinheiro et al., 2007). The sample stage is equipped with a x,y,z manipulator for positioning the sample into the focus plane with the help of a microscope. (Pinheiro et al., 2007; Veríssimo et al., 2007).

The microprobe lenses, scanning coils, collimator slits and chamber are mounted on a single concrete block, which rests on a layer of polystyrene to minimize the transmission of vibrations from the ground (Alves et al., 2000).

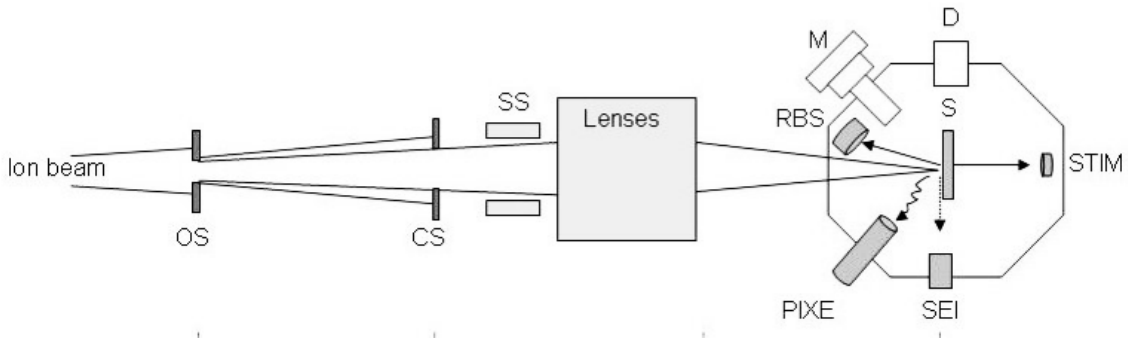


Figure 7. Lay-out of a nuclear microprobe installed at Centro Tecnológico Nuclear (ITN). ITN focusing system contains two sets of slits, the object slits (OS) and the collimation slits (CS) in addition to the lens system. The focused beam is raster scanned over the sample surface using scanning coils (SS) that are located before the lenses. The chamber configuration accommodates several detectors for X-rays (PIXE), for backscattered particles (Si surface barrier detector for RBS) for transmitted particles (collimated windowless photodiode for STIM), for secondary electrons (scintillator and photomultiplier system or a channeltron for SEI) and an additional position – D, for other detector. The sample stage (S) is equipped with a x,y,z manipulator for positioning the sample into the focus plane with the help of a microscope (M) (Adapted from Pinheiro et al. (2007)).

Samples are usually analyzed in vacuum to prevent unacceptable scattering of the beam. The final attainable beam's spatial resolution is dependent on several parameters such as accelerator stability, quality of the lens system, mechanical vibrations damping, and thermal stability (Veríssimo et al., 2007). Nevertheless, dimensions of 1–3 μm are easily attained on a routine basis for backscattering imaging and 0.5 μm for transmission imaging. The high spatial resolution of the beam coupled with a scanning range of 1–3 mm improves the imaging capabilities of the system and permits the scanning of a selected region of interest in the sample (Pinheiro et al., 2007; Veríssimo et al., 2007).

**Data acquisition and processing**

In a microprobe each event and spectra data are assigned to a digital x,y positional coordinate. When a detector detects an event, the small voltage pulse is read, converted in to a digital signal and sorted into a multichannel analyzer (usually 1024 or 2048 channels). A single map is obtained for a region of interest extracted from the spectral data (X-ray peak area, barrier area, etc.). In real-time the magnitude of a measured quantity is usually represented by a dynamic color gradient. The statistical treatment of the events occurring at each beam position can be used to produce quantitative elemental maps. To integrate this information commercially available data acquisition systems are used. These systems record full details of the experimental conditions (sample, detectors, beam parameters, etc.) and has many features to provide a convenient and flexible operating environment such as a library of X-ray energies to allow instantaneous identification of peaks in PIXE spectra, on-line simulation of RBS spectra, etc (Grime and Dawson, 1995).

## 1.7 Scope and objectives

The objective of this study was to assess the effects of 5mg $L^{-1}$ Ag NPs in the characteristics and performance of AGS in an anaerobic-aerobic SBR system treating synthetic textile wastewater. For that, the performance of two SBRs run in parallel, one supplied with Ag NPs and the other used as Ag NPs-free control, was evaluated in terms of COD and color removal efficiency. Additionally, this study

also aimed to assess the impacts of Ag NPs on granule formation and long-term stability; on sludge mass density; on cell membrane permeability; and on the major EPS components, i.e. PN and PS. Nuclear microscopy was also applied to image elemental distribution and to perform a quantitative elemental analysis of the Ag NPs-containing sludge samples.

# 2. Materials and methods

## 2.1. Experimental system and SBR cycle operation

The experimental system was composed of two anaerobic–aerobic sequencing batch reactors (SBRs). Both SBRs were fed with a synthetic textile wastewater containing a COD:N:P mass ratio of 100:3.7:37, ), avoiding the occurrence of nitrification. This solution was separately added to both SBRs, as carbon feed solution (Feed - C) and nitrogen dye-containing feed solution (Feed - N) (see section 2.2). One SBR was supplied with Ag NPs (SBR1) and the other was used as Ag NPs-free control (SBR2).

SBR1 and SBR2 were run in 6-h cycles with a hydraulic retention time (HRT) of 12h. Each cycle consisted of five discrete sequential phases, namely fill, reaction, with a mixed anaerobic stage followed by an aerated stage, settle, drain and idle, a quiescent period to complete the cycle time (Figure 8).

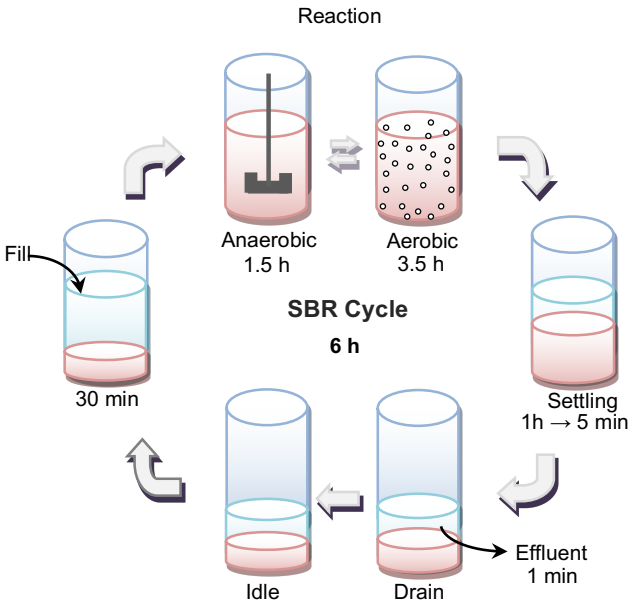


Figure 8. 6-h SBR cycle with five discrete sequential phases, namely fill, during which fresh feed was pumped into the reactor, reaction, with a mixed anaerobic stage followed by an aerated stage, settle, for biomass sedimentation, drain during which half of the operational volume was rapidly removed from the clarified supernatant, and idle, a quiescent period to complete the cycle time. The duration of each phase is also indicated.

These SBRs were run in parallel for 271 operating days. The Ag NPs was fed to SBR1 along a 178-days operational period followed by a 60-day period during which Ag NPs were absent from the feed. After this cleaning period, Ag NPs feeding was resumed.

The SBRs had a working volume of 1.5 L (height/diameter ratio of 2.5) and were fed with Feed -N and -C at the bottom with an exchange ratio of 50% and a volumetric organic loading rate (OLR) of

2.0 kg COD $m^3$ $d^{-1}$. At the end of the fill phase, SBR1 was supplied with Ag NPs at the top of the bioreactor (Figure 9). The feeding of the reactors was performed using peristaltic pumps (Mini-S 660, Ismatec, Switzerland), while the drain of the settled supernatant was achieved using gear pumps (Reglo-Z, Ismatec, Switzerland). Mechanical mixing was provided by magnetic stirrers during the non-aerated reaction. During the aerobic reaction, aeration (2 v.v.m) was supplied through air compressors (SPP-20 GJ-L, Hiblow, Japan) via a porous membrane diffuser at the bottom of each bioreactor. The pumping, aeration and agitation functions were automatically controlled, via an interface, by a dedicated software.

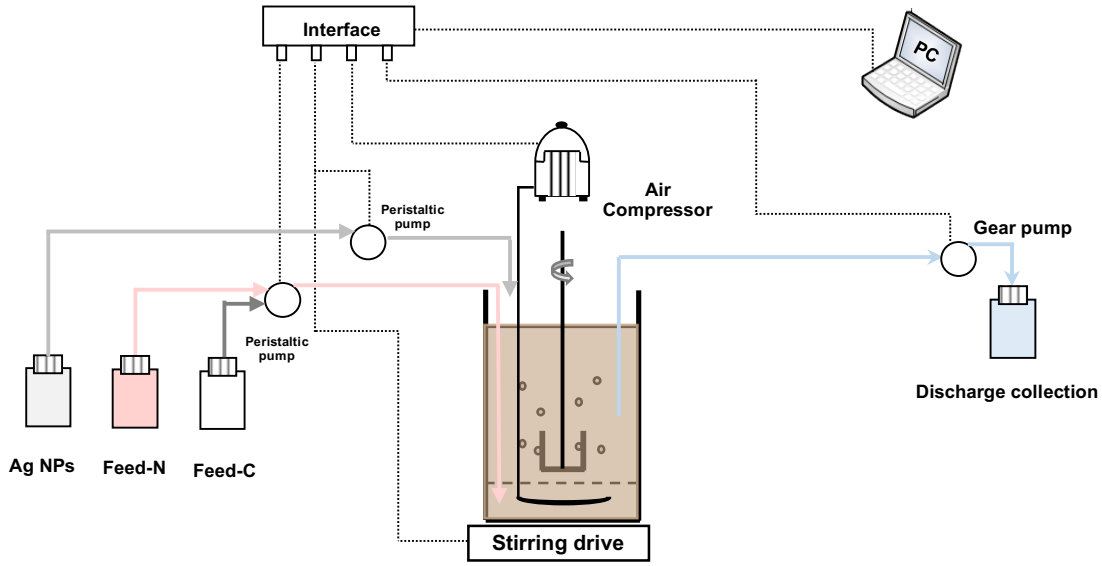


Figure 9. Representative SBR1 setup. SBR1 was fed with Feeds -N and -C at the bottom and at the end of the fill phase, was additionally supplied with Ag NPs at the top of the bioreactor. The feeding of the reactor was performed using peristaltic pumps, while the drain of the settled supernatant was achieved using a gear pump. Mechanical mixing was provided by a magnetic stirrer. Aeration (2 v.v.m) was supplied through an air compressor via a porous membrane diffuser at the bottom of the bioreactor. The pumping, aeration and agitation functions were automatically controlled, via an interface, by a dedicated software. SBR2 setup was similar to SBR1, except for the Ag NP supply.

## 2.2 Simulated textile wastewater

### 2.2.3 Feed-C preparation

The Feed-C solution was prepared by diluting the carbon source stock solution (100g $L^{-1}$) in distilled water to a COD content of 1000 mg $O_2$ $L^{-1}$ (1.15 g $L^{-1}$ Emsize E1) and supplemented with nutrients to the following concentrations: 27.5 mg $L^{-1}$ $CaCl_2$; 22.5 mg $L^{-1}$ $MgSO_4 \cdot 7H_2O$; 250 μg $L^{-1}$ $FeCl_3 \cdot 6H_2O$. Emsize E1 (Emsland-Stärke GmbH, Germany) is a starch derivative used as a sizing agent in the cotton textile industry. Under the alkaline conditions applied in the desizing step of cotton manufacture, the sizing agent is hydrolyzed and released in the wastewater. The preparation of the Emsize E1 stock solution (100 g $L^{-1}$) was based on one set of desizing conditions provided by the manufacturer (Lourenço et al., 2000). Thus, 100 g of Emsize E1 and 40 g of sodium hydroxide were dissolved in 500mL distilled water and stirred during 15 hours at room temperature. The hydrolyzed solution was then neutralized to pH 7.0 ± 0.05 with 37% HCl and diluted to 1 L with distilled water.

### 2.2.2 Feed-N preparation

The Feed - N was prepared with phosphorus and nitrogen salts, an azo dye (AR14, Chromotrope FB, Sigma Aldrich, 50% dye content) and other micro-nutrients to the following concentrations: 2310 mg $L^{-1}$ $Na_2HPO_4 \cdot 12H_2O$; 762 mg $L^{-1}$ $KH_2PO_4$; 143 mg $L^{-1}NH_4Cl$; 40 mg $L^{-1}$AR14; 40 µg $L^{-1}$ $MnSO_4 \cdot 4H_2O$, 57 µg $L^{-1}$ $H_3BO_3$, 43 µg $L^{-1}$ $ZnSO_4 \cdot 7H_2O$ and 35 µg $L^{-1}$ $(NH_4)_6Mo_7O_{24} \cdot 4H_2O$. The dye stock solution was prepared by dissolving AR14 in distilled water to a final concentration of 5.0 g $L^{-1}$ The AR14 concentration at the onset of the reaction phase (after the fill phase) was 20 mg $L^{-1}$.

### 2.2.3 Ag NPs feed suspension preparation and characterization

The feed suspension of Ag NPs was prepared by dispersing 100 mg of Ag NPs (in the form of nanopowder, <100 nm particle size, Sigma Aldrich) in 1L milli-Q water and sonicating it (VWR, Internation bvba/sprl, Belgium) during 60 minutes at 80W. After sonication, this suspension was diluted to 1L with milli-Q water to a final concentration of 50 mg $L^{-1}$. The Ag NPs concentration at the onset of the reaction phase (after the fill phase) was 5 mg $L^{-1}$.

The particle size distribution of the feed suspension of Ag NPs was determined by dynamic light scattering (DLS) (Zetasizer nanoZS, Malvern Instruments, UK).

## 2.3 SBR inoculation and aerobic granulation

SBR1 and SBR2 were inoculated with activated sludge flocs (5g TSS $L^{-1}$) harvested from a full-scale, conventional municipal WWTP (Chelas, Lisboa, Portugal). Aerobic granulation was induced by applying progressively smaller settling times, sufficient high shear stress and a feast/famine regime. The settling times were reduced from 1 hour to 5 minutes along the first 28 days of operation, according to Figure 10. Thereafter, the settling time was maintained in 5 minutes. The required shear stress was achieved by mechanical mixing during the anaerobic phase and by aeration in the aerobic phase. The SBRs were also fed in a short feeding time (30 minutes) in anaerobic conditions, allowing to establish a long famine phase.

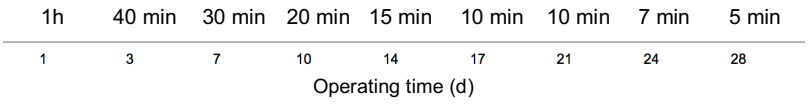


Figure 10. Settling times along the first 28 days of operating time. The settling times were reduced on Day 3, 7, 10, 14, 17, 24 and 28 of the experimental operating time.

## 2.4 SBR cycle monitoring

### 2.4.1 Total and volatile suspended solids

Total suspended solids (TSS) and volatile suspended solids (VSS) were measured on 10mL and 20 mL samples from the mixed liquor (ML) and from the effluent (E), respectively.

For TSS, glass microfiber filter discs (Whatman, GF/C, ø 47 mm) were washed with distilled water in a vacuum filtration system and dried in a drying balance (HB-43-S, Mettler-Toledo). The filter discs were heated in a muffle furnace (Nabertherm, L3/S27, Germany) at 550°C to eliminate any

adsorbed organic matter and were weighted in an analytical balance (Mettler AE160). Then, the mixed liquor SBR samples were filtered in the vacuum filtration system. Subsequently, the filter discs with samples were dried and weighted in the drying balance. The TSS content was determinate by the equation (10):

$$TSS = \frac{\text{mass (dry filter with sample )} - \text{mass (empty filter)}}{\text{Volume of sample}} \qquad (10)$$

For VSS, the dry filter discs with samples were heated in the muffle furnace at 550°. Next, the filter discs with the remaining ashes were weighted in the analytical balance. Thus, the VSS content was determinate by the equation (11):

$$VSS = \frac{\text{mass (filter with ashes)} - \text{mass (dry filter with sample)}}{\text{Volume of sample}} \qquad (11)$$

#### 2.4.2 Sludge volume index (SVI)

Sludge volume index (SVI) was determined by measuring the volume occupied by the sludge settled from 1 L of mixed liquor after settling times of 5 and 30 min in an Imhoff cone ($SVI_5$ and $SVI_{30}$, respectively), and dividing it by the mixed liquor TSS value.

#### 2.4.3 Chemical Oxygen Demand (COD)

For COD analysis, 10 mL samples were collected from SBR1 and SBR2 along the reaction phase of different treatment cycles. These samples were clarified by centrifugation (10 min at 4000 rpm), and measurements were performed on the supernatant.

The COD analysis method involves the use of a strong oxidizing chemical, potassium dichromate $Cr_2O_7^{2-}$, to oxidize the organic matter in solution to carbon dioxide and water under acidic conditions. So, in each tube, solutions were introduced by the following order: 1.5 mL of sample, 1 mL of solution potassium dichromate, and 2 mL of solution of $H_2SO_4$ with $Ag_2SO_4$ (adjuvant) solution. The tubes were put into a digester (thermoreactor TR420, Spectroquant, Merck) at 148 ºC, during 2 hours. After digestion, the tubes were allowed to cool to room temperature. Then, the digestates were discharged into 50mL-erlenmeyers and one drop of ferroine solution (the oxidation-reduction indicator) was added. The dichromate in excess was determined by titration with a 0.025M ferrous ammonium sulfate solution (FAS). The end of the titration was reached when the color of the solution changed from pale blue to strong orange/red. The same procedure was followed for the blank assays. The blank assays were prepared by substituting the sample volume by distilled water. A control was also prepared to standardize the titrant solution by substituting the sample volume by a standard potassium dichromate solution.

### 2.4.4 Color

For color analysis, 10 mL samples were collected from SBR1 and SBR2 along the reaction phase of different treatment cycles. These samples were clarified by centrifugation (10 min at 4000 rpm), and color measurements were performed on the supernatant.

The concentration of Acid Red 14 in these samples was determined spectrophotometrically, by reading the absorbance of samples at 515 nm (the wavelength of maximum absorbance in the visible range) using a Specord 200 spectrophotometer (Analytik Jena, Germany). Absorbance spectra between 200 and 800 nm were collected from solutions of Acid Red 14 with different concentrations and a calibration curve was established using the absorbance values at 515 nm. The concentration of dye in samples was determined based on the previously established calibration curve at 515 nm.

### 2.4.5 pH

For pH analysis, 10 mL samples were collected from SBR1 and SBR2 along the reaction phase of different treatment cycles. These samples were clarified by centrifugation (10 min at 4000 rpm), and pH measurements were performed on the supernatant using a Metrohm 6.0202.100 glass electrode connected to a Metrohm 691 potentiometer (Metrohm, Switzerland).

## 2.5 Cell membrane permeability analysis

For membrane permeability analysis, 5mL samples were collected at the beginning of the aerated phase of one treatment cycle on operational day 258. These samples were dewatered by centrifugation at 4000 rpm for 5 min and the pellet was ressuspended in 0.85% NaCl to their original volume. This steps was repeated 2 times. In the last time, the pellet was ressuspended in 2 mL 0.85% NaCl. Then, the sludge samples were stained using the LIVE/DEAD *Bac*Light Bacterial Viability Kit (Molecular Probes, Netherlands) and were observed at magnifications of 40x, under a transmission light microscope (BA200, Motic, China) fitted with a digital camera and respective software (Moticam 1000, Motic, China).

## 2.6 Extracellular polymeric substances (EPS) analysis

For extracellular polymeric substances (EPS) analysis, 5 mL samples duplicates were collected along the reaction phase of one treatment cycle on operational days 243, 250, 258 and 271. These samples were dewatered by centrifugation at 4000 rpm for 10 min and stored at -80ºC until EPS extraction and analysis were performed.

Before EPS extraction, the stored sludge samples, once at room temperature, were re-suspended in deionized water to their original volume. The resuspension was performed by mixing vigorously with a pipette until a homogeneous sludge suspension was obtained.

The extraction of the bound EPS from sludge samples was carried out by heating the mixture suspensions to 80 °C for 30 min in a water bath. Then, the suspensions were cooled down to room temperature and centrifuged at 4000 rpm for 20 min. Prior to EPS component analysis, the supernatant

was further filtered through glass microfiber filter discs (Whatman, GF/C, ø 25 mm). The protein (PN) content was determined with Pierce® BCA protein assay kit (Thermo Scientific, USA) using bovine serum albumin (BSA) as standard. The polysaccharide (PS) content was analyzed in accordance to the method described Dubois et al. (1956) with some modifications. Briefly, 1 mL of 5% phenol (w/w) in water was added to 1 mL of sample. Then, 5 mL of concentrated sulphuric acid was added rapidly, on the liquid surface. The mixtures were allowed to react for 10 min, then were mixed and allowed to react for another 30 min at room temperature. 300 µL of each tube was pipetted to a microplate and the absorbance was measured at 490 nm. Glucose was used as standard for method calibration, in a concentration range between 0 and 500 mg $L^{-1}$.

## 2.7 X-ray microtomography analysis

Sludge samples were collected directly from the Ag NPs-fed SBR1 and control SBR2 during the aerated reaction phase of one treatment cycle on operational day 243. These samples were lyophilized (Modulyo®, Edwards, US) and the material directly mounted onto an appropriate support in a self-supported mode.

X-ray microtomography is a non-destructive methodology that allowed a three-dimensional (3-D) observation of the samples. Digital radiographs can be produced using an X-ray cone incident on a rotating specimen. In this study a Skyscan1172 (Brucker®, USA) scanner was used. The experimental acquisition conditions included: X-ray source (voltage 59 kV, current = 167 µA, power 10W), direct irradiation without filtering with an exposure of 1000 ms/radiograph, rotation step of 0.5° (383 radiographs) and an image pixel size of 2.35 µm. The acquisition was performed by rotating the specimen over 180°. The instrument comprehends a 1.3 Megapixel camera which can reach spatial resolutions of 5 µm with a detail detectability of 2 µm. The maximum object diameter is 20 mm for standard operation and 37 mm with a camera offset. Reconstruction was performed with the NRecon (Brucker®) program with a GPUReconServer reconstruction engine. Around 1000 slices of the each sample were obtained after less than 1.5 minutes. 3D models and section analysis was performed with CTVox and Dataviewer free Brucker® software's. The CTvox allows the 3D virtual visualization (image or video) of the samples. The data set after acquisition consisted of transmission X-ray images presented in Hounsfield units (HU) or attenuation coefficient units ($mm^{-1}$).

## 2.8 Nuclear Microscopy

### 2.8.1. Sample preparation

Sludge samples were collected directly from the SBR during the aerated reaction phase of one treatment cycle on operational day 243. Aliquots of 50 µL of the sludge samples were directly deposited onto carbon conductive adhesive disks for microscopy (Agar Scientific, UK). The AGS were manually detached from flocculent sludge fraction under the microscope. The prepared sludge targets were then quench-frozen in liquid nitrogen to ensure biomass integrity (Pinheiro et al., 2007), transferred to a cryostat and allowed to dry at -25ºC. Granular structures were further encapsulated in a resin for microscopy (Tissue-Tek O.C.T. Compound). Then, it was rapidly quench-frozen in liquid nitrogen

followed by sectioning in a cryostat at -25ºC. Sections of 20 µm thickness were allowed to dry at -25ºC inside the cryostat. Before nuclear microscopy analysis, some sections were chosen under optical microscopy and were mounted in self supported mode.

#### 2.8.2 Experimental system and data acquisition

The samples were examined at the proton microprobe installed at the Van de Graaf accelerator of Centro Tecnológico e Nuclear/IST (Loures, Portugal). A focused 2.0 MeV proton beam of typically 3 µm was used to scan across a selected area of interest of the sample.

Data acquisition and map construction are performed with OMDAQ (Grime and Dawson, 1995). The spectra analysis and quantitative determination of elemental contents were carried out using the DAN32 (Grime, 2004) computer code. The program incorporates a graphical user interface to the PIXE analysis program and a RBS simulation and fitting module. The calculation of elemental concentrations is performed using the "Q factor" charge normalization method using simultaneous PIXE and RBS analysis (Grime 1996).

# 3. Results and Discussion

## 3.1 Ag NPs size and aggregation state

The particle size distribution in the feed suspension of Ag NPs (50 mg $L^{-1}$) is depicted in Figure 11. The average particle size in this solution was 155 ± 40 nm, which was larger than the product description (<100nm), indicating that aggregation of Ag NPs was involved.

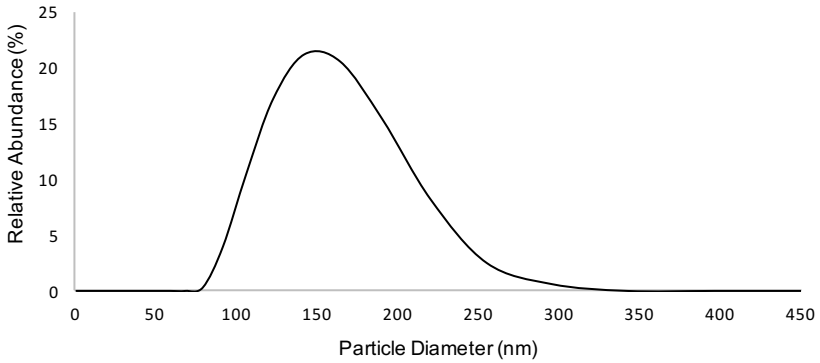


Figure 11. Size distribution of Ag NPs present in the feed solution (50mg $L^{-1}$).

The particle size of Ag NPs has a strong impact on their physicochemical processes and antimicrobial activities (Choi et al., 2008; Zhang et al., 2016). In general, it has been revealed that smaller Ag NPs have more pronounced antimicrobial activities (Agnihotri et al., 2014; Choi and Hu, 2008; Morones et al., 2005). Furthermore, Ag NPs size is affected by its aggregation state. Significant aggregation can greatly reduce specific surface area, bioavailability and toxicity of Ag NPs (Gu et al., 2014; Lok et al., 2006; Quan et al., 2015). Previously research involving the response of both individual microbial cells and sludge to the presence of Ag NPs were based on particles with a smaller diameter compared with that used in the current study (Choi and Hu, 2008; Gu et al., 2014; Liang et al., 2010;

Morones et al., 2005; Quan et al., 2015). Nonetheless, it has been reported that the silver released from Ag-functionalized textiles was in the form of particles larger than 450nm (Geranio et al. 2009; Lorenz et al. 2012).

Therefore, the Ag NPs size of the feed solution seemed to be reasonable in a textile wastewater treatment context.

## 3.2 Effects of Ag NPs on total suspended solids (TSS) measurements

The biomass content in a biological wastewater treatment reactor is usually assessed through the analysis of volatile suspended solids (VSS) and total suspended solids (TSS). As the method for TSS determination is faster than that of VSS, TSS values were commonly used as an indication of biomass content. Nonetheless, as TSS comprise biomass, non-biodegradable volatile suspended solids and inert inorganic suspended solids, the Ag NPs can have a contribution for the inorganic fraction, influencing the TSS measurement of the Ag NPs-fed SBR1. In order to assess the Ag NP influence on TSS measurements, the profiles of VSS/TSS (%) attained in the mixed liquor of the Ag NPs-fed SBR1 and in the Ag NPs-free control SBR2 were compared along the experimental period (Figure 12).

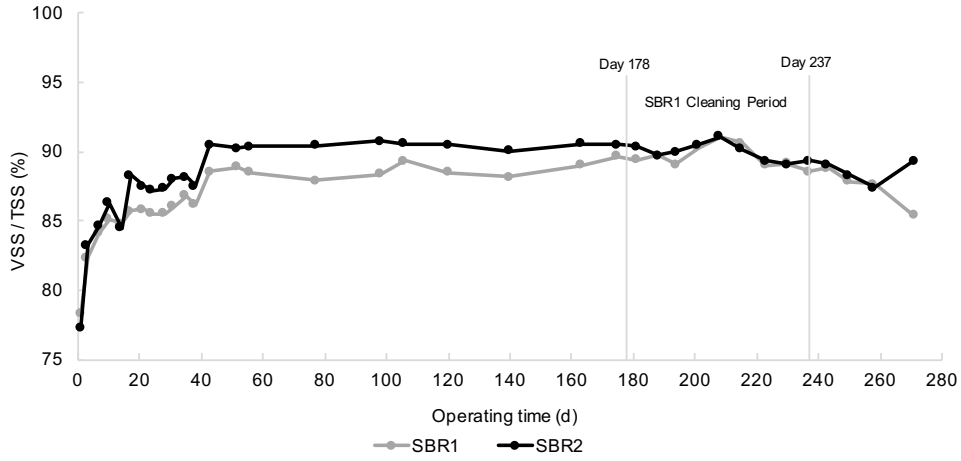


Figure 12. VSS/TSS (%) profiles attained in the mixed liquor of the Ag NPs-fed SBR1 and the Ag NPs- free control SBR2 along the experimental period of 271 days. The Ag NPs was fed to SBR1 along a 178-days operational period followed by a 60-day period during which Ag NPs were absent from the feed. After this cleaning period, Ag NPs feeding was resumed. The vertical line indicates the onset (Day 178) and the final (Day 237) of the cleaning period.

As shown in figure 12, after 20 days of operation, the VSS/TSS (%) values obtained in the mixed liquor of SBR1 along the period in which the reactor was fed with Ag NPs (up to day 178), were significantly lower than those for the Ag NPs-free control SBR2. Contrarily, during the cleaning period, the VSS/TSS (%) values were similar for both SBRs. After this period, Ag NPs feeding was resumed and again, after 20 days of operation, the VSS/TSS (%) values became lower in SBR1. These results suggest that the Ag NPs were retained by the filter (pore size 1.2 μm) during the filtration of SBR1 samples for TSS determination, contributing to the increase of the TSS values and, consequently, to the decrease of the corresponding ratio VSS/TSS (%). The Ag NPs retention can be due to the rejection of Ag NPs agglomerates having a size bigger than 1.2 μm or through the accumulation of Ag NPs

adsorbed on the biomass, which in turn is rejected by the filter.

Therefore, as the contribution of Ag NPs for the TSS values attained in SBR1 was significant, VSS values were used as an indication of biomass content, both in the SBR mixed liquor and in the discharged wastewater.

## 3.3 Effects of Ag NPs on granulation

The VSS content and SVI profiles obtained in both SBRs along the operational time are presented in Figure 13 and Figure 14, respectively. In the VSS profile, it is possible to note that in the first day of operation the level of biomass in the discharged effluent (EVSS) was high due to the poor settling properties of the flocculent sludge used as inoculum. Along the first 28 days of operation the settling time was gradually reduced from 1 hour to 5 minutes to promote aerobic granulation. The shortening of the settling time promotes the growth of fast-settling microorganism and the washout of flocculent sludge with poor settling properties (Adav et al., 2008; Gao et al., 2011; Qin et al., 2004). Thus, as expected, the EVSS of both SBRs increased on the days where the settling time was shortened. Nonetheless, in spite of the gradual decrease of the settling time, the biomass progressively accumulated in the mixed liquor (MLVSS) of both SBRs along the first 35 days of operation. At this point, due to the SBR geometry limitations, AGS could not continue to accumulate in the mixed liquor, leading to a loss of AGS in the effluent.

As can be seen in Figure 14, in general, the sludge initially also devolved excellent settling properties, as the $SVI_5$ and $SVI_{30}$ values consistently decreased in both SBRs up to day 35, reaching 62 and 40 mL gTSS-1 in SBR1, 62.4 and 39.6 mL $gTSS^{-1}$ in SBR2, respectively. Furthermore, both reactors presented progressively converging values of $SVI_5$ and $SVI_{30}$. Therefore, it was possible to conclude that aerobic granule formation was successfully achieved during this period, irrespective the presence of Ag NPs.

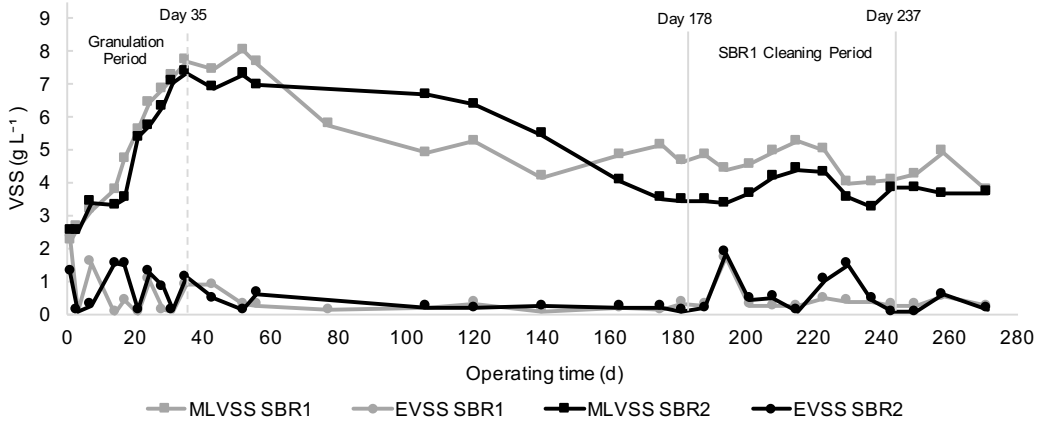


Figure 13. Volatile suspended solids profile obtained from the mixed liquor (MLVSS) and in the discharged effluent (EVSS) of the Ag NPs-fed SBR1 and of the Ag NPs-free control SBR2 along the experimental period of 271 days. The Ag NPs were fed to SBR1 along a 178-day operational period followed by a 60-day period during which Ag NPs were absent from the feed. After this cleaning period, Ag NPs feeding was resumed. The vertical dashed line indicates the end of the granulation period (Day 35), while the vertical solid lines indicate the onset (Day 178) and the end (Day 237) of the cleaning period.

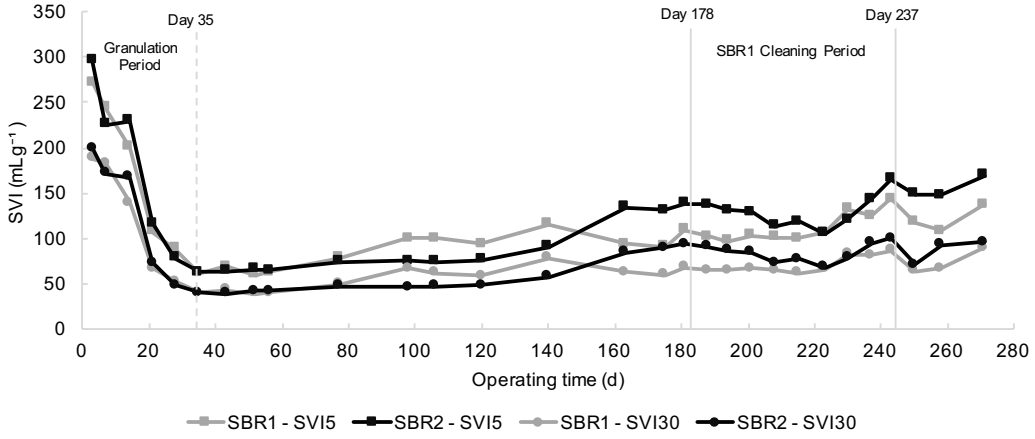


Figure 14. Sludge volume index (SVI) profiles along the experimental time of 271 days, including SVI values measured after 5 min settling (SVI5) and after 30 min settling (SVI30) for the Ag-NPs-fed SBR1 and the Ag NPs-free control SBR2. The Ag NPs were fed to SBR1 along a 178-day operational period followed by a 60-day period during which Ag NPs were absent from the feed. After this cleaning period, Ag NPs feeding was resumed. The vertical dashed line indicates the end of the granulation period (Day 35), while the vertical solid lines indicate the onset (Day 178) and the end (Day 237) of the cleaning period.

## 3.4 Effects of Ag NPs on AGS stability

Successful aerobic granulation was attained after 35 days of SBR operation and on day 56 of the operation the Ag NPs-fed SBR1 showed a loss in its MLVSS content (Figure 13), whereas the Ag NPs-free SBR2 only exhibited a significant reduction of biomass on day 120 of the operation. As expected, the SVI profile (Figure 14) trend was consistent with that observed in the MLVSS profile, since the biomass content present in the mixed liquor is dependent of the sludge setting properties. Specifically, while the granular sludge content of the Ag NPs-free SBR2 remained stable and maintained good settling properties up to day 120, the Ag NPs-fed SBR1 showed a deterioration of the sludge settling capacities on day 56, confirmed by the increase in the SVI values. Both the reduction of the biomass content in the mixed liquor and the loss of sludge settling capacities indicated the loss of AGS structural stability. Furthermore, the early AGS deterioration observed in the Ag NPs-fed SBR1 suggested that Ag NPs played a role on this phenomenon. It was noted that despite the MLVSS decrease in both SBRs, significant EVSS levels were not registered during this period. This can be explained by a loss of structural stability and consequent MLVSS decrease at specific cycles in which EVSS were not analyzed.

The loss of structural stability is one of the most serious barriers to full scale applications of AGS technology (Corsino et al., 2016; Lee et al., 2010; Liu and Tay, 2007). Outgrowth of filamentous organisms (Adav and Lee, 2008; Kreuk et al., 2007) and granule breakup due to the weaken of their core (Corsino et al., 2016; Lemaire et al., 2008; Toh et al., 2003; Zheng and Yu, 2007) are the major patterns of structural stability loss in AGS systems.

In the present study, outgrowth of filamentous organisms was not observed. In fact, the anaerobic feed mode and the high shear stress imposed in the system act as a selective pressure, restraining the proliferation of filamentous bacteria (Beun et al. 1999; Kreuk et al. 2007; Adav et al. 2008). Therefore, the weakening of the AGS core was likely the cause of the stability loss observed in

the long-term operation. This phenomenon is closely related to mass transfer and diffusion limitations throughout the granule structure, which limit the oxygen and substrate availability in its inner region. Under these conditions, certain starved anaerobic organisms start to consume EPS to sustain their growth. Furthermore, metabolic products, such as inhibitors, hydrolytic exoenzymes and toxic substances, accumulate in the inner region affecting the EPS matrix and the metabolic activity of functional microbes. These events can cause cell death and the appearance of cavities in the core of the granules, weakening their physical structure. Consequently, granules become more prone to break under shear stress (Toh et al., 2003; Zhang et al., 2015; Zhou et al., 2016).

The diameter of the granules and the clogging of their pores and channels have been pointed as the main reasons for the limitations in the flow of nutrients and oxygen from the bulk into the inner layers of the granular biomass (Corsino et al., 2016; Lemaire et al., 2008; Toh et al., 2003; Zheng and Yu, 2007). The diameter significantly influences the stability of the aerobic granules, since large granules are more prone to mass transfer and diffusion limitations. Zhang et al. (2015) reported that mature granules with small diameter (< 800 μm) were stable without disaggregation during an experiment period of 220 days. Verawaty et al. (2013) also showed that granules did equilibrate towards a common critical size of around 600–800 μm and that above this value granule breakage and attrition outweighed granule growth, causing an overall reduction in granule size. The granule size obtained was only up to 0.65 mm, indicating that the size was probably not the cause of AGS destabilization in the system. Therefore, the clogging of granule pores was possibly the key reason for core weakening and consequent AGS deterioration in the system. According to Lemaire et al. (2008), pore clogging is related to an excess of extracellular polymeric substances (EPS) production. Recently, Corsino et al. (2016) further reported that an enrichment in EPS proteins (PN), which are hydrophobic substances, can lead to an increase in granule hydrophobicity and density. As a result, granules become more compact and thick, limiting the penetration of nutrients.

In the current study, the presence of Ag NPs can have contributed to the pore clogging phenomenon, thus promoting the early loss of stability observed in AGS-SBR1. Specifically, Ag NPs can have accumulated within granule pores, leading directly to their clogging, or can have either caused a shift in the composition of the microbial consortium by an increase in EPS or PN producer organisms, or the existing microbial community may have activated the metabolic pathway of EPS or PN production leading to a premature excess of EPS or an enrichment in PN. Previous research suggested that bacteria acquire higher tolerance to Ag NPs through the production of more EPS (Sheng and Liu, 2011; Tan et al., 2015; Zhang et al., 2014). Thus, the increase in EPS production by AGS microorganisms was most probably a response to protect themselves from the toxic effects of the Ag NPs/$Ag^{+}$. In the study of Quan et al. (2015), despite the AGS SBR with Ag NPs showing an EPS level similar to that of the Ag NPs-free control SBR after 69 days of operation, its EPS components significantly changed, with an apparent PN content increase. These authors reported that one possible explanation for the elevated production of proteins was the induction of heat shock-like proteins as a defense mechanism against high concentrations of heavy metal ions. Another possible reason for the observed EPS changes was the additional mechanical shear stress promoted by collisions between Ag NPs agglomerates and aerobic granules, as it is known that shear stress stimulates the production of EPS (Adav et al., 2007;

Gao et al., 2011; Liu and Tay, 2004; Zhu et al., 2013).

The loss of AGS stability resulted in deterioration under shear stress with the formation of small fragments with poor settling characteristics. Part of these fragments flowed out with the effluent stream and part aggregated again, forming new granules. As result, in long-term operation, the MLVSS (Figure 13) and SVI (Figure 14) profiles obtained for both SBRs reached a dynamic steady-state in which granulation and degranulation continuously occurred. Thus, the mixed liquor of both SBRs can be considered as a hybrid system of both flocculent and granular sludge. It is noted that the values of SVI and MLVSS observed during the granulation phase (first 35 days of operation) were no longer attained, suggesting that the properties of newly formed granules differ from that of the granules initially formed due to the heterogeneity of structures with less biological activity from which they had to re-develop (Lemaire et al., 2008).

As can be seen in Figures 13 and 14, the steady-state values of MLVSS and SVI obtained for the Ag NPs-fed SBR1 differ from those of the control SBR2. In the SVI profile, the values obtained for SBR1 tended to be lower in the long-term, suggesting that the presence of Ag NPs had a positive influence on the sludge settling capacities. Reinforcing this idea, it was also noted that during the cleaning period, the $SVI_5$ and $SVI_{30}$ values gradually converged and, once the Ag NPs feeding was resumed, the values obtained for SBR1 were lower again. The SVI profile trend was consistent with the higher steady-state MLVSS values observed for the Ag NPs-fed SBR1, since the improved sludge settling capacities prevented the washout of granular sludge in the effluent stream.

These results are coherent with the effects of Ag NPs on the AGS loss of stability above discussed. Ag NPs can absorb and accumulate on the AGS, within the granule pores or on their surface, increasing directly their total density, thus improving their settling velocity. One the other hand, although a premature excess of EPS induced by the presence of Ag NPs may have induced the disintegration of the aerobic granules, EPS also contribute to a more compact and thick granular structure (Corsino et al., 2016). As a consequence, in the presence of Ag NPs, AGS can settle faster and pack more effectively in the SBR. The additional mechanical shear stress promoted by collisions between Ag NPs agglomerates and granules can not only induce the thickening of granules by enhancing EPS production, but also promote granule abrasion, resulting in smaller granules with a smoother outer surface and improved settling properties.

## 3.5 Effects of Ag NPs on sludge density

Microcomputerized tomography (μCT) allowed a three-dimensional (3D) reconstruction of the sludge samples from Ag NPs-fed SBR1 (Figure 15-A) and control SBR2 (Figure 16-A). A cross-section of each sample was also chosen (Figure 15-B and 16-B, respectively) and a representative attenuation profile was traced (Figure 15-C and 16-C, respectively). The 3D model of the Ag NPs-exposed sludge clearly showed more frequent high attenuation regions compared to that in the control. These high attenuation spots likely correspond to Ag NPs agglomerates disseminated in the biomass network, as X-rays are significantly more attenuated in Ag than in the biomaterial light element matrix. This can also be observed in more detail in the selected attenuation profiles. The attenuation profile of the Ag NPs exposed sludge sample showed sharp and well-defined peaks corresponding to particle features in the

cross-section, likely Ag NPs agglomerates. This pattern contrasted with the irregular and less prominent peaks of the attenuation profile obtained for the control sample, where the relationship between attenuation changes and particles are not so clear.

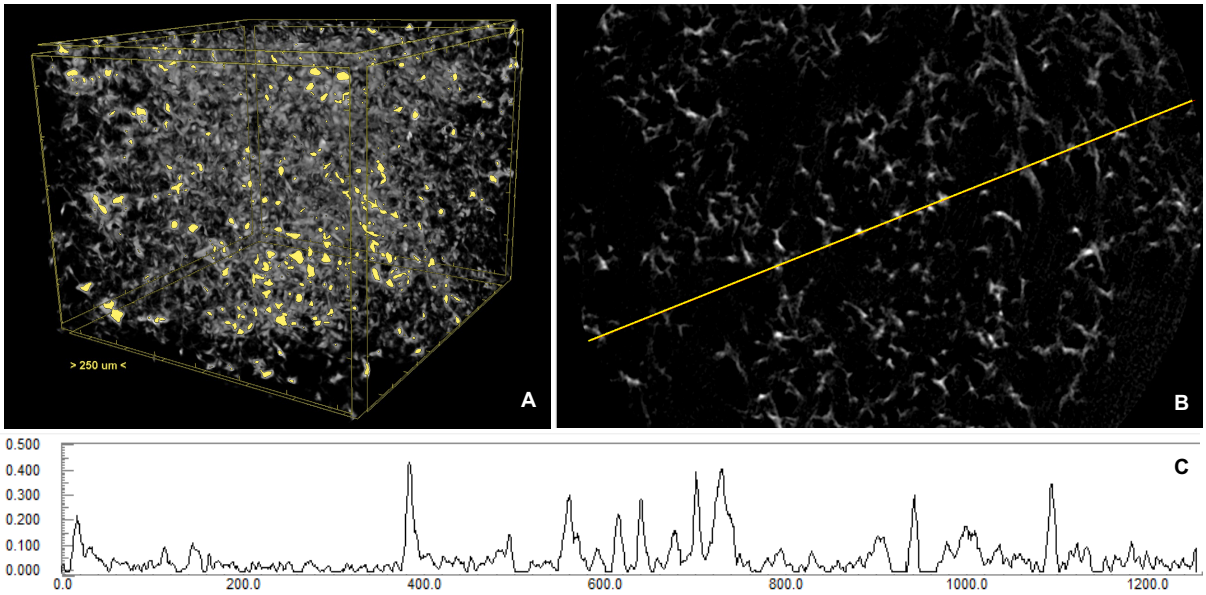


Figure 15. µCT analysis of the Ag NPs-fed SBR1 sludge sample. A - 3D model of sludge sample. Attenuation is represented by a grey scale: high attenuation – light grey, to low attenuation – dark grey. The high values of X-ray attenuation are highlighted with yellow color. B –Selected cross-section. Attenuation is also represented by a grey scale: high attenuation – light grey, to low attenuation – dark grey. The yellow row represents the attenuation profile represented in C. Attenuation units (y axis) are arbitrary, distance units (x axis) are in µm.

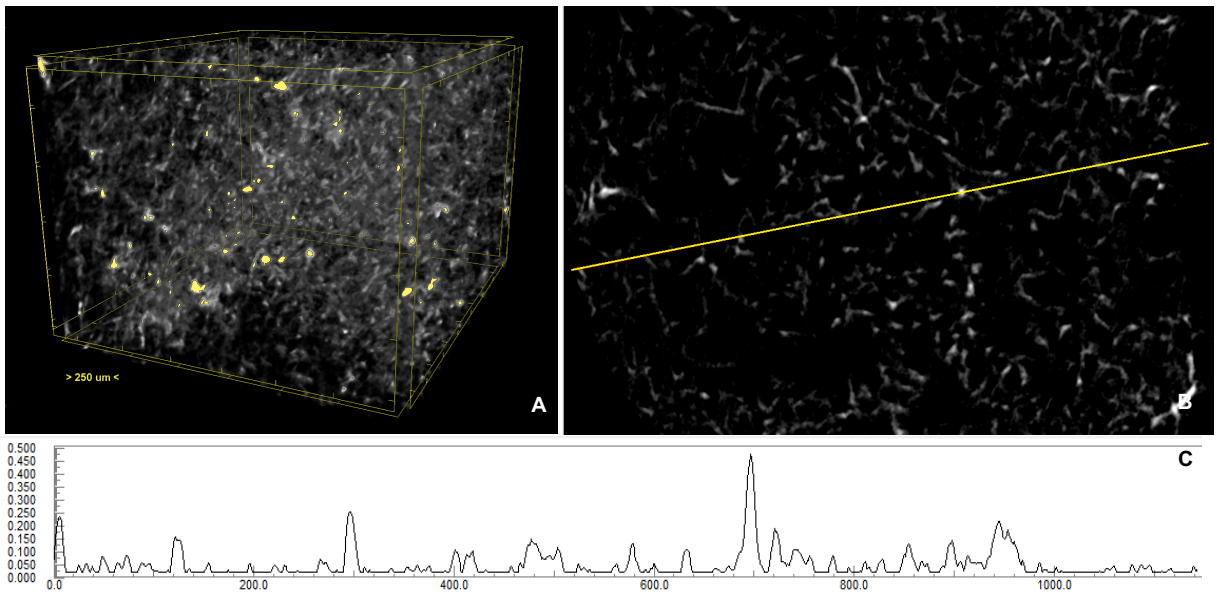


Figure 16. µCT analysis of the control SBR2 sludge sample. A - 3D model of sludge sample. Attenuation is represented by a grey scale: high attenuation – light grey, to low attenuation – dark grey. The high values of X-ray attenuation are highlighted with yellow color. B –Selected cross-section. Attenuation is also represented by a grey scale: high attenuation – light grey, to low attenuation – dark grey. The yellow row represents the attenuation profile represented in C. Attenuation units (y axis) are arbitrary, distance units (x axis) are in µm.

The different profiles of X-ray attenuation observed in the μCT analysis of the biomaterials can be interpreted as differences in density of the material due to the presence of Ag NPs, as the attenuation is proportional to the density of the specific elements present in the matrix (Rajczakowska et al., 2015).

Taking this into account, the differences in attenuation observed permitted to conclude that the Ag NPs accumulated in sludge can effectively contribute to an increase in sample mass density, which is in line with previous results as discussed in section 3.4.

## 3.6 Effects of Ag NPs on SBR treatment performance

### 3.6.1 COD removal

The carbon load removal performance of the SBRs was evaluated through measurements of residual soluble COD levels along the experimental period. The overall residual COD values registered along the reported experimental time are represented in Figure 17. The initial high residual COD levels attained in both SBRs were probably due to the change in the nature of the main carbon substrate, from domestic wastewater to a synthetic textile wastewater with hydrolyzed hydroxypropyl starch as the carbon source. However, the sludge in both SBRs rapidly adapted to the new carbon source, reaching stable COD removal levels within the 80 to 90% range after 17 days of operation. In the Ag NPs-fed SBR1, the COD removal yield decreased on day 77, probably due to the considerable loss of mixed liquor biomass on that day (Figure 13). After that day, both SBRs maintained stable COD removal yields during the whole experimental period, irrespective of the presence of Ag NPs. Also, Quan et al. (2015) showed that Ag NP-fed reactors maintained a high COD removal similar to the Ag NPs-free control reactor throughout the whole operational period. Nonetheless, these authors suggested that probably an influent COD of 1000 mg $O_2$ $L^{-1}$ was not sufficient to observe the influence of Ag NPs exposure in COD removal.

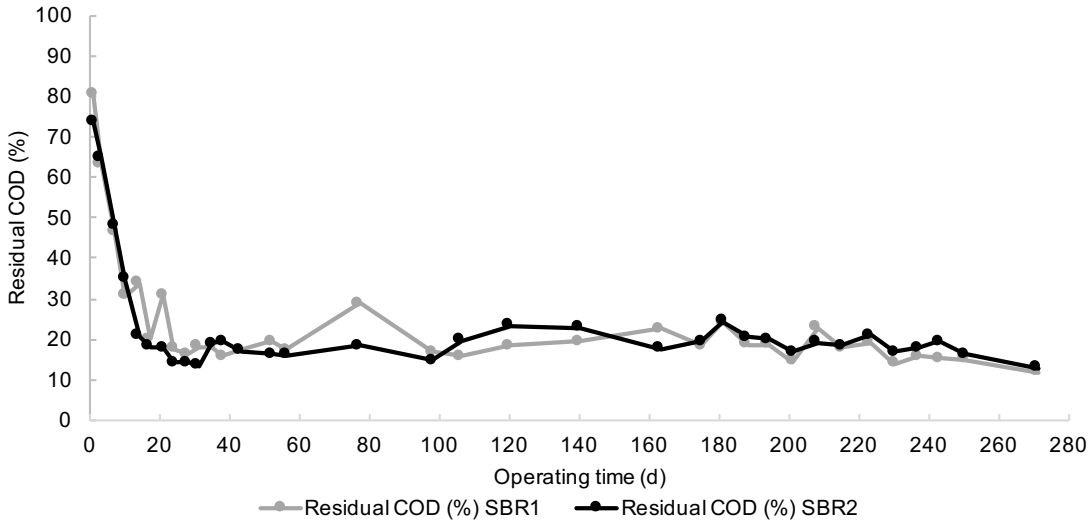


Figure 17. Overall residual COD yields in the Ag NPs-fed SBR1 and the Ag NPs-free control SBR2 along the experimental time of 271 days.

The residual COD profiles for SBR1 and SBR2 along the reaction phase of one treatment cycle selected as example (day 56) are shown in Figure 18. In the first 0.5h, the COD removal in the anaerobic phase reached up to 40% in both SBRs and thereafter, it was not further anaerobically removed from the mixed liquor. This profile suggests that, during the feast phase, easily biodegradable COD was taken up from the mixed liquor by slow-growing microorganisms (polyphosphate or glycogen accumulating organisms) and converted into storage polymers. When these microorganisms reached their maximum storage capacity, the removal of COD ceased. In the subsequent aerobic period an additional 40% of extracellular COD was removed from the mixed liquor and the storage polymers could have been used for growth throughout the granule at a relatively slow rate (de Kreuk and van Loosdrecht, 2004). The remaining 20% of residual COD comprises possibly non-biodegradable material.

The consumption of easily biodegradable substrates in the presence of oxygen can lead to the formation of filamentous outgrowth with consequent unstable granulation and poor settling biomass characteristics. Thus, a high removal yield of easily biodegradable COD during the anaerobic phase is determinant to enhance granule formation and stability (Kreuk et al., 2007). As the COD removal yield achieved in the anaerobic phase of SBR1 and SBR2 is similar to that achieved in the aerobic phase, it was possible to conclude that the microbial population present in both SBRs had a considerable capacity for anaerobic substrate uptake with intracellular polymer storage and, therefore, stable aerobic granules have been formed in the SBRs.

The COD removal profiles of SBR1 and SBR2 were similar, indicating that the presence of Ag NPs with a concentration of 5mg $L^{-1}$ at the onset of the reaction phase did not have a significant influence on the COD removal capacity of the aerobic granules. Similar behavior was observed for the remaining treatment cycles.

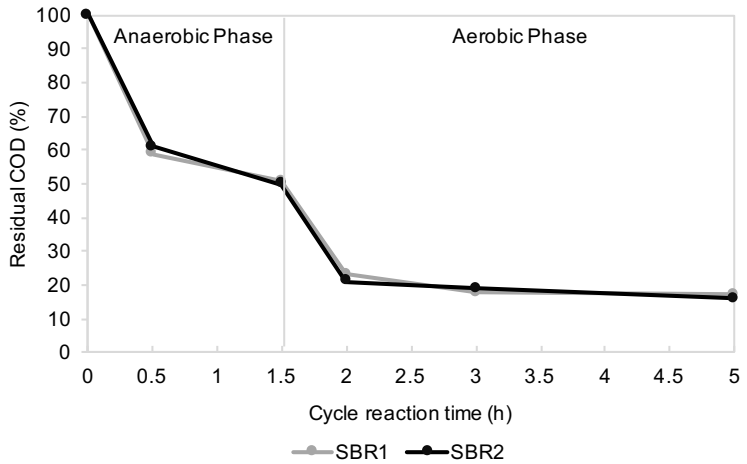


Figure 18. Residual COD profiles along the 5-h reaction phase of one typical SBR cycle (day 56) in the presence (SBR1) and absence (SBR2) of Ag NPs. Similar profiles were observed for the remaining treatment cycles. The vertical line indicates the onset of aeration.

### 3.6.2 Color Removal

The color removal performance of the SBRs was assessed through measurements of residual color levels along the experimental period. The overall residual color values registered along the reported experimental time are represented in Figure 19. The biomass rapidly adapted to the synthetic

textile wastewater containing the azo dye AR14 since color removal levels higher than 80% were attained after 3 days of operation in both SBRs. Similarly to COD, the color removal yield decreased on day 17, probably due to the considerable loss of biomass in the effluent on that day (Figure 13). As the biomass accumulated again in the both SBRs, color removal yield was also gradually recovered.

After the first 31 days, the color removal levels of SBR1 and SBR2 were similar along the reported experimental time, indicating that the presence of Ag NPs with a concentration of 5mg $L^{-1}$ at the onset of the reaction phase did not have a significant influence on the biodecolorization process of the azo dye AR14 by AGS.

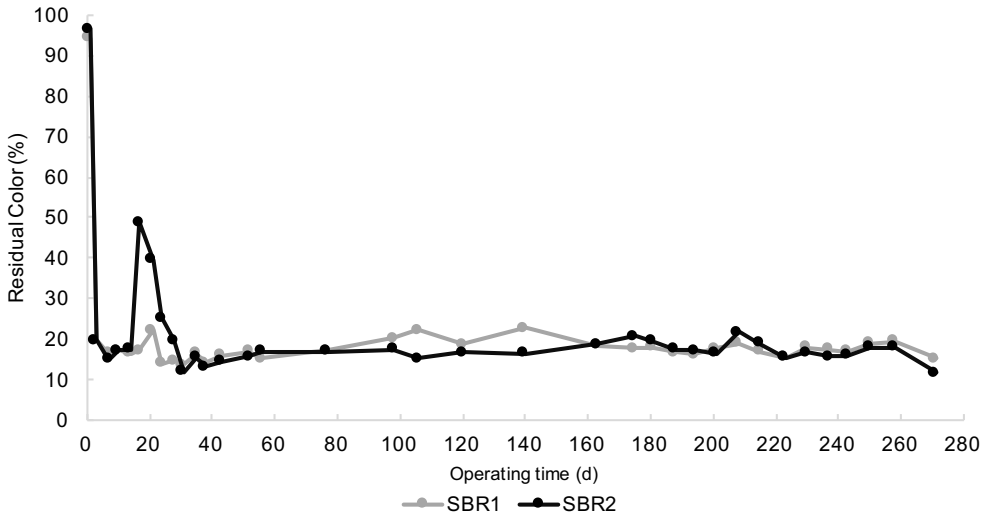


Figure 19. Overall residual color yields in the Ag NPs-fed SBR1 and the Ag NPs-free control SBR2 along the experimental time of 271 days.

Bacterial decolorization of azo dyes is generally accomplished through anaerobic azo bond reduction with colorless aromatic amine formation (Franca et al., 2015). Figure 20 represents the particular case of AR14 decolorization. Residual color profiles for SBR1 and SBR2 along the reaction phase of one SBR cycle selected as example (day 120) are shown in Figure 21. As expected, the color removal occurred almost solely in the anaerobic reaction phase. Both SBRs showed similar residual color profiles along the cycle reaction time, suggesting that the exposure to Ag NPs did not have a significant influence on the anaerobic biodecolorization process. Similar behavior was observed for the remaining treatment cycles.

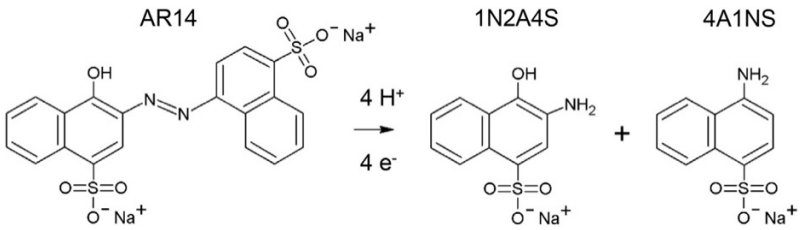


Figure 20. Acid Red 14 (AR14) descolorization reaction. The Azo bond present in the chemical structure of the dye (AR14) are reduce and two colorless aromatic amines, 1-naphthol-2-amino-4-sulfonic acid (1N2A4S) and 4-amino-naphthalene-1-sulfonic acid (4A1NS), are formed (Franca et al., 2015).

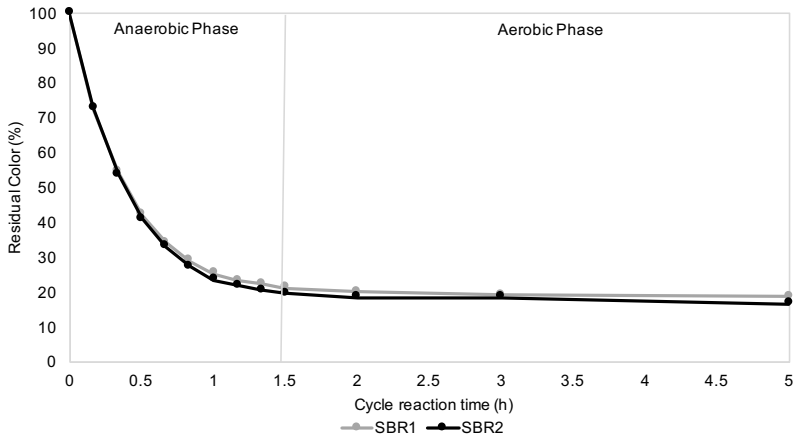


Figure 21. Residual color profiles along the 5-h reaction phase of a typical SBR cycle (day 120) in the Ag NPs- fed SBR1 and the Ag NPs-free control SBR2. Similar profiles were observed for the remaining treatment cycles. The vertical line indicates the onset of aeration.

Therefore, in the present system both COD and color removal yields and profiles of the Ag NPs-fed SBR1 and the Ag NPs-free control SBR2 showed to be similar along the reported experimental time, suggesting that the presence of Ag NPs did not have a significant influence in the SBR treatment performance.

## 3.6 Effects of Ag NPs on cell membrane permeability

Membrane permeability and sludge cell integrity were assessed using a mixture of SYTO 9 green-fluorescent nucleic acid stain and the red-fluorescent nucleic acid stain, propidium iodide (PI). These stains differ both in their spectral characteristics and in their ability to penetrate healthy bacterial cells. When used alone, the SYTO 9 stain generally labels all bacteria in a population – those with intact membranes and those with damaged membranes. In contrast, PI penetrates only bacteria with damaged membranes, causing a reduction in the SYTO 9 stain fluorescence when both dyes are present. Thus, comparing the stained cells present in sludge samples collected from the Ag NPs-fed SBR1 and the control SBR2 it was possible to infer the influence of Ag NPs on membrane permeability of the exposed sludge cells.

As can be seen in Figure 22 –A1 and –A2, the examined sludge from samples collected on day 258 consisted of AGS presenting a structure with a regular, smooth and spherical shape with a well-defined outer surface, surrounded by flocculent sludge with a loose, fluffy and irregular structure. The presence of Ag NPs could be further identified by a darker color in the Ag NPs-fed SBR1 sludge, mainly associated to the flocculent structures.

Both sludge fractions exposed to Ag NPs showed no significant difference compared to control in terms of dead cells (Figure 22 (B1 –B2)) and total cells (Figure 22 (C1–C2)), indicating that the cell membranes were not damaged in the presence of Ag NPs. Choi & Hu 2008 also assessed the membrane integrity of Ag NPs-exposed *Escherichia coli* cells using LIVE/DEAD assays and indicated that there was no evidence of cell membrane leakage in the presence of Ag NPs at 1mg/L. On the contrary, other studies demonstrated that Ag NPs attached to the sulphur-containing proteins present in the *Escherichia coli* membrane and their accumulation caused changes on membrane permeability

through the formation of pores, dissipation of the adenosine triphosphate (ATP) pool and proton motive force, and finally cell death (Gogoi et al., 2006; Lok et al., 2006; Morones et al., 2005; Sondi and Salopek-Sondi, 2004). Recently, Gu et al. (2014) and Quan et al. (2015) assessed the integrity and permeability of cells exposed to Ag NPs in AGS systems. Theses authors used the level of extracellular lactate dehydrogenase (LDH) released from damaged cells as an indicator of membrane permeability and integrity and revealed that exposure of AGS to high Ag NPs dosage (50 mg $L^{-1}$) induced the release of LDH. This indicated that the integrity of AGS cells was damaged in the presence of Ag NPs.

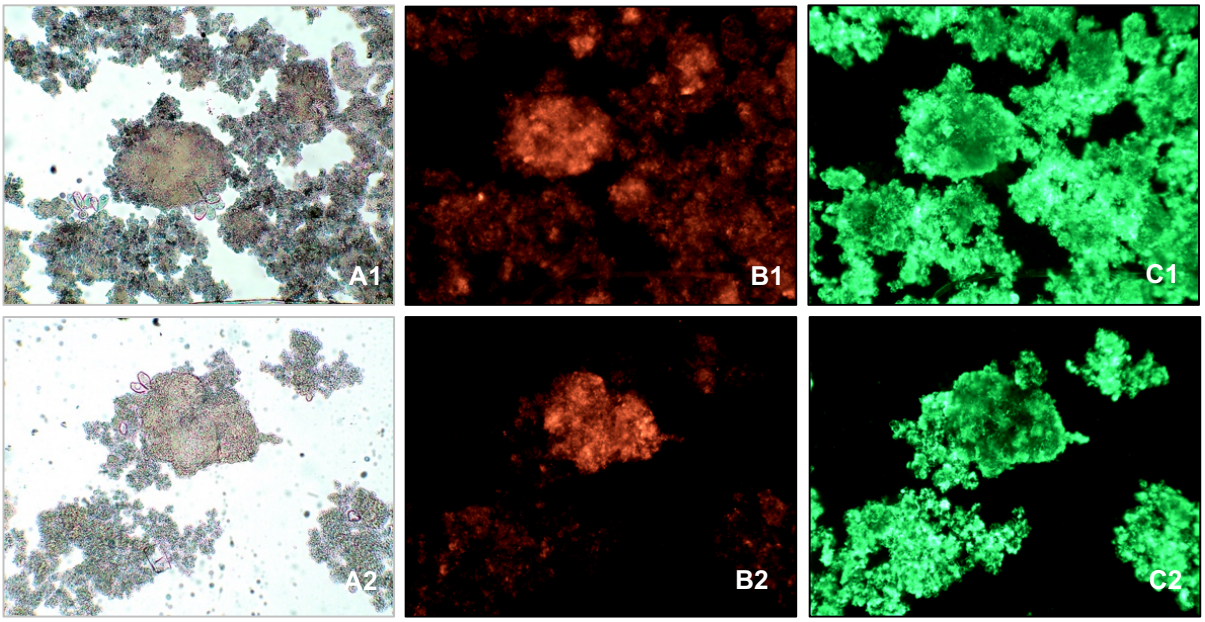


Figure 22. Ag NPs influence on cell membrane permeability inferred from LIVE/DEAD assays. Optical microscopy images of sludge samples from the Ag NPs-fed SBR1 (A1, B1 and C1) and the control SBR2 (A2, B2 and C2) without stain (A1 and A2), stained with propidium iodide (B1 and B2) and SYTO 9 (C1 and C2). The SYTO 9 stain labels all bacteria in a population (total cells). PI penetrates only bacteria with damaged membranes (dead cells).

Although the presence of Ag NPs may have contributed to the early loss of stability observed in AGS-SBR1, apparently it did not influence neither SBR treatment performance nor cell membrane integrity in the present system, contrarily to the reports of other authors, as mentioned before. In fact, wastewater treatment systems have very complex physicochemical and biological characteristics and many factors can affect the ecotoxicity of Ag NPs/$Ag^{+}$, including particle size and homoaggregation, the protective role of EPS and the AGS special structure.

### 3.7 Effects of Ag NPs on extracellular polymeric substances (EPS)

As discussed above, the microorganisms in AGS possibly induced alterations in EPS production as a response to the presence of Ag NPs, which further influenced the AGS structural stability and settling properties. Furthermore, it has been reported that the EPS components can play a significant protective role to the inner microorganisms against Ag NPs/$Ag^{+}$(Geyik and Çeçen, 2016; Kang et al., 2014; Sheng et al., 2010; Wang et al., 2016), which can possibly have contributed to the observed minimal effects of Ag NPs in membrane permeability and SBR treatment performance. Thus, to elucidate the mechanisms responsible for these events, EPS was extracted from samples of the Ag

NPs-fed SBR1 and from the Ag NPs-free control SBR2 mixed liquor along the reaction phase of different SBR cycles and their major constituents, i.e. proteins (PN) and polysaccharides (PS), were analyzed.

To our knowledge, a standard method for EPS extraction from aerobic granules is still not established. The extraction procedure must be selected for each case, considering the specific needs and constraints. The strategies of EPS extraction from aerobic granules are often inspired by protocols applied to activated sludge flocs. However, extracting EPS from aerobic granules is more difficult than from sludge flocs due to their low surface-to-volume ratio (Adav and Lee, 2008; Liu and Fang, 2002; Mcswain et al., 2005). Mcswain et al. 2005 extracted EPS from aerobic granules and reported that effective EPS extraction required pre-homogenization (980rpm) of the aggregates due to the large size of the granules. Adav & Lee 2008 also reported that using pre-ultrasound (120W) largely improved the EPS extraction from compact aerobic granules. Nonetheless, a harsh pre-treatment method, as homogenization (980rpm) or ultrasound (120W), can promote the occurrence of cell lysis and the release of intracellular components.

As verified previously in the current work, the mixed liquor of both SBRs on the operational period in which samples were collected can be considered as a hybrid system of both flocculent and granular sludge. Thus, considering the sludge characteristics and the comparative nature of the aim of this study, a milder method was preferred, decreasing the probability of occurrence of cell lysis in this step. In this way, samples were only pre-treated by mixing vigorously with a pipette until a homogeneous sludge suspension was obtained. Heat treatment was the extraction method chosen for being easy and inexpensive to perform, not requiring sophisticated equipment. Furthermore, comparing to other physical extraction techniques, this protocol is reported to lead to the highest EPS extraction efficiency (Antonelli et al., 2011). Besides, extract contamination by chemical reagents is avoided, making the subsequent analysis easier (Pal and Paul, 2008b; Sheng et al., 2010).

The extraction efficiency and the qualitative EPS composition varies significantly according to the selected method for EPS extraction, as can be confirmed in Table 2. In the present study, the PN and PS content yielded from the EPS extracted was between 44.7–72.4 mg $g^{-1}$ VSS and 31.5–49.2 mg $g^{-1}$ VSS for the control SBR2, respectively. The PN/PS ratio obtained for this SBR varied from 1.3 to 1.8. Both ranges of values are comparable with those reported in the literature for heat treatment (Table 2), validating the procedure used for EPS extraction.

Previous research provided direct experimental evidence that there is a dynamic change of aerobic granules-associated EPS during an SBR cycle comprising a short substrate feast phase and a relatively long famine phase (Wang et al. 2006; Zhu et al. 2012; Deng et al. 2016). It is also known that a large fraction of the EPS produced can be utilized by microorganisms as sources of carbon and energy during the famine phase (Ortega et al., 2009; Sheng et al., 2010; Wang et al., 2007). Therefore, the EPS production and consumption processes appear to be closely dependent on the availability of external substrate in each SBR cycle.

Figure 23 shows the mean PS profile obtained along the reaction phase of the studied AGS-SBR treatment cycles and a representative example of the residual COD profile (day 56) for the Ag NPs-fed SBR1 and the control SBR2. As expected, it was observed an increase of PS content in the first 0.5h, as easily biodegradable COD was removed from the mixed liquor. Subsequently, a decrease

in the PS content occurred during the starvation phase. It was also observed that the biodegradable EPS produced in the feast phase was consumed during the subsequent famine phase. Similar PS behavior was reported by Wang et al. (2006), Zhu et al. (2012) and Deng et al. (2016). Although there was a small difference between the average PS profile in the anaerobic phase of SBR1 and SBR2, the PS content values and their trend did not differ significantly. Therefore, this indicates that the presence of Ag NPs did not affect the dynamic change of PS along the reaction phase.

The average PN profile obtained along the reaction phase of the studied treatment cycles and a representative example of the pH profile (day 243) for the Ag NPs-fed SBR1 and the control SBR2 are shown in Figure 24. It was expected an increase in PN content, as COD was removed from the mixed liquor. Instead, a decrease of the PN content was observed during the anaerobic phase, similarly to the behavior detected in the pH profile. Although the phosphate buffer included in the synthetic textile wastewater was sufficient to maintain the pH in the range of 6.3 to 6.8, there is slight acidification was observed during the anaerobic phase. This behavior was probably due to the production of volatile fatty acids during the anaerobic fermentation of the carbon source. After the start of aeration, this trend was reversed and the PN profile acquired higher values. As mentioned before, EPS can be subdivided into bound EPS and soluble EPS. In this comparative study, it was only analyzed the bound-EPS fraction and it was considered as representative of the EPS present in the sludge samples. Nonetheless, whenever the pH of the medium moves away from the isoelectric point of a protein molecule, its solubility increases. Thus, it is possible that the reduction detected in the PN content of the bound EPS was related to the slight acidification of the medium in the anaerobic phase, as some proteins might have solubilized. Similar pH profiles were achieved for Ag NPs-fed SBR1 and control SBR2, suggesting that the presence of Ag NPs did not affect the pH profile. On the contrary, considerably higher PN levels were obtained for the Ag NPs-free SBR2 than for the Ag NPs-fed SBR1. This can be explained by limitations of the PN quantification method. The bicinchoninic acid (BCA) protein assay combines the reduction of $Cu^{2+}$ to $Cu^{+}$ by protein in an alkaline medium with the colorimetric detection of the $Cu^{+}$ by BCA. The color development results from the reaction of two molecules of BCA with one $Cu^{+}$, forming the complex 2(BCA)–Cu. Nonetheless, this reaction is strongly influenced by four amino acid residues, including cysteines (Cys). Specifically, in the presence of proteins enriched in Cys, the $Cu^{+}$ can form the complex BCA–Cu–Cys and Cys–Cu–Cys, in addition to the 2(BCA)–Cu complex, producing an overestimated result (Huang et al., 2010; Olson and Markwell, 2007). Therefore, as Ag NPs/$Ag^{+}$ has a strong affinity with the thiol (−SH) group of Cys present in EPS proteins (Behra et al., 2013; Le Ouay and Stellacci, 2015; Levard et al., 2012; Mcgillicuddy et al., 2016), it is possible that Ag NPs/$Ag^{+}$ hinder the formation of these complexes. This means that the PN levels observed for the Ag NPs-free SBR2 could have been overestimated by limitations of the method. Although this result has prevented the study of the behavior of PN along the reaction phase of the studied treatment cycles, it permitted to conclude that the Ag NPs/$Ag^{+}$ interacted with this EPS component, suggesting that PN possibly take part in the reported protective role of EPS to the inner microorganisms against Ag NPs/$Ag^{+}$ in this system.

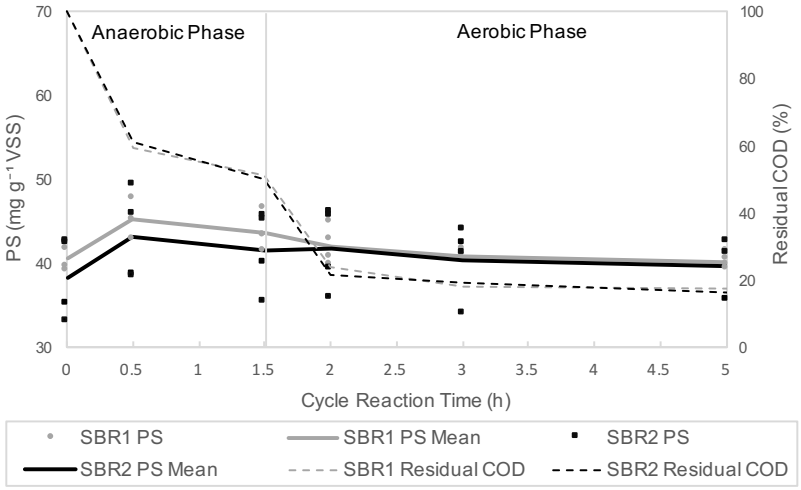


Figure 23. Average PS profile obtained along the reaction phase of the studied treatment cycles and a typical example of the residual COD profile (day 56) for the Ag NPs-fed SBR1 and the control SBR2. The vertical line indicates the onset of aeration.

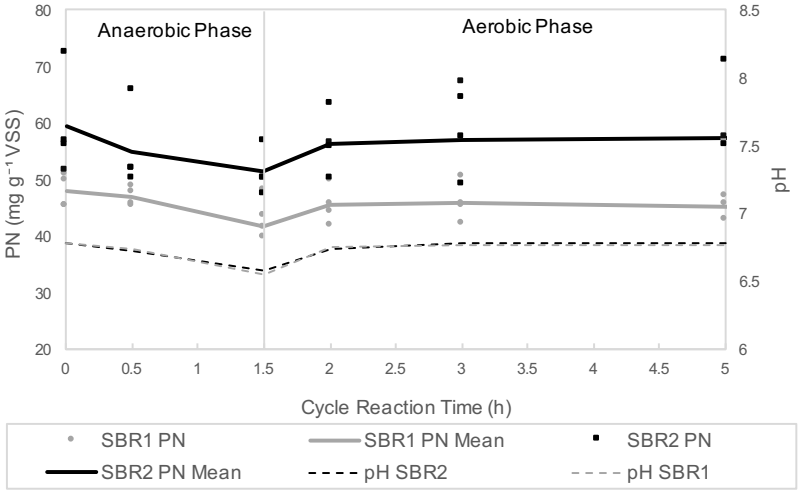


Figure 24. Average PN profile obtained along the reaction phase of the studied treatment cycles and a typical example of the pH profile (day 243) for the Ag NPs-fed SBR1 and the control SBR2. The vertical line indicates the onset of aeration.

## 3.8 Sludge components characterization and Ag NPs distribution

Nuclear microscopy was applied to image elemental distribution, as well as to perform a quantitative elemental analysis of the Ag NPs-containing sludge samples. Both flocculent and granular sludge were present in the SBR samples collected for nuclear microscopy examination. The sample preparation methodology adopted aimed the separation of these two sludge fractions and ensure that elemental contents and Ag NPs burdens in AGS and flocculent sludge could be properly analyzed and estimated. As can be observed in Figure 25–A, the flocculent sludge was separated from the AGS, although some remaining flocculent sludge involving the granule could not be completely detached. In AGS, it was also possible to distinguish an external gel-like layer surrounding the spheroid structure of the granule. Similar gel-like layers, mainly constituted by loosely bound EPS (LB-EPS), have previously been reported by Sheng et al. (2010). Also, Corsino et al. (2016), through microscopic observations,

noted the development of a gelatinous film at the surface of aerobic granules and associated it to an excess of EPS. Additionally, it was evident in the Figure 25–B3 that the flocculent matrix shrunk during the dehydration process, contrarily to the granular sludge (Figure 25 B1–B2). This can have occurred due to the high water content and loose structure characteristic of flocculent sludge (Gao et al., 2011).

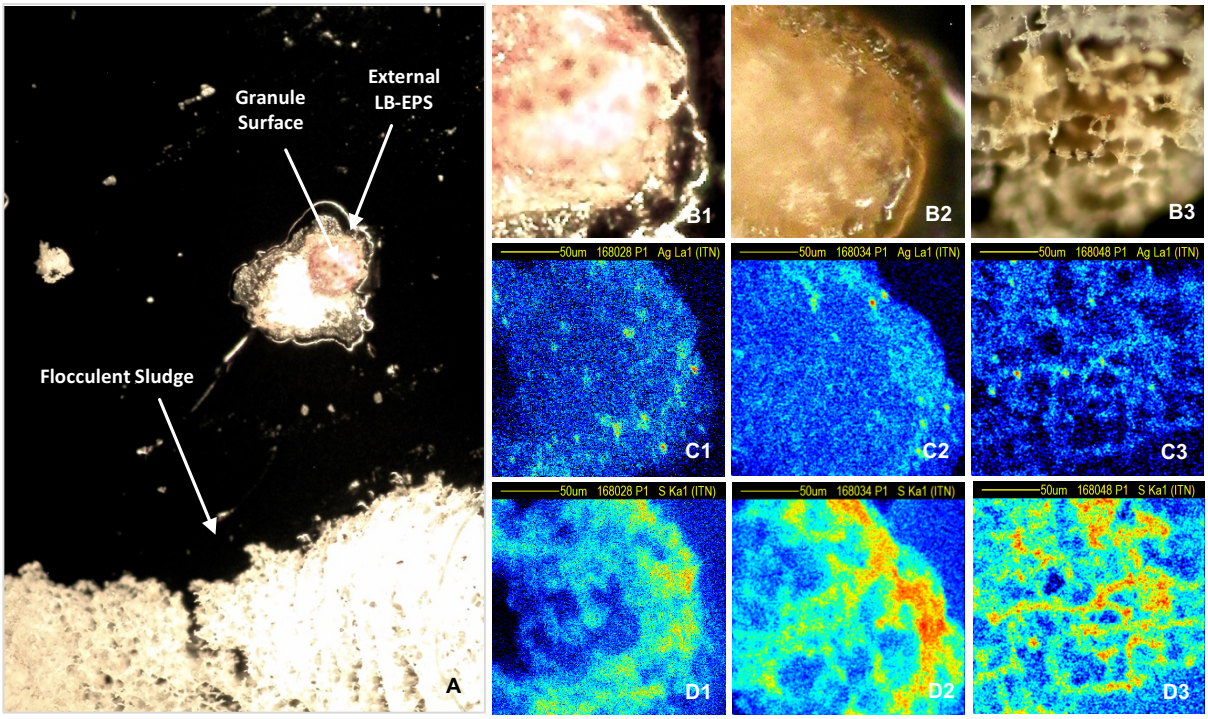


Figure 25. Sludge morphological characterization. Optical micrographs of AGS and flocculent sludge (100x magnification). Dehydrated sample showing a manually isolated AGS granule surrounded by external EPS and flocculent sludge (A); details of AGS surface (B1–B2) and dehydrated flocs (B3). Nuclear microscopy elemental distribution maps of Ag (C1-C3) and S (D1-D3) of AGS and flocculent sludge depicted above (B1–B3). Content gradient is represented by a color dynamic scale: high content – red, low content – blue. Sludge samples were collected directly from the Ag NPs-fed SBR1 during the aerated reaction phase of one treatment cycle on operational day 243.

The nuclear microscopy examination of the sludge showed that the presence of Ag NPs could be easily visualized in both AGS structures and flocculent sludge. Ag NPs typically clustered in agglomerates presenting a dimension < 10 µm, which were invariably distributed throughout the AGS and flocculent sludge, but were not observed in the surrounding medium. The images of Ag distribution showed an apparent predominance of Ag NPs agglomerates on the AGS regions coated with the gelatinous film (Figure 25 C1–C2), while Ag deposits on the exposed surface regions of the granules seem to be less important. This result is consistent with the reported affinity of EPS for metals (Geyik and Çeçen, 2016; Kang et al., 2014; Sheng et al., 2010; Wang et al., 2016). Specifically, the loose network of LB-EPS may facilitate the physical retention of Ag NPs and promote the capture of Ag NPs in its structure (Geyik & Çeçen 2016). However, because of the sample preparation methodology adopted part of the dispersible EPS layer was dragged to the edges of the spheroid structure. This means that in the native sludge most probably this layer is distributed uniformly on the granule surface, as well as the Ag associated to it. This also imply that the external EPS layer may prevent Ag NPs to

interact with the inner layer of the granules. In turn, the images of Ag distribution in flocculent sludge (Figure 25 –C3) showed Ag NPs clusters uniformly distributed along the characteristic laminar like structure. Furthermore, as can be easily visualized in PIXE maps presented in Figure 25 C(1–3) and D(1–3), the S distribution in both sludge structures seemed to follow the Ag distribution. The S content is related with protein content, as proteins contain abundant thiol (–SH) groups. Therefore, this pattern suggested the Ag NPs/$Ag^{+}$ interact with extracellular proteins present in EPS matrix, which is line with the interaction previously discussed in EPS protein quantification (section 3.7).

Ag NPs clusters, which can be visualized in the PIXE Ag distribution maps, may be embedded in both sludge structures. This means that RBS spectra analysis in these regions often has to account for Ag at a certain depth below the surface and both matrix estimation and depth distribution of Ag are therefore not straightforward. In addition, the depth of biomaterial (either AGS or flocculent sludge) that could be probed with 2.0 MeV protons was approximately 4-6 µm, which definitely limited the capability of assessing Ag profiles in these structures. Taking these limitations and derived uncertainties into account and for comparison purposes, the Ag quantification in the surface of AGS and flocculent sludge was carried out. The amount of Ag, whether associated to flocculent sludge or AGS surface, did not significantly differ (Figure 26). This suggests that Ag NPs remained attached or entrapped in the surface of both sludge structures in a similar manner. Nonetheless, this does not mean that there were no differences in the inner layers of the sludge components.

The elements present in AGS are also present in flocculent sludge (Table 3). However, the quantitative approach showed a higher S content in flocculent sludge (Figure 27), whereas P, K, and Ca were mainly associated to the AGS (Table 3). No significant variations in the concentrations of Cl, Mn and Zn were found in the sludge components. The higher S content of flocculent sludge suggested a higher protein content, according to the relation previously mentioned. In fact, the flocculent sludge due to their large specific surface area with a loose structure can favor the contact between Ag NPs and cells. Thus, cells as response against the toxic effects of the Ag NPs/Ag+ can have enhanced the EPS production (Sheng and Liu, 2011; Tan et al., 2015; Zhang et al., 2014), presumably in the form of proteins (Quan et al., 2015). On the other hand, the presence of high contents of P, K and Ca in granule structures is consistent with their higher cellular density (Quan et al., 2015). P forms the sugar-P backbone of DNA and RNA. Living cells use P to transport cellular energy with adenosine triphosphate (ATP), necessary for every cellular process that uses energy. ATP is also important for phosphorylation, a key regulatory event in cells. Phospholipids are also the main structural components of all cellular membranes. In addition, microbial cells maintain controlled intracellular levels of Ca and K to ensure cellular functions, such as metabolism, cell division, and membrane potential.

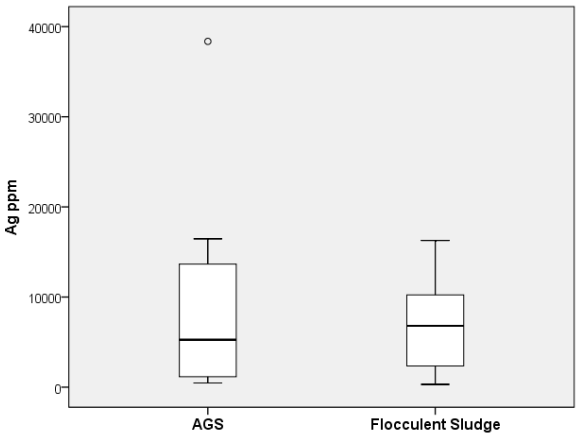


Figure 26. Box plot of the Ag concentrations in AgNPs clusters identified on the surface of AGS and flocculent sludge. The box represents the 25% and 75% interquartiles (IQ) and the dividing horizontal line indicates the median; whiskers indicate the maximum and minimum values, excluding the identified outliers (open circles).

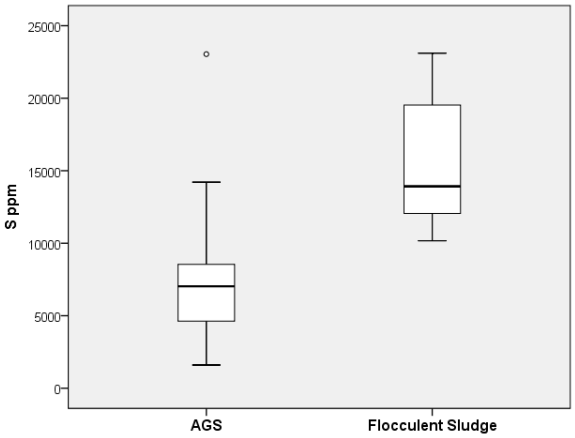


Figure 27. Box plot of the S concentrations in AGS and flocculent sludge. The box represents the 25% and 75% interquartiles (IQ) and the dividing horizontal line indicates the median; whiskers indicate the maximum and minimum values, excluding the identified outliers (open circles).

Table 3. Elemental concentrations present in AGS and Flocculent Sludge (mg/kg dry weight). Data summarized as median (IQ50%) and interquartiles 25% (IQ 25%) and 75% (IQ 75%). Significant differences, $p<0.05$, for Mann-Whitney non-parametric test are also indicated (*).

| Elements (mg/kg dry weight) | AGS | | | Flocculent Sludge | | |
|---|---|---|---|---|---|---|
| | IQ 25% | IQ 50% | IQ 75% | IQ 25% | IQ 50% | IQ 75% |
| **Ag** | 1015 | 5262 | 15974 | 1841 | 6802 | 10918 |
| **S** | 4421 | 7028 | 8947 | 11960 | 13922 | 20078* |
| **P** | 20173 | 39715 | 77079 | 16076 | 18659 | 22351* |
| **Cl** | 9834 | 33227 | 42635 | 9998 | 12401 | 15005 |
| **K** | 24738 | 37723 | 61847 | 22356 | 26871 | 34741 * |
| **Ca** | 3991 | 4917 | 13085 | 2884 | 3705 | 4696 * |
| **Mn** | 13 | 18 | 38 | 10 | 23 | 27 |
| **Zn** | 31 | 44 | 109 | 34 | 48 | 87 |

To explore the Ag distribution in AGS, sections of these spheroid structures were examined (Figure 28). In AGS sections an evident predominance of Ag NPs agglomerates were associated to the outer layers of the spheroid structures (Figure 28 –B1 and B2). The quantitative approach also confirmed the significantly higher Ag concentration present in the outer layer of the granule (Figure 28 –C). These results suggested that the outer layers of AGS hinder the dispersion of Ag NPs into the central part of the granule, which is in agreement with the results obtained in the granule surface analysis, as discussed above. Therefore, the retention of Ag NPS on the granule surface layers may protect the microbial communities present in the inner layers against Ag NPs/$Ag^{+}$ toxicity. These results are in line with that reported by Quan et al. (2015). These authors suggested that the special physical structure of AGS in

which microbes aggregate tightly and are encapsulated by dense layers of EPS allowed the microbial community to remain stable after long-term exposure (69 days) to 5 and 50 mg/L of Ag NPs.

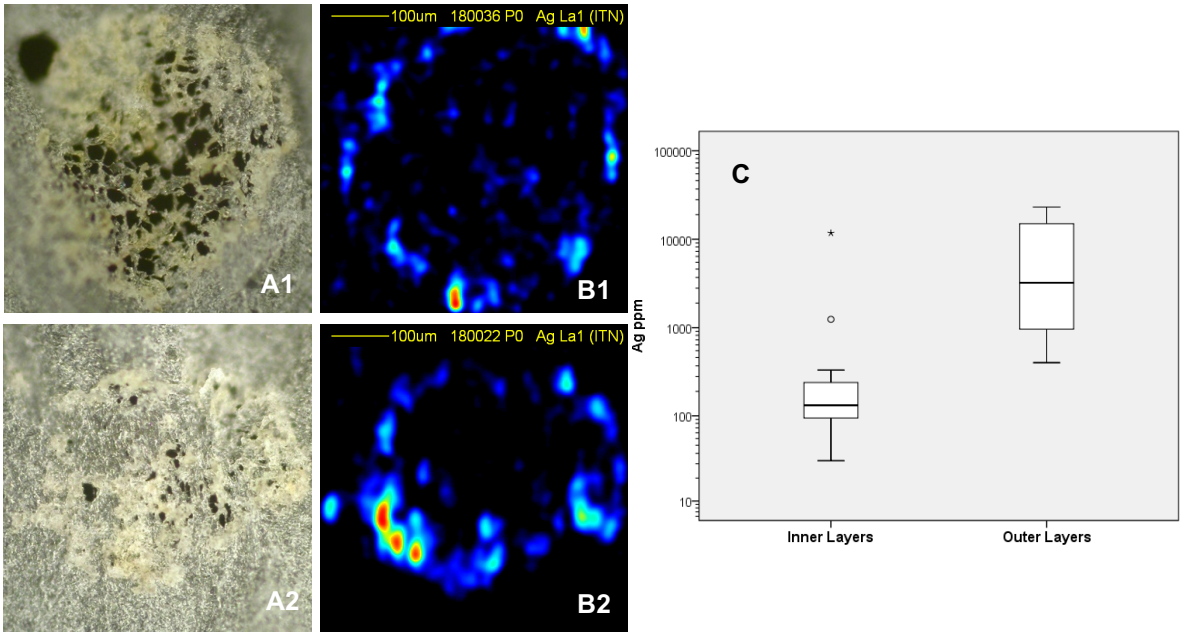


Figure 28. Ag distribution in granule sections. Optical microscopy images of two sections of different granules (A1 and A2) and the corresponding PIXE maps of Ag distribution (B1–B2). In the Ag maps the content gradient is represented by a color dynamic scale: high content – red, low content – blue. C – Box plot of the logarithm of Ag concentration in Ag NPs clusters identified on the inner and outer layer of AGS. The box represents the 25% and 75% interquartiles (IQ) and the dividing horizontal line indicates the median; whiskers indicate the maximum and minimum values.

# 4. Conclusions

The current study represents one of the first reports assessing the effects of silver nanoparticles on the characteristics and performance of AGS during the treatment of synthetic textile wastewater in an anaerobic-aerobic SBR system, including the granulation step. Successful granule formation was achieved after 35 days of operation, irrespective of the presence of Ag NPs. Although the exposure to Ag NPs had induced an early deterioration of the granules, in the long term Ag NPs seemed to have a positive influence on their settling properties.

The accumulation of Ag NPs within the granule pores and on their surface, a premature excess of EPS production or an enrichment in the protein fraction of EPS induced by Ag NPs, as well as the additional mechanical shear stress promoted by collisions between Ag NPs agglomerates and the granules seemed to be the main mechanisms involved in both early AGS loss of stability and improved sludge settling capacities. Furthermore, the presence of Ag NPs apparently did not influence neither SBR treatment performance nor cell membrane integrity in the present system. The quantitative analysis of the EPS major fractions suggested that Ag NPs interact with the protein fraction, which was further confirmed by nuclear microscopy. The examination of Ag NPs-containing samples through nuclear microscopy also showed that < 10μm Ag NPs agglomerates were presumably distributed uniformly in the surface of both granular and floc-like structures, although in AGS they were preferentially associated

to an external gel-like EPS layer. A quantitative nuclear microscopy approach revealed that the amount of Ag, whether associated to flocculent sludge or AGS surface, did not significantly differ. This analysis also evidenced a higher protein content for flocculent sludge, whereas granule structures appeared to have a higher cellular density. The Ag distribution in cross sectioned AGS samples demonstrated that the outer layers of the granules greatly hindered the dispersion of Ag NPs into the central part, which may have protected the microbial communities present in the inner layers against Ag NPs/$Ag^+$ toxicity.

This study demonstrated that AGS has the ability to withstand Ag NPs/$Ag^+$ toxicity, since neither SBR treatment performance nor cell membrane integrity were affected under the conditions tested. Nonetheless, the Ag NPs seemed to have negatively influenced the structural stability of AGS, which is one of the most serious barriers to full scale applications of AGS technology. The use of nuclear microscopy allowed the detailed compartmentalization of Ag NPs in sludge sample components, providing new and relevant information concerning the pattern of Ag NPs retention. Thus, the reported results also highlighted the potential application of nuclear microscopy for characterizing the fate of Ag NPs in wastewater treatment systems based in AGS technology.

# 5. Future Work

This study provided various evidences that Ag NPs interact with the EPS matrix of AGS, mainly with PN. Nonetheless, in this preliminary study it was not possible to quantity this EPS component, which prevented the study of the behavior of PN along the reaction phase of the SBR treatment cycles. As such, the PN quantification should be optimized in order to assess the dynamic change of EPS during the SBR cycles along the whole experimental period. This would enable to further study the effects of Ag NPs on aerobic granules-associated EPS during textile wastewater treatment with AGS, including granulation and long-term SBR operation.

Moreover, it would be important to complement these studies with the analysis of the interaction of Ag NPs with the microbial consortium present in AGS. For example, this information would allow to know whether the Ag NPs induced a shift in the diversity of the microbial communities toward an increase in EPS- or PN-producer organisms.

Furthermore, as the particle size and the concentration of Ag NPs has a strong impact on their physicochemical properties and antimicrobial activities, the effects of Ag NPs with different particle sizes and concentrations on textile wastewater treatment with AGS should also be assessed.

# 6. References

Adav, S.S., Lee, D., Show, K., Tay, J., 2008. Aerobic granular sludge : Recent advances. Biotechnol. Adv. 26, 411–423.

Adav, S.S., Lee, D.J., 2008. Extraction of extracellular polymeric substances from aerobic granule with compact interior structure. J. Hazard. Mater. 154, 1120–1126.

Adav, S.S., Lee, D.J., Lai, J.Y., 2007. Effects of aeration intensity on formation of phenol-fed aerobic

granules and extracellular polymeric substances. Appl. Microbiol. Biotechnol. 77, 175–182.

Agnihotri, S., Mukherji, S., Mukherji, S., 2014. Size-controlled silver nanoparticles synthesized over the range 5–100 nm using the same protocol and their antibacterial efficacy. RSC Adv. 4, 3974–3983.

Alves, C., Breese, H., Alves, E., Paúl, A., da Silva, M.R., da Silva, M.F., Soares, J.C., 2000. Micron-scale analysis of SiC/SiCf composites using the new Lisbon nuclear microprobe. Nucl. Instruments Methods Phys. Res. Sect. B Beam Interact. with Mater. Atoms 161–163, 334–338.

Antonelli, M., Bialek, K., Teli, A., Citterio, S., Malpei, F., 2011. Influence of thermal extraction of extracellular polymeric substances on cell integrity in activated sludge and membrane bioreactor samples. Water Environ. Res. 83, 100–106.

Azeredo, J., Oliveira, R., Lazarova, V., 1998. A new method for extraction of exopolymers from activated sludges. Water Sci. Technol. 37, 367–370.

Babu, B.R., Parande, a K., Raghu, S., Kumar, T.P., 2007. Cotton Textile Processing : Waste Generation and Effluent Treatment. J. Cotton Sci. 153, 141–153.

Behra, R., Sigg, L., Martin, J.D.C., Herzog, F., Minghetti, M., Jonhston, B., Petri-Fink, A., Rothen-Rutishauser, B., 2013. Bioavailability of silver nanoparticles and ions: from a chemical and biochemical perspective. J R Soc Interface 10, 15.

Benn, T.M., Westerhoff, P., 2008. Nanoparticle silver released into water from commercially available sock fabrics. Environ. Sci. Technol. 42, 4133–4139.

Beun, J.., Hendriks, A., van Loosdrecht, M.C.., Morgenroth, E., Wilderer, P.., Heijnen, J.., 1999. Aerobic granulation in a sequencing batch reactor. Water Res. 33, 2283–2290.

Beun, J.J., Dircks, K., Van Loosdrecht, M.C.M., Heijnen, J.J., 2002. Poly-b-hydroxybutyrate metabolism in dynamically fed mixed microbial cultures. Water Res. 36, 1167–1180.

Bisschops, I., Spanjers, H., 2003. Literature review on textile wastewater characterisation. Environ. Technol. 24, 1399–1411.

Blaser, S.A., Scheringer, M., MacLeod, M., Hungerbühler, K., 2008. Estimation of cumulative aquatic exposure and risk due to silver: Contribution of nano-functionalized plastics and textiles. Sci. Total Environ. 390, 396–409.

Blomqvist, A., 1996. Food and Fashion: Water Management and Collective Action Among Irrigation Farmers and Textile Industrialists in South India.

Bourven, I., Simon, S., Guibaud, G., 2013. Influence of extraction method on size exclusion chromatography fingerprints of EPS from wastewater sludges. Environ. Technol. 1–12.

Brigé, A., Motte, B., Borloo, J., Buysschaert, G., Devreese, B., Van Beeumen, J.J., 2008. Bacterial decolorization of textile dyes is an extracellular process requiring a multicomponent electron transfer pathway. Microb. Biotechnol. 1, 40–52.

Carmen, Z., Daniela, S., 2010. Textile Organic Dyes – Characteristics , Polluting Effects and Separation / Elimination Procedures from Industrial Effluents – A Critical Overview. Org. Pollut. ten years after Stock. Conv. - Environ. Anal. Updat. 55–86.

Carmona, a., Devès, G., Ortega, R., 2008. Quantitative micro-analysis of metal ions in subcellular compartments of cultured dopaminergic cells by combination of three ion beam techniques. Anal. Bioanal. Chem. 390, 1585–1594.

Caudan, C., Filali, A., Lefebvre, D., Spérandio, M., Girbal-Neuhauser, E., 2012. Extracellular polymeric substances (EPS) from aerobic granular sludges: Extraction, fractionation, and anionic properties. Appl. Biochem. Biotechnol. 166, 1685–1702.

Chan, Y.J., Chong, M.F., Law, C.L., Hassell, D.G., 2009a. A review on anaerobic–aerobic treatment of industrial and municipal wastewater. Chem. Eng. J. 155, 1–18.

Chan, Y.J., Chong, M.F., Law, C.L., Hassell, D.G., 2009b. A review on anaerobic–aerobic treatment of industrial and municipal wastewater. Chem. Eng. J. 155, 1–18.

Chen, H., Zhou, S., Li, T., 2010. Impact of extracellular polymeric substances on the settlement ability of aerobic granular sludge. Environ. Technol. 31, 1601–1612.

Chequer, F.M.D., Oliveira, G.A.R. De, Ferraz, E.R.A., Cardoso, J.C., Zanoni, M.V.B., Oliveira, D.P. De, 2013. Textile Dyes: Dyeing Process and Environmental Impact. Eco-Friendly Text. Dye. Finish. 151–176.

Choi, O., Deng, K.K., Kim, N.-J., Ross, L., Surampalli, R.Y., Hu, Z., 2008. The inhibitory effects of silver nanoparticles, silver ions, and silver chloride colloids on microbial growth. Water Res. 42, 3066–3074.

Choi, O., Hu, Z., 2008. Size dependent and reactive oxygen species related nanosilver toxicity to nitrifying bacteria. Environ. Sci. Technol. 42, 4583–4588.

Citeve, 2012. Estudo das dificuldades das empresas do setor têxtil e vestuário no cumprimento de legislação ambiental 52.

Commission, E., 2012. Types and uses of nanomaterials, including safety aspects, European Commission.

Corsino, S.F., Capodici, M., Torregrossa, M., Viviani, G., 2016. Fate of aerobic granular sludge in the long-term: The role of EPSs on the clogging of granular sludge porosity. J. Environ. Manage. 183, 541–550.

D'Abzac, P., Bordas, F., Van Hullebusch, E., Lens, P.N.L., Guibaud, G., 2010. Extraction of extracellular polymeric substances (EPS) from anaerobic granular sludges: Comparison of chemical and physical extraction protocols. Appl. Microbiol. Biotechnol. 85, 1589–1599.

Dasgupta, J., Sikder, J., Chakraborty, S., Curcio, S., Drioli, E., 2015. Remediation of textile effluents by membrane based treatment techniques: A state of the art review. J. Environ. Manage. 147, 55–72.

de Kreuk, M.K., van Loosdrecht, M.C.M., 2004. Selection of slow growing organisms as a means for improving aerobic granular sludge stability. Water Sci. Technol. 49, 9–17.

Deng, S., Wang, L., Su, H., 2016. Role and influence of extracellular polymeric substances on the preparation of aerobic granular sludge. J. Environ. Manage. 173, 49–54.

Dignac, M.F., Urbain, V., Rybacki, D., Bruchet, A., Snidaro, D., Scribe, P., 1998. Chemical description of extracellular polymers: Implication on activated sludge floc structure. Water Sci. Technol. 38, 45–53.

dos Santos, A.B., Cervantes, F.J., van Lier, J.B., 2007. Review paper on current technologies for decolourisation of textile wastewaters: Perspectives for anaerobic biotechnology. Bioresour. Technol. 98, 2369–2385.

Dubois, M., Gilles, K. a., Hamilton, J.K., Rebers, P. a., Smith, F., 1956. Colorimetric method for determination of sugars and related substances. Anal. Chem. 28, 350–356.

Dudkiewicz, A., Tiede, K., Loeschner, K., Jensen, L.H.S., Jensen, E., Wierzbicki, R., Boxall, A.B. a, Molhave, K., 2011. Characterization of nanomaterials in food by electron microscopy. TrAC - Trends Anal. Chem. 30, 28–43.

Ebeling, J.M., Sibrell, P.L., Ogden, S.R., Summerfelt, S.T., 2003. Evaluation of chemical coagulation-flocculation aids for the removal of suspended solids and phosphorus from intensive recirculating aquaculture effluent discharge. Aquac. Eng. 29, 23–42.

Eduok, S., Hendry, C., Ferguson, R., Martin, B., Villa, R., Jefferson, B., Coulon, F., 2015. Insights into the effect of mixed engineered nanoparticles on activated sludge performance. FEMS Microbiol. Ecol. 1–9.

Eyvaz, M., Gürbulak, E., Arslan, S., Prof, A., Yüksel, E., 2016. A review of state-of-the-art technologies in dye-containing wastewater treatment - The textile industry case, in: Textile Wastewater Treatment. pp. 1–4.

Franca, R.D.G.G., Vieira, A., Mata, A.M.T.T., Carvalho, G.S., Pinheiro, H.M., Lourenço, N.D., 2015. Effect of an azo dye on the performance of an aerobic granular sludge sequencing batch reactor treating a simulated textile wastewater. Water Res. 85, 327–336.

Frolund, B., Palmagren, R., Keiging, K., Nielsen, P.H., 1996. Extraction of extracellular polymers from activated sludge using a cation exchange resin. Wat. Res. Vol. 30, 1749–1758.

Gao, D., Liu, L., Liang, H., Wu, W.-M., 2011. Aerobic granular sludge: characterization, mechanism of granulation and application to wastewater treatment. Crit. Rev. Biotechnol. 31, 137–52.

Geranio, L., Heuberger, M., Nowack, B., 2009. The Behavior of Silver Nanotextiles during Washing 43, 8113–8118.

Geyik, A.G., Çeçen, F., 2016. Exposure of activated sludge to nanosilver and silver ion: Inhibitory effects and binding to the fractions of extracellular polymeric substances. Bioresour. Technol. 211, 691–697.

Geyik, A.G., Çeçen, F., 2015. Variations in extracellular polymeric substances (EPS) during adaptation of activated sludges to new feeding conditions. Int. Biodeterior. Biodegrad. 105, 137–145.

Ghaly, A., Ananthashankar, R., Alhattab, M., Ramakrishnan, V., 2013. Production, Characterization and Treatment of Textile Effluents: A Critical Review. J. Chem. Eng. Process Technol. 5, 1–19.

Giesen, A., Bruin, L.M.M. De, Niermans, R.P., Roest, H.F. Van Der, 2013. Advancements in the application of aerobic granular biomass technology for sustainable treatment of wastewater.

Gogoi, S.K., Gopinath, P., Paul, A., Ramesh, A., Ghosh, S.S., Chattopadhyay, A., 2006. Green Fluorescent Protein-Expressing Escherichia c oli as a Model System for Investigating the Antimicrobial Activities of Silver Nanoparticles. Langmuir 22, 9322–9328.

Goi, A., Trapido, M., 2002. Hydrogen peroxide photolysis, Fenton reagent and photo-Fenton for the degradation of nitrophenols: A comparative study. Chemosphere 46, 913–922.

Gontier, E., Ynsa, M.-D., Bíró, T., Hunyadi, J., Kiss, B., Gáspár, K., Pinheiro, T., Silva, J.-N., Filipe, P., Stachura, J., Dabros, W., Reinert, T., Butz, T., Moretto, P., Surlève-Bazeille, J.-E., 2008. Is there penetration of titania nanoparticles in sunscreens through skin? A comparative electron and ion

microscopy study. Nanotoxicology 2, 218–231.

Grassi, M., Kaykioglu, G., Belgiorno, V., Lofrano, G., 2012. Emerging Compounds Removal from Wastewater. Green Chem. Sustain. 15–38.

Grime, G.W., 2004. Dan32 : Recent Developments In The Windows Interface To GUPIX 8–10.

Grime, G.W., Dawson, M., 1995. Recent developments in data acquisition and processing on the Oxford scanning proton microprobe. Nucl. Instruments Methods Phys. Res. Sect. B Beam Interact. with Mater. Atoms 104, 107–113.

Gu, L., Li, Q., Quan, X., Cen, Y., Jiang, X., 2014. Comparison of nanosilver removal by flocculent and granular sludge and short- and long-term inhibition impacts. Water Res. 58, 62–70.

Gürses, A., Açıkyıldız, M., Güneş, K., Sadi Gürses, M., 2016. Dyes and Pigments 88.

Holkar, C.R., Jadhav, A.J., Pinjari, D. V., Mahamuni, N.M., Pandit, A.B., 2016. A critical review on textile wastewater treatments: Possible approaches. J. Environ. Manage. 182, 351–366.

Hong, Y.G., Gu, J.D., 2010. Physiology and biochemistry of reduction of azo compounds by Shewanella strains relevant to electron transport chain. Appl. Microbiol. Biotechnol. 88, 637–643.

Huang, T., Long, M., Huo, B., 2010. Competitive binding to cuprous ions of protein and BCA in the bicinchoninic acid protein assay. Open Biomed. Eng. J. 4, 271–278.

Jang, N., Ren, X., Kim, G., Ahn, C., Cho, J., Kim, I.S., 2007. Characteristics of soluble microbial products and extracellular polymeric substances in the membrane bioreactor for water reuse. Desalination 202, 90–98.

Jiang, C., Pang, S., Ouyang, F., Ma, J., Jiang, J., 2010. A new insight into Fenton and Fenton-like processes for water treatment. J. Hazard. Mater. 174, 813–817.

Kang, F., Alvarez, P.J.J., Zhu, D., 2014. Microbial Extracellular Polymeric Substances Reduce Ag + to Silver Nanoparticles and Antagonize Bactericidal Activity Microbial Extracellular Polymeric Substances Reduce Ag + to Silver Nanoparticles and. Environ. Sci. Technol. 48, 316–322.

Keck, A., Klein, J., Kudlich, M., Stolz, A., Knackmuss, H.J., Mattes, R., 1997. Reduction of azo dyes by redox mediators originating in the naphthalenesulfonic acid degradation pathway of Sphingomonas sp. strain BN6. Appl. Environ. Microbiol. 63, 3684–3690.

Kiser, M.A., Ryu, H., Jang, H., Hristovski, K., Westerhoff, P., 2010. Biosorption of nanoparticles to heterotrophic wastewater biomass. Water Res. 44, 4105–4114.

Kreuk, M.K., Kishida, N., Van Loodsdrecht, M.C.M., 2007. Aerobic Granular Sludge - State of the Art.

Kreuk, M. De, van Loosdrecht, M., 2004. Aerobic granular sludge technology : An alternative to activated sludge? Water Sci. Technol. 49, 1–7.

Le Ouay, B., Stellacci, F., 2015. Antibacterial activity of silver nanoparticles: A surface science insight. Nano Today 10, 339–354.

Lee, D.J., Chen, Y.Y., Show, K.Y., Whiteley, C.G., Tay, J.H., 2010. Advances in aerobic granule formation and granule stability in the course of storage and reactor operation. Biotechnol. Adv. 28, 919–934.

Lemaire, R., Webb, R.I., Yuan, Z., 2008. Micro-scale observations of the structure of aerobic microbial granules used for the treatment of nutrient-rich industrial wastewater. ISME J. 2, 528–541.

Levard, C., Hotze, E.M., Lowry, G. V., Brown, G.E., 2012. Environmental transformations of silver

nanoparticles: Impact on stability and toxicity. Environ. Sci. Technol. 46, 6900–6914.

Li, X.F., Li, Y.J., Liu, H., Hua, Z.Z., Du, G.C., Chen, J., 2008. Correlation between extracellular polymeric substances and aerobic biogranulation in membrane bioreactor. Sep. Purif. Technol. 59, 26–33.

Li, Y., Lv, J., Zhong, C., Hao, W., Wang, Y., Zhu, J., 2014. Performance and role of N-acyl-homoserine lactone (AHL)-based quorum sensing (QS) in aerobic granules. J. Environ. Sci. (China) 26, 1615–1621. doi:10.1016/j.jes.2014.05.028

Liang, Z., Das, A., Hu, Z., 2010. Bacterial response to a shock load of nanosilver in an activated sludge treatment system. Water Res. 44, 5432–5438.

Lin, H., Zhang, M., Wang, F., Meng, F., Liao, B.Q., Hong, H., Chen, J., Gao, W., 2014. A critical review of extracellular polymeric substances (EPSs) in membrane bioreactors: Characteristics, roles in membrane fouling and control strategies. J. Memb. Sci. 460, 110–125.

Liu, H., Fang, H.H.P., 2002. Extraction of extracellular polymeric substances (EPS) of sludges. J. Biotechnol. 95, 249–256.

Liu, J., Yu, S., Yin, Y., Chao, J., 2012. Methods for separation, identification, characterization and quantification of silver nanoparticles. TrAC Trends Anal. Chem. 33, 95–106.

Liu, Y., Tay, J.-H., 2004. State of the art of biogranulation technology for wastewater treatment. Biotechnol. Adv. 22, 533–563.

Liu, Y., Wang, Z.-W., Qin, L., Liu, Y.-Q., Tay, J.-H., 2005. Selection pressure-driven aerobic granulation in a sequencing batch reactor. Appl. Microbiol. Biotechnol. 67, 26–32.

Liu, Y.Q., Tay, J.H., 2007. Characteristics and stability of aerobic granules cultivated with different starvation time. Appl. Microbiol. Biotechnol. 75, 205–210.

Lok, C.-N., Ho, C.-M., Chen, R., He, Q.-Y., Yu, W.-Y., Sun, H., Tam, P., Chiu, J.-F., Che, C.-M., 2006. Proteomic analysis of the mode of antibacterial action of silver nanoparticles. J. Proteome Res. 5, 916–924.

Lorenz, C., Windler, L., von Goetz, N., Lehmann, R.P., Schuppler, M., Hungerbühler, K., Heuberger, M., Nowack, B., 2012. Characterization of silver release from commercially available functional (nano)textiles. Chemosphere 89, 817–824.

Lourenço, N.D., Franca, R.D.G., Moreira, M.A., Gil, F.N., Viegas, C.A., Pinheiro, H.M., 2015. Comparing aerobic granular sludge and flocculent sequencing batch reactor technologies for textile wastewater treatment. Biochem. Eng. J. 104, 57–63.

Lourenço, N.D., Novais, J.M., Pinheiro, H.M., 2003. Analysis of secondary metabolite fate during anaerobic-aerobic azo dye biodegradation in a sequential batch reactor. Environ. Technol. 24, 679–686.

Lourenço, N.D., Novais, J.M., Pinheiro, H.M., 2000. Reactive textile dye colour removal in a sequencing batch reactor. Water Sci. Technol. 42, 321–328.

Lv, J., Wang, Y., Zhong, C., Li, Y., Hao, W., Zhu, J., 2014. The effect of quorum sensing and extracellular proteins on the microbial attachment of aerobic granular activated sludge. Bioresour. Technol. 152, 53–58. doi:10.1016/j.biortech.2013.10.097

Majcen, A., Križanec, B., Vajnhand, S., Volmajer, J., 2012. Textile Finishing Industry as an Important Source of Organic Pollutants. Org. Pollut. Ten Years After Stock. Conv. - Environ. Anal. Updat. 2,

29–56.

Malik, A., Akhtar, R., Grohmann, E., 2014. Environmental deterioration and human health: Natural and anthropogenic determinants. Environ. Deterior. Hum. Heal. Nat. Anthropog. Determ. 1–421. doi:10.1007/978-94-007-7890-0

Maria, F., Chequer, D., Dorta, D.J., Oliveira, D.P. De, 2011. Azo Dyes and Their Metabolites : Does the Discharge of the Azo Dye into Water Bodies Represent Human and Ecological Risks ? Adv. Treat. Text. Effl. 27–48.

Masupha, T.M., 2007. Water Management at a textile industry : a case study in Lesotho 1–106.

Mattioli, D., Florio, L. De, Giordano, A., Tarantini, M., Enea, S., Ipts, M.A., Bianchi, R., Depur, B.L., Mornasco, F., Witters, H., Genné, I., Vito, S., Spanjers, H., Bisschops, I., Associates, L., Hanke, G., Loos, R., Ies, J.L., Osset, P., Ecobilan, C.V., Centexbel, I.D.V., 2005. E-Water 1–18.

Mcgillicuddy, E., Murray, I., Kavanagh, S., Morrison, L., Fogarty, A., Cormican, M., Dockery, P., Prendergast, M., Rowan, N., Morris, D., 2016. Silver nanoparticles in the environment: Sources, detection and ecotoxicology. Sci. Total Environ. 575, 231–246.

Mcswain, B.S., Irvine, R.L., Hausner, M., Wilderer, P. a, 2005. Composition and Distribution of Extracellular Polymeric Substances in Aerobic Flocs and Granular Sludge Composition and Distribution of Extracellular Polymeric Substances in Aerobic Flocs and Granular Sludge. Appl. Environ. Microbiol. 71, 1051–1057.

Morones, J.R., Elechiguerra, J.L., Camacho, A., Holt, K., Kouri, J.., Ramírez, J.T., Yacaman, J.M., 2005. The bactericidal effect of silver nanoparticles. Nanotechnology 16, 2346–53.

Muda, K., Aris, A., Salim, M.R., Ibrahim, Z., 2013. Sequential Anaerobic-Aerobic Phase Strategy Using Microbial Granular Sludge for Textile Wastewater Treatment. Biomass Now – Sustain. Growth Use 231–264.

Muda, K., Aris, A., Salim, M.R., Ibrahim, Z., Yahya, A., van Loosdrecht, M.C.M., Ahmad, A., Nawahwi, M.Z., 2010. Development of granular sludge for textile wastewater treatment. Water Res. 44, 4341–4350.

Mulware, S.J., 2015. The Review of Nuclear Microscopy Techniques : An Approach for Nondestructive Trace Elemental Analysis and Mapping of 2015.

Nielsen, P.H., Jahn, A., 1999. Extraction of EPS, in: Microbial Extracellular Polymeric Substances. pp. 49–69.

Nor-Anuar, A., Ujang, Z., van Loosdrecht, M.C.M., de Kreuk, M.K., Olsson, G., 2012. Strength characteristics of aerobic granular sludge. Water Sci. Technol. 65, 309.

O'Neill, C., Hawkes, F.R., Hawkes, D.L., Lourenço, N.D., Pinheiro, H.M., Delée, W., 1999. Colour in textile effluents - Sources, measurement, discharge consents and simulation: A review. J. Chem. Technol. Biotechnol. 74, 1009–1018.

Olson, B.J.S.C., Markwell, J., 2007. Assays for determination of protein concentration. Curr. Protoc. Protein Sci. Chapter 3, Unit 3.4.

Ortega, R., Devès, G., Carmona, A., 2009. Bio-metals imaging and speciation in cells using proton and synchrotron radiation X-ray microspectroscopy. J. R. Soc. Interface 6 Suppl 5, S649–S658.

Pal, A., Paul, A.K., 2008a. Microbial extracellular polymeric substances:central elements in heavy metal

bioremediation. Indian J. Microbiol. 48, 49–64.

Pal, A., Paul, A.K., 2008b. Microbial extracellular polymeric substances: Central elements in heavy metal bioremediation. Indian J. Microbiol. 48, 49–64. doi:10.1007/s12088-008-0006-5

Pandey, A., Singh, P., Iyengar, L., 2007. Bacterial decolorization and degradation of azo dyes. Int. Biodeterior. Biodegrad. 59, 73–84.

Pang, Y.L., Abdullah, A.Z., 2013. Current status of textile industry wastewater management and research progress in malaysia: A review. Clean - Soil, Air, Water 41, 751–764.

Pearce, C.I., Lloyd, J.R., Guthrie, J.T., 2003. The removal of colour from textile wastewater using whole bacterial cells: A review. Dye. Pigment. 58, 179–196.

Pereira, L., Alves, M., 2012. Dyes-Environmental Impact and Remediation. Environ. Prot. Strateg. Sustain. Dev. 111–162.

Pereira, L., Coelho, A. V., Viegas, C.A., Santos, M.M.C. dos, Robalo, M.P., Martins, L.O., 2009. Enzymatic biotransformation of the azo dye Sudan Orange G with bacterial CotA-laccase. J. Biotechnol. 139, 68–77.

Pinheiro, H.M., Touraud, E., Thomas, O., 2004. Aromatic amines from azo dye reduction: Status review with emphasis on direct UV spectrophotometric detection in textile industry wastewaters. Dye. Pigment. 61, 121–139.

Pinheiro, T., Pallon, J., Alves, L.C., Veríssimo, A., Filipe, P., Silva, J.N., Silva, R., 2007. The influence of corneocyte structure on the interpretation of permeation profiles of nanoparticles across skin. Nucl. Instruments Methods Phys. Res. Sect. B Beam Interact. with Mater. Atoms 260, 119–123. doi:10.1016/j.nimb.2007.02.014

Pinheiro, T., Ynsa, M.D., Alves, L.C., 2007. Imaging biological structures with a proton microprobe, in: Modern Research and Educational Topics in Microscopy. pp. 237–244.

Pronk, M., Abbas, B., Al-zuhairy, S.H.K., Kraan, R., Kleerebezem, R., van Loosdrecht, M.C.M., 2015a. Effect and behaviour of different substrates in relation to the formation of aerobic granular sludge. Appl. Microbiol. Biotechnol. 99, 5257–5268.

Pronk, M., de Kreuk, M.K., de Bruin, B., Kamminga, P., Kleerebezem, R., van Loosdrecht, M.C.M., 2015b. Full scale performance of the aerobic granular sludge process for sewage treatment. Water Res. 84, 207–217.

Qin, L., Tay, J.H., Liu, Y., 2004. Selection pressure is a driving force of aerobic granulation in sequencing batch reactors. Process Biochem. 39, 579–584.

Quan, X., Cen, Y., Lu, F., Gu, L., Ma, J., 2015. Response of aerobic granular sludge to the long-term presence to nanosilver in sequencing batch reactors: Reactor performance, sludge property, microbial activity and community. Sci. Total Environ. 506–507, 226–233.

Radetić, M., 2013. Functionalization of textile materials with silver nanoparticles. J. Mater. Sci. 48, 95–107.

Rajczakowska, M., Stefaniuk, D., Łydżba, D., 2015. Microstructure Characterization by Means of X-ray Micro-CT and Nanoindentation Measurements. Stud. Geotech. Mech. 37.

Rashed, M.N., 2013. Adsorption Technique for the Removal of Organic Pollutants from Water and Wastewater. Org. Pollut. - Monit. Risk Treat. 167–194.

Rawat, D., Mishra, V., Sharma, R.S., 2016. Detoxification of azo dyes in the context of environmental processes. Chemosphere 155, 591–605.

Rodrigues, C., 2013. Textile dyeing wastewater treatment by single and integrated processes of coagulation , chemical oxidation and biological degradation.

Russ, R., Rau, J., Stolz, A., 2000. The function of cytoplasmic flavin reductases in the reduction of azo dyes by bacteria. Appl. Environ. Microbiol. 66, 1429–1434.

Saratale, R.G., Saratale, G.D., Chang, J.S., Govindwar, S.P., 2011. Bacterial decolorization and degradation of azo dyes: A review. J. Taiwan Inst. Chem. Eng. 42, 138–157.

Sarayu, K., Sandhya, S., 2012. Current technologies for biological treatment of textile wastewater-A review. Appl. Biochem. Biotechnol. 167, 645–661.

Shafer, M.M., Overdier, J.T., Armstong, D.E., 1998. Removal, partitioning, and fate of silver and other metals in wastewater treatment plants and effluent-receiving streams. Environ. Toxicol. Chem. 17, 630–641.

Sheng, G.-P., Yu, H.-Q., Li, X.-Y., 2010. Extracellular polymeric substances (EPS) of microbial aggregates in biological wastewater treatment systems: A review. Biotechnol. Adv. 28, 882–894.

Sheng, Z., Liu, Y., 2011. Effects of silver nanoparticles on wastewater biofilms. Water Res. 45, 6039–6050.

Singh, S.N., 2014. Microbial Degradation of Synthetic Dyes in Wastewaters 367.

Solís, M., Solís, A., Pérez, H.I., Manjarrez, N., Flores, M., 2012. Microbial decolouration of azo dyes: A review. Process Biochem. 47, 1723–1748.

Som, C., Wick, P., Krug, H., Nowack, B., 2011. Environmental and health effects of nanomaterials in nanotextiles and fa??ade coatings. Environ. Int. 37, 1131–1142.

Sondi, I., Salopek-Sondi, B., 2004. Silver nanoparticles as antimicrobial agent: A case study on E. coli as a model for Gram-negative bacteria. J. Colloid Interface Sci. 275, 177–182.

Stolz, A., 2001. Basic and applied aspects in the microbial degradation of azo dyes. Appl. Microbiol. Biotechnol. 56, 69–80.

Tan, J.-M., Qiu, G., Ting, Y.-P., 2015. Osmotic membrane bioreactor for municipal wastewater treatment and the effects of siler nanoparticles on system performance. J. Clean. Prod. 88, 287–97.

Tay, J., Liu, Q., Liu, Y., 2001. Microscopic observation of aerobic granulation in sequential aerobic sludge blanket reactor 168–175.

Tay, J.H., Liu, Q.S., Liu, Y., 2002. Characteristics of Aerobic Granules Grown on Glucose and Acetate in Sequential Aerobic Sludge Blanket Reactors. Environ. Technol. 23, 931–936.

Tay, J.H., Liu, Q.S., Liu, Y., 2001. The effects of shear force on the formation, structure and metabolism of aerobic granules. Appl. Microbiol. Biotechnol. 57, 227–233.

Tay, J.H., Tay, S.T.L., Ivanov, V., Pan, S., Jiang, H.L., Liu, Q.S., 2003. Biomass and porosity profiles in microbial granules used for aerobic wastewater treatment. Lett. Appl. Microbiol. 36, 297–301.

Toh, S., Tay, J., Moy, B., Ivanov, V., Tay, S., 2003. Size-effect on the physical characteristics of the aerobic granule in a SBR. Appl. Microbiol. Biotechnol. 60, 687–695.

Vajnhandl, S., Valh, J.V., 2014. The status of water reuse in European textile sector. J. Environ. Manage. 141, 29–35.

Van Der Zee, F.P., Villaverde, S., 2005. Combined anaerobic-aerobic treatment of azo dyes - A short review of bioreactor studies. Water Res. 39, 1425–1440.

Vandevivere, P.C., Bianchi, R., Verstraete, W., 1998. Review Treatment and Reuse of Wastewater from the Textile Wet-Processing Industr y : Review of Emerging Technologies. J. Chem. T echnol. Biotechnol 72, 289–302.

Ventura, B.D.C.C., Marin, M.A.M., 2013. Azo Dyes : Characterization and Toxicity – A Review. Text. Light Ind. Sci. Technol. 2(2) 2, 85–103.

Verawaty, M., Tait, S., Pijuan, M., Yuan, Z., Bond, P.L., 2013. Breakage and growth towards a stable aerobic granule size during the treatment of wastewater. Water Res. 47, 5338–5349.

Veríssimo, A., Alves, L.C., Filipe, P., Silva, J.N., Silva, R., Ynsa, M.D., Gontier, E., Moretto, P., Pallon, J., Pinheiro, T., 2007. Nuclear microscopy: a tool for imaging elemental distribution and percutaneous absorption in vivo. Microsc. Res. Tech. 70, 302–9.

Verma, A.K., Dash, R.R., Bhunia, P., 2012. A review on chemical coagulation/flocculation technologies for removal of colour from textile wastewaters. J. Environ. Manage. 93, 154–168.

Voelker, D., Schlich, K., Hohndorf, L., Koch, W., Kuehnen, U., Polleichtner, C., Kussatz, C., Hund-Rinke, K., 2015. Approach on environmental risk assessment of nanosilver released from textiles. Environ. Res. 140, 661–672.

Wang, Q., Kang, F., Gao, Y., Mao, X., Hu, X., 2016. Sequestration of nanoparticles by an EPS matrix reduces the particle-specific bactericidal activity. Sci. Rep. 6, 21379.

Wang, Z., Liu, L., Yao, J., Cai, W., 2006. Effects of extracellular polymeric substances on aerobic granulation in sequencing batch reactors. Chemosphere 63, 1728–1735.

Wang, Z., Xue, M., Huang, K., Liu, Z., 2011. Textile dyeing wastewater treatment, in: Advances in Treating Textile effluentTreating Textile Effluent. pp. 91–116.

Wang, Z.W., Liu, Y., Tay, J.H., 2007. Biodegradability of extracellular polymeric substances produced by aerobic granules. Appl. Microbiol. Biotechnol. 74, 462–466.

Wang, Z.W., Liu, Y., Tay, J.H., 2005. Distribution of EPS and cell surface hydrophobicity in aerobic granules. Appl. Microbiol. Biotechnol. 69, 469–473.

Watt, F., 2006. A nuclear microscopy study of trace elements Ca , Fe , Zn and Cu in atherosclerosis 249, 646–652.

Watt, F., Chen, X., Chen, C., Udalagama, C.N.B., Kan, J.A. Van, Bettiol, A.A., 2013. Nuclear Instruments and Methods in Physics Research B Whole cell structural imaging at 20 nanometre resolutions using MeV ions. Nucl. Inst. Methods Phys. Res. B 306, 6–11.

Windler, L., Height, M., Nowack, B., 2013. Comparative evaluation of antimicrobials for textile applications. Environ. Int. 53, 62–73.

Winkler, M.-K.H., Bassin, J.P., Kleerebezem, R., de Bruin, L.M.M., van den Brand, T.P.H., van Loosdrecht, M.C.M., 2011. Selective sludge removal in a segregated aerobic granular biomass system as a strategy to control PAO–GAO competition at high temperatures. Water Res. 45, 3291–3299.

Winkler, M.-K.H., Kleerebezem, R., de Bruin, L.M.M., Verheijen, P.J.T., Abbas, B., Habermacher, J., van Loosdrecht, M.C.M., 2013. Microbial diversity differences within aerobic granular sludge and

activated sludge flocs. Appl. Microbiol. Biotechnol. 97, 7447–7458.

Winkler, M.K.H., Kleerebezem, R., Khunjar, W.O., de Bruin, B., van Loosdrecht, M.C.M., 2012. Evaluating the solid retention time of bacteria in flocculent and granular sludge. Water Res. 46, 4973–4980.

Xavier, J.B., Kreuk, M.K.D.E., Picioreanu, C., Loosdrecht, M.C.M.V.A.N., 2007. Multi-Scale Individual-Based Model of Microbial and Bioconversion Dynamics in Aerobic Granular Sludge 41, 6410–6417.

Yang, D., Zhao, R., 2015. Advanced Oxidation Processes (AOPs) in Wastewater Treatment. Water Pollut. 1, 167–176.

Zhang, C., Hu, Z., Deng, B., 2016. Silver nanoparticles in aquatic environments: Physiochemical behavior and antimicrobial mechanisms. Water Res. 88, 403–427.

Zhang, C., Liang, Z., Hu, Z., 2014. Bacterial response to a continuous long-term exposure of silver nanoparticles at sub-ppm silver concentrations in a membrane bioreactor activated sludge system. Water Res. 50, 350–358.

Zhang, C., Zhang, H., Yang, F., 2015. Diameter control and stability maintenance of aerobic granular sludge in an A/O/A SBR. Sep. Purif. Technol. 149, 362–369.

Zhang, L., Feng, X., Zhu, N., Chen, J., 2007. Role of extracellular protein in the formation and stability of aerobic granules. Enzyme Microb. Technol. 41, 551–557.

Zheng, Y.-M., Yu, H.-Q., Sheng, G.-P., 2005. Physical and chemical characteristics of granular activated sludge from a sequencing batch airlift reactor. Process Biochem. 40, 645–650.

Zheng, Y.M., Yu, H.Q., 2007. Determination of the pore size distribution and porosity of aerobic granules using size-exclusion chromatography. Water Res. 41, 39–46.

Zhou, J. heng, Zhang, Z. ming, Zhao, H., Yu, H. tian, Alvarez, P.J.J., Xu, X. yang, Zhu, L., 2016. Optimizing granules size distribution for aerobic granular sludge stability: Effect of a novel funnel-shaped internals on hydraulic shear stress. Bioresour. Technol. 216, 562–570.

Zhu, L., Dai, X., Lv, M., Xu, X., 2013. Correlation analysis of major control factors for the formation and stabilization of aerobic granule. Environ. Sci. Pollut. Res. 20, 3165–3175.

Zhu, L., Lv, M. Le, Dai, X., Yu, Y.W., Qi, H.Y., Xu, X.Y., 2012. Role and significance of extracellular polymeric substances on the property of aerobic granule. Bioresour. Technol. 107, 46–54.